QUANTUM CHEMICAL STUDIES AND KINETICS OF GAS REACTIONS

Except where reference is made to the work of others, the work described in this dissertation is my own or was done in collaboration with my advisory committee. This dissertation does not include proprietary or classified information.

_____

Hasan Sayin

Certificate of Approval:

_____	_____
Thomas E. Albrecht-Schmitt Associate Professor Chemistry and Biochemistry	Michael L. McKee, Chair Professor Chemistry and Biochemistry
_____	_____
Thomas R. Webb Associate Professor Chemistry and Biochemistry	Rik Blumenthal Associate Professor Chemistry and Biochemistry

_____

Joe F. Pittman
Interim Dean
Graduate School

QUANTUM CHEMICAL STUDIES AND KINETICS OF GAS REACTIONS

Hasan Sayin

A Dissertation

Submitted to

the Graduate Faculty of

Auburn University

in Partial Fulfillment of the

Requirements for the

Degree of

Doctor of Philosophy

Auburn, Alabama
December 15, 2006

QUANTUM CHEMICAL STUDIES AND KINETICS OF GAS REACTIONS

Hasan Sayin

_____
Hasan Sayin

_____
Date of Graduation

VITA

Hasan Sayin, the first child of Battal Sayin (father) and Esma Sayin (mother), was born on June 07, 1978, in Malatya, Turkey. He graduated from Bogazici (Bosphorus) University in Istanbul, Turkey with a Bachelor of Science degree in Chemistry on July 4, 2002. He entered the Ph.D. program in the Department of Chemistry, Auburn University in August, 2002. He joined Dr. Michael McKee's research group and studied quantum mechanical calculations and kinetics of gas reactions.

DISSERTATION ABSTRACT

QUANTUM CHEMICAL STUDIES AND KINETICS OF GAS REACTIONS

Hasan Sayin

Doctor of Philosophy, December 15, 2006
(B.S Bogazici (Bosphorous) University, 2002)

138 Typed Pages

Directed by Michael L. McKee

Potential energy surfaces and reaction mechanisms were calculated using various computational methods such as density-functional and wave-function methods. High-level computational methods were used to obtain accurate rate constants. Theoretical background and computational methods are introduced in Chapter 1. Chapter 2 and Chapter 3 show potential energy surface and kinetic calculations of important atmospheric reactions. Chapter 4 covers the theoretically challenging molecule F_2NOF which has not yet been synthesized experimentally.

The potential energy surface and the rate constants for reaction of XO (X=Cl, Br, I) with dimethyl sulfide (DMS) have been computed at high levels of theory in Chapter 2.

Natural bond orbital (NBO) analysis of XO-DMS and the branching ratios of the each pathways are computed.

In Chapter 3 the reaction of NO with ClO has been studied theoretically using density-functional and wave-function methods (B3LYP and CCSD(T)). Variational transition-state theory was used to calculate the rate constant for disappearance of reactants (k_{dis}) and for formation of products (k_{obs}) in the range of 200-1000K at the high-pressure limit.

The mechanism of dissociation of F_2NOF has been studied using various computational methods in Chapter 4. Rate constant calculations have been performed to understand the product formation. The calculated results showed that the formation of F_3NO is favored thermodynamically but not favored kinetically.

ACKNOWLEDGMENTS

I would like to acknowledge Prof. Michael L. McKee for setting a high standard of excellence for me and for giving me wonderful opportunities to do research in his group. He has been an invaluable source of knowledge and inspiration during my graduate life in Auburn. Dr. Nida McKee deserves special mention for her help in my graduate life in Auburn.

I would like to thank my committee members, Prof. Thomas E. Albrecht-Schmitt, Prof. Thomas R. Webb and Prof. Rik Blumental for their contributions towards my dissertation.

I am also grateful to my friends, Eren Orhun, Denem Orhun and their parents, Prof. Emrah Orhun, Dr. Deniz Orhun for their encouragement and help in Auburn.

Finally, if there were not heroic efforts of my father Battal Sayin and my mother Esma Sayin and the patience of my sisters Gül Sayin and Demet Sayin, all of whom supported and encouraged me to take my Ph.D., I certainly could never have accomplished anything.

Style Manual or Journal manual used: Journal of the American Chemical Society

Computer software used: Mac-MS word 2001, CS ChemDraw Std. 9.0 for Mac, KaleidaGraph 3.6

TABLE OF CONTENTS

LIST OF FIGURES

CHAPTER 2

LIST OF TABLES

CHAPTER 2

CHAPTER 3

CHAPTER 4

The research presented herein has resulted in the following publications:

Sayin, H.; McKee, M. L. Computational Study of the Reactions between XO (X=Cl, Br, I) and Dimethyl Sulfide, *J. Phys. Chem. A* 2004, *108*, 7613.

Sayin, H.; McKee, M. L. Theoretical Study of the mechanism of NO_2 production from NO + ClO, *J. Phys. Chem. A* 2005*, 109*, 4736.

Sayin, H.; McKee, M. L. Dissociation Mechanism of a Stable Intermediate: Perfluorohyrodxylamine, *J. Phys. Chem. A,* 2006*, 110,* 10880.

CHAPTER 1

GENERAL INTRODUCTION

Chemicals structures and reactions are simulated numerically by computational algorithms that are based on the fundamental laws of physics. Chemists can study a chemical event by running calculations on computers rather than by doing reactions and synthesizing compounds experimentally. Unstable intermediates and transition states can be modeled by computational chemistry, which can provide information about molecules and reactions that is impossible to obtain through observation alone.

There are two broad areas in computational chemistry, molecular mechanics[1] and electronic structure theory[1]. They involve the same basic types of calculations such as computing the energy of a particular molecular structure, performing geometry optimizations, and computing the vibrational frequencies of molecules. Molecular mechanics predicts the structures and properties of molecules by using classical physics but does not treat the electrons in a molecular system. Electronic effects are included in force fields through parametrization. Molecular mechanics computations are inexpensive computationally and are used for very large systems containing thousands of atoms. However this technique has many limitations. Since it neglect electrons, it cannot treat chemical problems where electronic effects are dominant. For example, it cannot describe processes that involve bond formation or bond breaking.

If we are interested in describing the electron distribution in detail, there is no way other than quantum mechanics. Electronic structure methods use quantum mechanics rather than classical physics. Electrons are very light particles and cannot be described correctly by classical mechanics. Quantum mechanics implies that the energy and the other properties of a molecule can be obtained by solving the Schrödinger equation:[1,2,3]

$$\hat{H}\Psi = E\Psi \qquad (1)$$

The exact solutions for the Schrödinger equation are not computationally practical. Therefore various mathematical approximations are applied to solve the Schrödinger equation. There are three major classes of electronic structure methods which are semi-empirical methods,[4,5] ab initio methods[6] and density functional methods.[7]

Semi-empirical methods such as AM1,[8] MINDO/3[8,9] and PM3[10,11] use parameters derived from experimental data to simplify the computation. They solve an approximate form of the Schrödinger equation. Different semi-empirical methods are classified by their parameter sets. Semi-empirical calculations are relatively inexpensive compared to ab initio and provide reasonable descriptions of molecular systems and fairly accurate in predictions of energies and structures for many systems.

Ab initio methods use no experimental parameters in their computations. Their computations depend on the laws of quantum mechanics. Ab initio computations provide high quality predictions for many systems.

A third class of electronic structure methods used widely is called density functional methods (DFT). DFT methods are similar to ab initio methods. DFT is less

expensive than ab initio methods. Since they include the effects of electron correlation, they can give the benefits of some more expensive ab initio methods at a cheaper cost.

The field of computational fluid dynamics, process simulation and design, combustion, and atmospheric chemistry are just a few of the areas that need accurate rate constants for chemical reactions. Predicting rate constants is in fact a major goal of computational chemistry. Calculations of rate constants require the accuracy of the dynamical theory and the efficiency in obtaining accurate potential-energy information.

Direct dynamics calculations provide a practical approach to the calculation of chemical reaction rates and achieve a greater understanding of dynamical bottlenecks, tunneling mechanisms, and kinetic isotope effects in chemical reactions. Direct dynamics approach is based on the output (energies, gradients, and hessians) of electronic structure calculations. Their weakness is a fairly high cost in terms of computer time because so many electronic structure calculations are involved.

1.1 Schrödinger Equation

The Austrian physicist Erwin Schrödinger proposed an equation to find the wavefunction of any system in 1926. The Schrödinger equation for a particle of mass m moving in one dimension with energy E is given in eq 2.

$$-\frac{\hbar^2}{2m}\frac{d^2\Psi}{dx^2} + V(x)\Psi = \mathrm{E}\Psi \qquad (2)$$

V(x) is the potential energy of the particle and depends on the position x; $\hbar$ ($\hbar = h/2\pi$) is the modification of Planck's constant (h) and Ψ is the wave function of the system with respect to time.

The energy and many other properties of the particle can be obtained by solving the Schrödinger equation for Ψ. For many real-world problems the energy distribution does not change with time t, and it is useful to determine how the stationary states change with position x (independent of the time t). For every time-independent Hamiltonian H, there exist a set of quantum states, Ψ_n, known as energy eigenstates and corresponding real numbers E_n satisfying the eigenvalue equation in eq 3.

$$\hat{H}\Psi_n(x)=E_n\Psi_n(x) \tag{3}$$

Such a state has a definite total energy, whose value E_n is the eigenvalue of the state vector with the Hamiltonian. This eigenvalue equation is referred as the time-independent Schrödinger equation. Equation 3 is a non-relativistic description of the system, which is not valid when the velocities of particles approach the speed of light.

1.2 The Born-Oppenheimer Approximation

As nuclei are much heavier than electrons, their velocities are much smaller. Therefore the Schrödinger equation can be separated into two parts; one part describes the electronic wave function for a fixed nuclear geometry, and another part describes the nuclear wave function, where the energy from the electronic wave function plays the role of a potential energy. This separation is called the Born-Oppenheimer (BO)

approximation.[1,2] In another way, the nuclei look fixed to the electrons, and electronic motion can be described as occurring in a field of fixed nuclei in BO approximation.

The full Hamiltonian for the molecular system can be written as given in eq 4.

$$\hat{H} = T^{elec} + T^{nucl} + V^{nucl\text{-}elec} + V^{elec} + V^{nucl} \quad (4)$$

T and V terms are kinetic and potential energy terms, respectively. The Born-Oppenheimer approximation allows solving two parts of the problem independently, so we can construct an electronic Hamiltonian which neglects the kinetic energy term from the nuclei as given in eq 5.

$$\hat{H}^{elec} = T^{elec} + V^{nucl\text{-}elec} + V^{elec} + V^{nucl} \quad (5)$$

This Hamiltonian is used in the Schrödinger equation to describe the motion of electrons in the field of fixed nuclei shown in eq 6.

$$\hat{H}^{elec}\Psi^{elec} = E^{eff}\Psi^{elec} \quad (6)$$

Solving this equation for the electronic wavefunction will produce the effective nuclear potential function E^{eff}. It depends on the nuclear coordinates and describes the potential energy surface for the system. E^{eff} is also used as the effective potential for the nuclear Hamiltonian, shown in eq 7.

$$H^{nucl} = T^{nucl} + E^{eff} \quad (7)$$

This Hamiltonian is used in the Schrödinger equation for nuclear motion, to describe the vibrational, rotational, and translational states of the nuclei. Solving the nuclear Schrödinger equation approximately is necessary for predicting the vibrational spectra of molecules.

1.3 Hartree-Fock Theory

Hartree-Fock theory[1,2] is one of the fundamental concepts of electronic structure theory. It depends on molecular orbital (MO) theory, that uses one-electron wave function or orbitals to construct the full wave function. Molecular orbitals are the product of Hartree-Fock theory, and Hartree-Fock is not an exact theory: it is an approximation to the electronic Schrödinger equation. The approximation is that we pretend that each electron feels only the average Coulomb repulsion of all the other electrons. This approximation makes Hartree-Fock theory much simpler than the real problem, which is an N-body problem. Unfortunately, in many cases this approximation is rather serious and can give poor answers. It can be corrected by explicitly accounting for electron correlation by density functional theory (DFT), many-body perturbation theory (MBPT),[12] configuration interaction (CI),[13,14] and other means.

It is important to remember that these orbitals are mathematical constructions which approximate reality. Only for hydrogen atom (or other one-electron systems, like He^+) are orbitals exact eigenfunctions of the full electronic Hamiltonian. As long as we are content to consider molecules near their equilibrium geometry, Hartree-Fock theory

often provides a good starting point for more elaborate theoretical methods which are better approximations to the electronic Schrödinger equation.

1.4 Basis set

The approximation involves expressing the molecular orbitals as linear combination of a pre-defined set of one-electron functions known as basis functions.[15] These basis functions are usually centered on the atomic nuclei and so bear some resemblance to atomic orbitals. Larger basis sets more accurately approximate the orbitals by imposing fewer restrictions on the locations of the electrons in space. An individual molecular orbital is defined in eq 8,

$$\phi_i = \sum_{\mu=1}^{N} c_{\mu i}\chi_\mu \tag{8}$$

where the coefficients $c_{\mu i}$ are known as the molecular orbital expansion coefficients. χ_μ refers to an arbitrary function in the same way ϕ_i refers to an arbitrary molecular orbital.

Ab initio methods try to derive information by solving the Schrödinger equation without fitting parameters to experimental data. Actually, ab initio methods also make use of experimental data, but in a somewhat more subtle fashion. Many different approximate methods exist for solving the Schrödinger equation, and the one to use for a specific problem is usually chosen by comparing the performance against known experimental data. Therefore experimental data guides selection of the computational model, rather than directly entering the computational procedure.

Basis sets[2] are one of the approximations inherent in essentially all ab initio methods. Expanding an unknown function, such as a molecular orbital, in a set of known functions is not an approximation, if the basis set is complete. However, a complete basis set means that an infinite number of functions must be used, which is impossible in actual calculations. The smaller the basis, the poorer the representation.

There are two types of basis functions commonly used in quantum mechanics calculations. These are Slater-type orbitals (STO)[16] and Gaussian-type orbitals (GTO).[1,2] STOs are not appropriate for numerical computations of multi-centered integrals while solving the Schrödinger equation due to high cost in computer time. Therefore their practical use in quantum-mechanical calculations is now limited. Eventhough most quantum mechanics programs use GTOs as basis functions, GTOs have difficulty in describing the proper behavior near the nucleus. Neverthless, GTOs have the important advantage that evaluating a GTO integral while solving the Schrödinger equation takes much less computer time than a STO integral evaluation. Therefore, GTOs are preferred and are generally used in computational calculations. STOs and GTOs functional forms are given in eq 9 and eq 10, respectively.

$$\phi_{\varsigma,n,l,m}(r,\theta,\varphi) = NY_{l,m}(\theta,\varphi)r^{n-1}e^{-\varsigma r} \qquad 9$$

$$\phi_{\varsigma,n,l,m}(r,\theta,\varphi) = Nx^{l_x}y^{l_y}z^{l_z}e^{-\varsigma r^2} \qquad 10$$

After deciding the type of function (STO/GTO) and the location (nuclei), the most important factor is the number of functions to be used. The smallest number of functions possible is a minimum basis set. For hydrogen and helium this means a single s-function.

For the first row in the periodic table it means two s-functions (1s and 2s) and one set of p-functions ($2p_x$, $2p_y$ and $2p_z$). For the second-row elements, three s-functions (1s, 2s and 3s) and two sets of p-functions (2p and 3p) are used.

The next improvement in the basis sets is a doubling of all basis functions, producing a Double Zeta (DZ) type basis set.[1,2] A DZ basis set employs two s-function for hydrogen (1s and 1s'), four s-functions (1s, 1s', 2s and 2s') and two sets of p-functions for first-row elements, and six s-functions and four sets of p-functions for second-row elements. For instance, 3-21G basis have two sets of functions in the valence region. The number of basis function for 3-21G and 6-31G basis sets are the same, but the 6-31G basis set has more GTOs than 3-21G. Therefore a 6-31G basis set describes molecular properties better than a 3-21G basis set. However we can use 3-21G for very large molecules for which 6-31G is too expensive. Doubling the number of basis functions allows a much better description of electron distribution in chemical bonding. The chemical bonding occurs between valence orbitals. For example doubling the 1s-functions in carbon allows for a better description of the 1s-electrons. However, the 1s-orbital is independent of the chemical environment. A variation of DZ type basis only doubles the number of valence orbitals, producing split valence basis sets. In actual calculations a doubling of the core orbitals would rarely be considered, and the term DZ basis is also used for split valence basis sets or sometimes VDZ, for valence double zeta.[1]

The next step in basis set size is a Triple Zeta (TZ).[1] This basis set contains three time as many functions as the minimum basis set, i.e. six s-functions and three p-functions for the first row elements. Some of the core orbitals may again be saved by only splitting the valence, producing a triple split valence basis set. For example, a 6-

311G basis set uses three sets of basis functions for each valence atomic orbital. The names Quadruple Zeta (QZ) and Quintuple Zeta (5Z) for the next-level basis sets are also used.[1]

In most cases higher angular-momentum functions are also important; these are denoted polarization functions.[1,2] For example, the C-H bond in HCN is primarily described by the hydrogen s-orbitals and the carbon s- and p_z-orbitals. It is clear that the electron distribution along the bond will be different than that perpendicular to the bond. If only s-functions are present on the hydrogen, this can not be described. However, if a set of p- orbitals is added to the hydrogen, the p_z component can be used for improving the description of the C-H bond. The p-orbital introduces a polarization of the s-orbitals. Similarly d- orbitals can be used for polarizing p-orbitals, f-orbitals for polarizing d-orbitals etc. 6-31G(d) basis set is a VDZ polarized set which adds six d-type functions to the 6-31G basis set on each atom other than hydrogen. The 6-31G(d,p) basis set adds three p-type functions to the 6-31G(d) basis set on each hydrogen.

The basis sets can be also improved by adding diffuse functions that are large-size versions of s- and p-type functions.[1,2] They allow orbitals to occupy a larger region of space. Basis sets with diffuse functions are important for systems where electrons are relatively far from the nucleus: molecules with lone pairs, anions and other systems with significant negative charge, systems in their excited states, systems with low ionization potentials, and so on. The 6-31+G(d) basis set is formed from the 6-31G(d) basis set by adding four diffuse functions (s, p_x, p_y, p_z) on each non-hydrogen atom. The 6-31++G(d) set also includes one diffuse s-type function on each hydrogen atom.

Basis sets for atoms beyond the third row of the periodic table are handled differently. For these very large nuclei, electrons near the nucleus are treated in an approximate way, via effective core potentials (ECPs).[17] This treatment includes some relativistic effects, which are important in these atoms. The ECPs and associated basis sets of Hay-Wadt,[18] Stevens and co-workers,[19] and Stuttgart-Dresden ECP[20] are widely used and implemented in many computational chemistry packages.

1.5 Restricted and Unrestricted Hartree-Fock

If the system has an even number of electrons and a singlet type of wave function (a closed-shell system), such wave functions are known as Restricted Hartree-Fock (RHF).[17] Open-shell systems may also be described by the restricted type wave functions where the part of the doubly occupied orbitals is forced to be the same: this is known as Restricted Open-shell Hartree-Fock (ROHF).[17] In other words, it uses doubly occupied molecular orbitals as far as possible and then singly occupied orbitals for the unpaired electrons

For open-shell systems, an unrestricted method,[17] capable of treating unpaired electrons is needed. For this case, the alpha and beta electrons are in different orbitals, resulting in two sets of molecular orbital expansion coefficients. The two sets of coefficients result in two sets of Fock matrices and ultimately to a solution producing two sets of orbitals. These separate orbitals produce proper dissociation to separate atoms, correct delocalized orbitals for resonant systems, and other attributes characteristic of open-shell systems. However eigenfunctions are not pure spin states, but contain some

amount of spin contamination from higher states (for example, doublets are contaminated to some degree by states corresponding to quartets and higher states).

1.6 Electron Correlation Methods

The Hartee-Fock method generates solutions to the Schödinger equation where the real electron-electron interection is replaced by an average interaction. With sufficiently large basis sets, the HF wave function is able to account for 99% of the total energy, but the remaining 1% is often very important for describing chemical phenomena. The difference in energy between the HF and the lowest possible energy in a given basis set is called the Electron Correlation (EC) energy.[10]

There are four main methods for calculating electron correlation: Configuration Interaction (CI), Many-Body Perturbation Theory (MBPT), Coupled-Cluster (CC)[21] and Density Functional Theory (DFT).

The HF method determines the best one-determinant trial wave function within the given basis set. Therefore it is clear that in order to improve on HF results, the starting point must be trial wave function which contains more than one determinant. As the HF solution usually gives 99% of the correct answer, electron correlation methods normally use the HF wave function as a starting point for improvements.

Configuration Interaction (CI) methods begin by noting that the exact wave function Ψ can not be expressed as a single determinant, as HF theory assumes. The additional determinants beyond the HF are constructed by interchanging one or more occupied orbitals within the Hartree-Fock determinant with a virtual (unoccupied) orbital. These can be denoted according to how many occupied HF MOs have been replaced by

virtual MOs, i.e. Slater determinants which are singly, doubly, triply, quadruply etc. excited relative to the HF determinant, up to a maximum of N excited electrons. These determinants are often referred to as Singles (S), Doubles (D), Triples (T), Quadruples (Q) etc. If all possible determinants (full CI) in a given basis set are included, all the electron correlation (in the given basis) can be recovered. For an infinite basis set the Schrödinger equation is then solved exactly. Methods which include electron correlation are two-dimensionals, the larger the one-electron expansion (basis set size) and the larger the many-electron expansion (number of determinants), the better are the results.

The multi-configuration self-consistent field (MCSCF)[3] can be considered as a CI where not only the coefficients in front of the determinants are optimized, but also the MOs used for constructing the determinants are made optimum. The MCSCF optimization is iterative just like the SCF procedure. (If the "multi-configuration" is only one, it is simply HF) Increasing the number of configurations in an MCSCF will recover more and more of the dynamical correlation (correlating the motion of the electrons), until at the full CI limit, the correlation treatment is exact. MCSCF methods are mainly used for generating a qualitatively correct wave function.

The major problem with MCSCF methods is selecting the necessary configurations to include for the property of interest. One of the most popular approaches is the Complete Active Space Self-Consistent Field (CASSCF) method (also called Full Optimized Reaction Space, FORS).[22] The selection of configurations is done by partitioning the MOs into active and inactive spaces. The active MOs will typically be some of the highest occupied and some of the lowest unoccupied MOs from a HF

calculation. The inactive MOs either have 2 or 0 electrons, i.e. always doubly occupied or empty. Within the active MOs, a full CI is performed, and all the proper symmetry-adapted configurations are included in the MCSCF optimization. The active space must be decided manually, by considering the problem and the computational expense. A common notation is [n,m]-CASSCF, indicating that n electrons are distributed in all possible ways in m orbitals.

Another approach to electron correlation is Møller-Plesset perturbation theory.[1,2] Qualitatively, Møller-Plesset perturbation theory adds higher excitations to Hartree-Fock theory as a non-iterative correction, using the techniques from the mathematical physics known as many-body perturbation theory.

Perturbation theory is based upon dividing the Hamiltonian (eq 11) into two parts:

$$\hat{H} = \hat{H}_0 + \lambda\hat{H}' \tag{11}$$

$\hat{H}_0$ is a reference Hamilton operator and $\hat{H}'$ is a perturbation Hamilton operator. λ is variable parameter determining the strength of the perturbation.

The zero-order wave function is the HF determinant, and the zero-order energy is just a sum of MO energies. Since the first-order energy is exactly the HF energy, electron correlation starts at order 2 with the choice of H_0 (see eq 12 and eq 13).

$$\text{MP0} = \text{E(MP0)} = \sum_{i=1}^{N} \varepsilon_i \tag{12}$$

$$\text{MP1} = \text{MP0} + \text{E(MP1)} = \text{E(HF)} \tag{13}$$

The lowest-energy solution to the unperturbed problem is the HF wave function, additional higher-energy solutions are excited Slater determinants, analogously to the CI method. When a finite basis set is employed it is only possible to generate a finite number of excited determinants. Therefore the expansion of the many-electron wave function is truncated. Well-known truncated MP methods are MP2 (truncation after 2nd-order), MP3, MP4 and so forth. MP2 typically accounts for 80-90% of the correlation energy, and it is the most economical method for including electron correlation. High order of MP methods such as MP3 and MP4 are available in case MP2 is inadequate. However, MP4 is more used compared to MP3 because MP3 calculations are known to provide little improvement over MP2 results.[1]

Perturbation methods add all types of corrections (S,D,T,Q, etc.) to the reference wave function to a given order (2,3,4,etc.). The idea in Coupled Cluster (CC) methods is to include all corrections of a given type to infinite order. CC methods include the effects of single and double excitation, effectively adding higher-order excitation than MP4. CC calculations are similar to CI methods in that the CC wavefunction is expressed as an exponential of excitations operating on a single Slater determinant, which solves the size-consistency problem of CI methods. The cluster operator is a sum of excitations of singles and doubles, etc. These excitations are commonly truncated at double excitations to give Coupled Cluster Singles and Doubles (CCSD).[23] Like QCISD(T)[24], triple excitations are included perturbatively to CCSD, which is called CCSD(T)[24] . Coupled Cluster (CCSD) and quadratic (QCISD) methods with triple excitations (CCSD(T) and QCISD(T)) often gives similar quality in terms of accuracy of energies and geometries.

Standard coupled-cluster theory is based on a single-determinant reference wave function. Coupled cluster is somewhat more tolerant of a poor reference wave function than MP methods due to the summation of contributions to infinite order. Since the singly excited determinants allow the MOs to relax in order to describe the multi-reference character in the wave function, the magnitude of the singles amplitude is an indicator of how good the HF single determinant is as a reference. The quality of CCSD wave function is evaluated by the T_1-diagnostic.[25] Specifically, if $T_1 < 0.02$, the CCSD(T) method is expected to give results close to the full CI limit for the given basis set. If T_1 is larger than 0.02, it indicates that the reference wave function has significant multi-determinant character, and multi-reference coupled cluster should be employed.

The foundation for Density Functional Theory (DFT) is the proof by Hohenberg and Kohn[1,2,26] that the ground-state electronic energy is determined completely by the electron density ρ. Following on the work of Kohn and Sham, the approximate functionals employed by current DFT methods partition the electronic energy into several terms where E^T is the kinetic energy term, E^V is the potential energy of the nuclear-electron attraction and of the repulsion between pairs of nuclei, E^J is the electron-electron repulsion term and E^{XC} is the exchange-correlation term and includes the remaining part of the electron-electron interactions (eq 14). E^{XC} includes the exchange energy arising from the antisymmetry of the quantum mechanical wavefunction and dynamic correlation in the motions of the individual electrons.

$$E = E^T + E^V + E^J + E^{XC} \qquad (14)$$

E^{XC} is usually divided into exchange and correlation parts, which actually correspond to same-spin and mixed-spin interactions, respectively (eq 15).

$$E^{XC}(\rho) = E^{X}(\rho) + E^{C}(\rho) \tag{15}$$

Pure DFT methods are defined by pairing an exchange functional with a correlation functional. For example, the well-known BLYP functional pairs Becke's gradient-corrected exchange functional with the gradient-corrected correlation functional of Lee, Yang and Parr.[27,28]

Self-consistent Kohn-Sham DFT calculations are performed in an iterative manner that is similar to an SCF computation. This similarity to the methodology of Hartree-Fock theory was pointed out by Kohn and Sham. E^{XC} is formulated by including the mixture of Hartree-Fock and DFT exchange along with DFT correlation by Becke (eq 16).

$$E_{hybrid}^{XC} = c_{HF} E_{HF}^{X} + c_{DFT} E_{DFT}^{XC} \tag{16}$$

where the c's are constants. B3LYP[29] functionals are currently the most widely used functionals for molecular calculations because they give good equilibrium geometries, vibrational frequencies, and accurate reaction energies. Even though DFT methods include electron correlation, they take almost the same computer resources as HF calculations which neglect electron correlation. It is also known that B3LYP results are equal to MP2 in terms of geometries and relative energies. On the other hand, DFT

methods often fail to reproduce excited-state properties and non-bonded interaction such as hydrogen bonding and van der Waals interactions.

Time-dependent density functional theory (TDDFT)[30,31] has been introduced to calculate excitation energies and oscillator strengths. In this case, the Kohn-Sham (KS) orbital energies and various exchange integrals are used in place of matrix elements of the Hamiltonian. TDDFT is usually most successful for low-energy excitations, because the KS orbital energies for orbitals that are high in the virtual manifold are typically quite poor. Further developments aimed at correcting systematic errors in TDDFT offer great promise for future applications.

1.7 Kinetics

The study of chemical kinetics is a fundamental part of chemistry. Chemistry is the study of reactions; therefore determination of the rates is important. The results of kinetic studies give information which can be applied in different ways. For example many important phenomena, such as combustion or stratospheric ozone depletion, involve many reaction steps. If we want to understand these processes fully, determination of the rate of each step is necessary. The advantages of such knowledge would be significant such as in developing more efficient combustion processes or reducing ozone depletion. Recent developments in experimental techniques and computational methods have allowed detailed studies of elementary reaction rates. The variation of such rates with temperature or pressure can give microscopic insights into the molecular mechanisms of these reactions.

1.7.1 Bimolecular Reactions

One of the basic aims of theoretical reaction kinetics is to understand why some reactions are fast and others slow, why some reactions have strong positive temperature dependencies and others none. Obviously we need to compare our theoretical expressions with experimental data or empirical expressions for the temperature dependence of the rate coefficient. Initially we will limit ourselves to trying to match the Arrhenius expression[32] [$k=A\exp(-E_a/RT$]. Rate constant, Arrhenius constant, activation energy, and temperature are denoted by k, A, E_a, T, respectively. Although this expression is not perfect, it is a good starting point for kinetics.

First of all I will start with the collision theory[33] in which the molecules are thought of as hard, structureless spheres. Then a more detailed theory which is statistical, rather than collisional, will be described. This is the famous transition state theory[33] (TST) which was developed in the 1930s and has been used in much of the discussion of rate processes.

1.7.1.a Collision theory

Collision theory is a pictorially simple model that provides a good initial visualization of bimolecular reaction. It emphasizes the importance of collision events providing the energy for reaction, and predicts qualitatively the form of temperature dependence of the rate coefficient. The predicted values for A are far from the experimental results. There are some disadvantages in collision theory.

Firstly, the 'hard sphere' assumption has completely ignored the structure of the molecules. Secondly, it is assumed that molecules react instantaneously. In practice the

changes in structure take place over a finite period. The structure of the reaction complex will evolve and this must be considered. Finally it is assumed that there are no interactions between molecules until they come into contact. Because of these drawbacks, we must turn to transition state theory (TST) to make further progress.

1.7.1.b Transition State Theory

Once simple collision theory was found to be inadequate, another was developed in the 1930s, initially by Wigner and Pilzer, later extended by Eyring and known as activated complex theory or now more commonly as transition state theory. Transition state theory refers to the details of how reactions become products. In order for a reaction to occur, the transition state must pass through some critical configuration in this space. Because of the nature of the potential function used to express the energy of the system as a function of atomic positions, the system energy possesses a saddle point.

The essential feature of the transition state theory is that there is a "concentration" of the species at the saddle point, the activated complex, that is in equilibrium with reactants and products. The Boltzmann distribution governs the concentration of that activated complex, and the rate of reaction is proportional to that concentration. Since the concentration of activated complex is small because its energy is higher than that of the reactants, this critical configuration represents the regulator of the rate of flow of reactants to products.

The concentration of the activated complex is not the only factor involved because the frequency of its dissociation into products plays an important role. Therefore, the rate can be expressed in eq 17.

$$\text{Rate} = \begin{pmatrix}\text{Activated complex}\\ \text{concentration}\end{pmatrix}\begin{pmatrix}\text{Decomposition frequency}\\ \text{of the activated complex}\end{pmatrix} \quad (17)$$

In order for the activated complex to separate into products, one bond (the one being broken) must acquire sufficient vibrational energy to separate. When it separates, one of the 3N-6 vibrational degrees of freedom is lost and is transformed into translational degrees of freedom of the products. Central to the ideal of transition state theory is the assumption that the activated complex is in equilibrium with the reactants (eq 18).

$$A + B \rightleftharpoons [AB]^{\ddagger} \longrightarrow \text{Products} \quad (18)$$

For the formation of the activated complex, $[AB]^{\ddagger}$, the equilibrium constant is given in eq 19.

$$K^{\ddagger} = \frac{[AB]^{\ddagger}}{[A][B]} \quad (19)$$

Reaction rate can be written in terms of the equilibrium constant as eq 20.

$$\text{Rate} = \frac{kT}{h} K^{\ddagger} [A][B] \quad (20)$$

Equilibrium constant $K^{\ddagger}$ is also equal to $\exp(-\Delta G^{\ddagger}/RT)$. Therefore the rate constant is given in eq 21.

$$k = \frac{kT}{h} K^{\ddagger} = \frac{kT}{h} \exp(-\Delta G^{\ddagger} / RT) \tag{21}$$

1.7.1.c Variational Transition State Theory

Transition state theory is exact if and only if no trajectories cross the transition-state dividing surface more than once. When the transition state theory is not exact, the transition state theory overestimates the exact (equilibrium) rate constant. One should therefore pick the transition-state dividing surface to minimize the flux through it. Variational transition state theory[34-37] (VTST) has been developed in which the position of the transition state is varied until the maximum value of $\Delta G^{\ddagger}$ is found. Note that VTST always provides an equal or a better estimate of the rate constant than TST.

1.8 Unimolecular Reactions

A unimolecular reaction[38] is in principle the simplest kind of elementary reaction, since it involves the isomerization or decomposition of a single isolated reactant molecule (A) through an activated complex ($A^{\ddagger}$) which involves no other molecule (eq 22).

$$A \rightarrow A^{\ddagger} \rightarrow \text{Products} \tag{22}$$

At the beginning of the twentieth century, many gas-phase reactions were known to be first-order processes and were thought to be first order under all conditions. Many reactions such as pyrolyses of simple ketones, aldehydes and ethers, have been found not to be unimolecular processes according to the modern definition. Despite the complexity, the earlier studies of these reactions were important in the development of unimolecular reaction theory. It was difficult to understand how first order processes could result if molecules were energized by bimolecular collisions that would be expected to be second order processes. Lindemann explained this phenomena by predicting that the rate coefficient should decrease with pressure, with the reaction eventually becoming second order overall.

Lindemann theory[39] overcomes the disadvantages of earlier theories. The four main concepts of the theory are given below (a-c)

(a) By collisions, a certain fraction of the molecules become energized. The rate of the energization process depends upon the rate of bimolecular collisions. This process can be written as eq 23 where

$$A + M \xrightarrow{k_1} A^* + M \qquad (23)$$

M represent a product molecule, an added 'inert' gas molecule, or a second molecule of reactant. In the simple Lindemann theory k_1 is energy-independent.

(b) Energized molecules are de-energized by collision. This is the reverse of process eq 23 and may be written as eq 24.

$$A^* + M \xrightarrow{k_2} A + M \qquad (24)$$

The rate constant k_2 is energy-independent. The superscript * indicates the energized species.

(c) The unimolecular dissociation process eq 24 also occurs with a rate constant independent of the energy content of A^* (eq 25).

$$A^* \xrightarrow{k_3} B+C \qquad (25)$$

Before starting to RRKM theory, we will explain the definition of partition functions which are important in the RRKM theory. If a molecular system can be written in a series of quantized energy levels with total energy E_0, E_1, E_2, ..., then the partition function Q for the molecule is defined as in eq 26.

$$Q = g_0\exp(-E_0/kT) + g_1\exp(-E_1/kT) + g_2\exp(-E_2/kT) + ... \qquad (26)$$

$$= \sum_{i=0}^{\infty} g_i \exp(-E_i/kT)$$

where g_i is the degeneracy of the energy level E_i. The degeneracy is alternatively the number of different independent wave-functions of the system with total energy E_i or the number of physically distinct ways of the energy can be distributed in the molecule. Therefore the sum can be taken over all energy levels rather than evaluating $\Sigma\exp(-E_i/kT)$ over all quantum states (some of the same energy), which is mathematically more

complicated. For a given system, Q depends only on the temperature and on the zero chosen for the energy scale. If the energy zero is shifted down by an amount ΔE all the energies are increased by ΔE. Therefore each exponential term in eq 26 is multiplied by exp(-ΔE/kT) and Q is simply multiplied by the same factor.

Partition functions can be considered for certain degrees of freedom of the molecule rather than for a whole molecule. It is common to consider separately the electronic, vibrational, rotational and translational partition functions, Q_e, Q_v, Q_r and Q_t. If the total energy can be written as $E_{tot} = E_e + E_v + E_r + E_t$, the molecular partition function is the product of the individual functions ($Q = Q_e \cdot Q_v \cdot Q_r \cdot Q_t$). In the same way all the degrees of freedom of one type do not need to be considered together. For instance, Q_v can be factorized into contributions for different vibrations. Such an approach may be useful if an approximate treatment of Q_v is valid for some vibrations but not for others.

1.8.1 RRKM Theory

This theory was developed by R.A. Marcus[40] and O.K.Rice[41] and is known by the names of these authors or very often by the initials RRKM. In RRKM theory, the main difference from the previous theories is the calculation of the rate constant k_1 by quantum statistical mechanics. The reaction scheme used in the RRKM theory comprises the reactions shown in eq 27 and eq 28.

$$A + M \underset{k_2}{\overset{dk_{1(E^*\to E^*+dE^*)}}{\rightleftharpoons}} A^*_{(E^*\to E^*+dE^*)} + M \qquad (27)$$

$$A^*_{(E^*)} \xrightarrow{k_\alpha(E^*)} A^{\ddagger} \xrightarrow{k^{\ddagger}} \text{Products} \qquad (28)$$

In this theory k_1 is evaluated as a function of energy by a quantum statistical-mechanical treatment instead of the classical treatment. E^* is the total non-fixed energy in the active degrees of freedom of a given energized molecule A^* ($E^* = E^{\ddagger}_v + E^*_r$; $E^{\ddagger}_v$ and E^*_r are the vibrational and rotational part of E^*, respectively). In this scheme, a careful distinction has been made between the energized molecule A^* (sometimes called active molecule) and the activated complex $A^{\ddagger}$ (occasionally called the activated molecule).

The energized molecule A^* is basically an A molecule which is characterized loosely by having enough energy to react. The energy distribution will not usually be such that reaction occurs immediately. However, there will be many quantum states of the energized molecule in a given small energy range and only a few of these can undergo conversion to products. Moreover, the energized molecules will not react instantaneously even when one of these relatively rare quantum states is reached, since the vibrational modes involved in the reaction will not be in the correct phase at first. The energized molecules thus have lifetimes to decomposition which are much greater than the periods of their vibrations. The actual lifetimes to de-energization or decomposition depend on the values of $k_2[M]$ and $k_\alpha[E^*]$ respectively. They are typically in the range 10^{-9} to 10^{-4} s.

The activated complex $A^{\ddagger}$ is basically a species which is recognizable as being intermediate between reactant and products. It is characterized by having a configuration corresponding to the top of an energy barrier between reactant and products. The energy profile along the reaction coordinate involves a potential energy barrier E^0 (the critical energy requirement) between reactant and products and this must be surmounted for

reaction to occur. The activated complex is a molecule which lies in an arbitrarily small range at the top of the barrier. The activated complex is thus unstable to movement in either direction along the reaction coordinate and, in contrast to an energized molecule, has no measurable life.

The unimolecular rate constant for RRKM can be expressed as in eq 29.

$$k_{uni} = \frac{L^{\neq} Q_1^{+}}{h Q_1 Q_2} \int_{E^* = E_0}^{\infty} \frac{\{\sum P(E_{vr}^{+})\} \exp(-E^*/\mathrm{k}T) dE^*}{1 + k_\alpha(E^*)/k_2[M]} \tag{29}$$

$L^{\neq}$ is the statistical factor which concerns the possibility of a reaction that can proceed by several distinct paths which are kinetically equivalent. For example the dissociation of H_2O to OH+H, for which $L^{\neq}=2$ since either of the two identical OH bonds are broken. $Q_1^{\ddagger}$ and Q_1 are the partition functions for the adiabatic rotations in the activated complex and the A molecule respectively. Q_2 is the partition function for the active degrees of freedom of the reactant molecule A. $E^{\ddagger}$ is the total non-fixed energy in the active degrees of freedom of a given activated complex $A^{\ddagger}$ ($E^{\ddagger} = E^{\ddagger}_v + E_r^{\ddagger} + x$; x is the translational energy of $A^{\ddagger}$ in the reaction coordinate $E^{\ddagger}_v$ and $E^{\ddagger}_r$ are the vibrational and rotational contributions to E^{+}). $\Sigma P(E^{\ddagger}_{vr})$ is the sum of the numbers of vibrational-rotational quantum states at all the quantized energy levels of energy less than or equal to $E^{\ddagger}$. It is simply the total number of vibrational-rotational quantum states of the activated complex with energies $\leq E^{\ddagger}$ Planck and Boltzmann gas constants are denoted by *h* and k, respectively.

1.8.2 The High Pressure Limit

The high-pressure limit is easily obtained from eq 29 by putting [M] → ∞, when the k_{uni} becomes the pressure-independent first-order rate constant k_∞. The rate constant at high pressure can be expressed in eq 30.

$$k_\infty = L^{*} \frac{\mathrm{kT}}{h} \frac{Q^{\ddagger}}{Q} \exp(-E_0 / \mathrm{k}T) \tag{30}$$

Q and $Q^{\ddagger}$ are the complete vibrational-rotational partition functions for the reactant and the activated complex ($Q=Q_1Q_2$ and $Q^{\ddagger}=Q_1^{\ddagger}Q_2^{\ddagger}$).

1.8.3 The Low-Pressure Limit

In the limit of very low pressures the first-order rate constant from eq 29 becomes proportional to the pressure. The rate constant at the low pressure (k_{bim}), that is the second-order rate constant, is given by eq 31, in which Q_2^{*} is the partition function for energized molecules (specifically those of A molecules which have non-fixed energy greater than E_0) using the ground state of A for the zero of energy.

$$k_{bim} = \lim_{[M]->0} \left(\frac{k_{uni}}{[M]}\right) = \frac{k_2 Q_2^{*}}{Q_2} \tag{31}$$

Equation 31 can be written in terms of the partition function $Q_2^{*'}$ for the ground state of energized molecules. The two partition functions are related by the equation $Q_2^{*'} = Q_2^{*}\exp(E_0/kT)$ and k_{bim} is given by eq 32. The terms $k_2\exp(E_0/kT)$ in this

$$k_{bim} = \frac{Q_2^{*'}}{Q_2} k_2 \exp(-E_0/kT) \tag{32}$$

equation correspond to Lindemann's k_1. The density of quantum states increases rapidly with energy and $Q_2^{*'}$ is therefore greater than Q_2.

It has already been seen that the Arrhenius activation energy of a unimolecular reaction varies with pressure. The RRKM theory does not lead to any simple equation for this variation, but the theoretical activation energy E_{ARR} at any pressure may be obtained in the usual way from the first-order rate constants calculated at a series of temperatures. The basic reason for the variation of E_{ARR} with pressure is the change in the energy distribution of reacting molecules. At sufficiently low pressures, all the molecules which become energized react. The rate constant k_1 decreases rapidly as the energy increases. Therefore the reaction of molecules with energies near the critical energy is favored. At high pressures there is a competition between reaction and collisional de-energization. The energized molecules with energies near the critical energy have long lifetimes before reaction. Therefore they can be de-energized rather than rapidly reacting with molecules having higher energies.

1.8.4 Adiabatic Rotations

An adiabatic rotation means that the angular momentum stays constant during the conversion of the energized molecule to an activated complex. In another way, the rotation stays in the same quantum state throughout this process. Since the energy of the rotation is given by $E_J=(h^2/8\pi^2 I)J(J+1)$, the energy will change as the geometry of the molecule and hence the moment of inertia I changes. In most cases where such effects are worth considering, $I^{\ddagger}>I$ so that $E_J>E_J^{\ddagger}$ and the adiabatic rotations release energy into the other (active) degrees of freedom of the molecule. This increases the multiplicity of available quantum states of the complex and the specific rate constant k_α. An alternative interpretation is that this 'centrifugal effect' allows part of the adiabatic rotational energy to be used for overcoming the potential energy barrier, thus effectively reducing E_0. In bond fission reactions the moment of inertia can change substantially, amounting to an effective reduction of E_0 by more than kT and increase in k_∞ by more than a factor of e.

1.9 References

(1) Jensen F. *Introduction to computational Chemistry*, Wiley: New York, **1999**.

(2) Hehre, W. J.; Radom, L.; Schleyer, P. v. R.; Pople, J. A. *Ab initio Molecular Orbital Theory*, Wiley and Sons: New York, **1986**.

(3) Levine, I. N. *Quantum Chemistry, Fifth Ed.*, Prentice-Hall, Inc.; New Jersey, **2000**.

(4) Thiel, W. *Tetrahedron* **1988**, *44*, 7393.

(5) Dewar, M. J. S.; Zoebisch, E. G.; Healy, E. F.; Stewart, J. J. P. *J. Am. Chem. Soc*. **1985**, *107*, 3902.

(6) (a) Hehre, W. J.; Stewart, F. R.; Pople, J. A. *J. Chem. Phys.* **1969**, *51*, 2657.

(b) Newton, M. D.; Lathan, W. A.; Hehre, W. J.; Pople, J. A. *J. Chem. Phys.* **1969**, *51*, 3927.

(c) Hehre, W. J.; Pople, J. A. *J. Am. Chem. So*c. **1970**, *92*, 2191.

7) Hohenberg, P.; Kohn, W. *Phys. Rev*. **1964**, *136*, B864.

8) Dewar, M. J. S.; Thiel, W. *J. Am. Chem. Soc*. **1977**, *99*, 4499.

9) Bingham, R. C.; Dewar, M. J. S. *J. Am. Chem. Soc*. **1975**, *97*, 1285.

10) Stewart, J. J. P. *J. Comp. Chem*. **1989**, *10*, 209.

11) Stewart, J. J. P. *J. Comp. Chem*. **1989**, *10*, 221.

12) Bartlett, R. J. *Ann. Rev. Phys. Chem*. **1981**, *32*, 359.

13) Krishnan, R.; Schlegel, H. B.; Pople, J. A. *J. Chem. Phys*. **1980**, *72*, 4654.

14) Raghavachari, K.; Pople, J. A. *Int. J. Quant. Chem*. **1981**, *20*, 167.

15) Foresman, J. B.: Frisch, A. *Exploring Chemistry with Electronic Structure Methods, 2nd Ed.*, Gaussian Inc.: Pittsburgh, **1996**.

16) Slater, J. C. *Phys. Rev*. **1930**, *36*, 57.

17) Cramer, C. J. *Essentials of Computational Chemistry*, John Wiley & Sons Inc.: New York, **2002**.

18) Hay, P. J.: Wadt,W. R. *J. Chem. Phys*. **1985**, *82*, 270.

19) Stevens, W. J.; Basch, H.; Krauss, M. *J. Chem. Phys*. **1984**, *81*, 6026

20) Dolg, M.; Wedig, U.; Stoll, H.; Preuss, H. *J. Chem. Phys*. **1987**, *86*, 866.

21) Pople, J. A.; Krishnan, R.; Schlegel, H. B.; Binkley, J. S. *Int. J. Quant. Chem*. **1978**, *14*, 545.

22) Bernardi, F.; Bottini, A.; McDougall, J. J. W.; Robb, M. A.; Schlegel, H. B. *Far. Synp. Chem. Soc.* **1984**, *19*, 137.

23) Cizek, J. *Adv. Chem. Phys*. 1969, *14*, 35.

24) Pople, J. A.; Head-Gordon, M.; Raghavachari, K. *J. Chem. Phys*. **1987**, *87*, 5968.

25) Lee, T. J.; Taylor, P. R. *Int. J. Quantum Chem. Symp*. **1989**, *23*, 199.

26) Parr, R. G.; Yang, W. *Density-Functional Theory of Atoms and Molecules*, Oxford Univ. Press: Oxford, **1989**.

27) Lee, C.; Yang, W.; Parr, R. G. *Physical Review B,* **1988**, *37*, 785.

28) Miehlich, B.; Savin, A.; Stoll, H.; Preus, H. *Chem. Phys. Lett*. 1989, *157*, 200.

29) Becke, A. D. *J. Chem. Phys*. **1993**, *98*, 5648.

30) Stratmann, R. E.; Scuseria, G. E.; Frisch, M. J. *J. Chem. Phys.* **1998**, *109*, 8218.

31) Bauernschmitt, R.; Ahlrichs, R. *Chem. Phys. Lett*. **1996**, *256*, 454.

32) Arrhenius, S. *Zeitschrift fur Physikalische Chemie* **1889**, *4*, 226.

33) Weston, R. A, Jr.; Schwarz, H. A. *Chemical Kinetics*, Prentice-Hall, Inc., Englewood Cliffs: New Jersey, **1972**.

34) Truhlar, D. G.; Garrett, B. C. *Acc. Chem. Res*. **1980**, *13*, 440.

35) Bishop, D. M.; Laidler, K. J. *Trans. Faraday Soc*. **1970**, *66*, 1685

36) Keck, J. C. *J. Chem. Phys.* **1960**, *32*, 1035.

37) Keck, J. C. *Adv. Chem. Phys.* **1967**, *13*, 85.

38) Forst, W. *Unimolecular Reactions,* Cambridge University Press: Cambridge, **2003**.

39) Lindemann, F. A. *Trans. Faraday Soc*., **1920**, *17*, 598

40) Marcus, R. A. *J. Chem. Phys*. **1952**, *20*, 359.

41) Marcus, R. A.; Rice, O. K. *J. Phys. and Colloid Chem.* **1951**, *55*, 894.

CHAPTER 2

COMPUTATIONAL STUDY OF THE REACTIONS BETWEEN XO (X=Cl, Br, I) AND DIMETHYL SULFIDE

2.1 Introduction

Dimethyl sulfide (DMS) is the most important reduced sulfur compound in the troposphere where it plays a major role regulating the climate through formation of cloud condensation nuclei in the troposphere.[1] Therefore, it is of great importance to understand the mechanism of DMS atmospheric transformations.[2-4] Unfortunately, there are many uncertainties in understanding the eventual fate of DMS in the atmosphere because of the lack of understanding of the oxidation mechanism. DMS, which is naturally emitted by oceanic phytoplankton, can reach the troposphere and react with halogen monoxide radicals in the catalytic ozone-loss cycle (eq 1).[5]

$$DMS + XO \rightarrow DMSO + X \quad (X=Cl, Br, I) \tag{1a}$$

$$O_3 + X \rightarrow O_2 + XO \tag{1b}$$

A better understanding of the reactions of XO with DMS will permit a quantitative assessment of the importance of these reactions in atmospheric models.

The experimental measurements of the reaction rates between XO and DMS (X=Cl, Br, I) are collected in Table 1.[6-16] While the hydrogen abstraction pathway is the major pathway in the reaction of Cl and NO_3 with DMS, this pathway does not appear to be important in the reaction of XO (X=Cl, Br, I) with DMS. Instead, only the oxygen-atom transfer (OAT) pathway is observed, with DMSO as the single product detected in high yield.

As seen from Table 1, there is fairly good agreement on rate constants of ClO and BrO reactions with DMS. On the other hand, the rate constant varies by almost four orders of magnitude for the IO + DMS reaction. At the slow end, the reaction would not be an important atmospheric loss process for DMS, while it would be on the fast end. One of the goals of the present study is to determine the rate constant for the IO + DMS reaction as accurately as possible.

From the experimental exothermicities[17] for the reactions of ClO, BrO and IO with DMS to form Cl, Br, and I plus DMSO (–22.4 kcal·mol^{-1}, —27.5 kcal·mol^{-1}, and –29.0 kcal·mol^{-1}, respectively), one would expect the reactivity order ClO < BrO < IO. The reactions of ClO and BrO follow this trend, but the variations in the rate constant determinations for the IO reaction are too large to determine whether the trend is followed.

We will consider two possible reaction pathways; (a) oxygen-atom transfer (OAT) from XO (X=Cl, Br, I) to DMS and (b) abstraction of hydrogen by XO (X=Cl, Br, I) (eq 2-3).

$$MeSCH_3 + XO \rightarrow MeS(O)CH_3 + X \qquad (2)$$

$$MeSCH_3 + XO \rightarrow MeSCH_2 + HOX \ (X=Cl, Br, I) \qquad (3)$$

For X=Cl, an additional pathway is considered, the abstraction of hydrogen from DMSO by chlorine atom (eq 4) which is exothermic for X=Cl but

Table 1. Experimental and theoretical rate constant ($cm^3 \cdot s^{-1}$) for XO + DMS (X=Cl, Br, I) at 298K

	Pressure(torr)	Exptl. k	Ref	Calc. k[a]
ClO+DMS				
Flow tube MS	1.8-5.1(He)	$(9.5\pm2.0)\times10^{-15}$	6	3.0×10^{-15}
Flow tube MS	0.5-2	$(3.9\pm1.2)\times10^{-15}$	7	
BrO+DMS[b]				
Flow tube MS	1.8-5.1(He)	$(2.7\pm0.5)\times10^{-13}$	6	8.7×10^{-13}
Flow tube MS		$(2.7\pm0.2)\times10^{-13}$	8	
Laser photolysis absorption	60-100(N_2)	$(4.4\pm0.6)\times10^{-13}$	9	
Cavity ring down spectroscopy	100(N_2)	4.2×10^{-13}	10	
IO+DMS				
Smog chamber FTIR	760(N_2)	$(3\pm1.5)\times10^{-11}$	11	1.5×10^{-11}
Flow tube MS	1(Ne)	$(1.5\pm0.5)\times10^{-11}$	12	
Laser photolysis absorption	40-300 (N_2,O_2,air)	$<3.5\times10^{-14}$	13	
Flow tube MS	1.58-5.1(He)	$(8.8\pm2.1)\times10^{-15}$	6	
Flow tube MS	1.1-1.4(He)	$(1.5\pm0.2)\times10^{-14}$	14	
Flow tube MS	2.5-2.7(He)	$(1.6\pm0.1)\times10^{-14}$	15	
Cavity ring down spectroscopy	100(N_2)	$(2.5\pm0.2)\times10^{-13}$	16	

[a] This work.

[b] The rate constant for the BrO + MeSH reaction at 298K is 4.54×10^{-14} $cm^3 \cdot s^{-1}$. Aranda, A.; Díaz de Mera, Y.; Rodríguez, D.; Salgado, S.; Martínez, E. *Chem. Phys. Lett.* **2002**, *357*, 471.

$$MeS(O)CH_3 + Cl \rightarrow MeS(O)CH_2 + HCl \quad (4)$$

endothermic for X=Br and I.

2.2 Method

All calculations were made using the Gaussian 98 program[18] system. Optimization and frequency calculations were carried out at the B3LYP/6-311+G(d,p) level (X=Cl and Br) and B3LYP/6-311+G(d,p)/ECP (X=I). All imaginary frequencies for transition states were tested by using the graphical program (MOLDEN)[19] to make sure that the motion was appropriate for converting reactants to products. For X=Cl, G3B3[20] energies have been determined using B3LYP/6-31G(d) geometries. For X=Br and I, a series of single-point calculations (using B3LYP/6-311+G(d,p) or B3LYP/6-311+G(d,p)/ECP geometries) have been combined to form G2B3(MP2)[21,22] and G3B3(MP2)[22,24] energies with only slight deviations from the standard procedure. The G3B3(MP2) energies were not determined for X=I because the method has not been defined for the iodine atom.

G2B3(MP2) theory corresponds effectively to calculations at the QCISD(T)/6-311+G(3df,2p) level with zero-point vibrational energies (ZPE) and higher-level corrections (HLC). The G2B3(MP2) method was extended by Radom and co-workers[22] to bromine- and iodine-containing compounds using basis sets which include effective core potentials (ECP)[25] and first-order spin-orbit corrections (SOC) for Br and I atoms (ΔESO). Recently, the G3B3(MP2) method has been extended to X=Br where all-electron basis sets are used on bromine.[24] In the calculations presented here (and a slight deviation from the standard G2B3(MP2) and G3B3(MP2) methods), SOC will be

included for X, XO, XO/DMS complexes and XO/OAT transition states (X=Cl, Br, I). The XO radicals have $^2\Pi$ ground states and are expected to have large SOCs. The XO/DMS complexes (and to a lesser extent XO/OAT transition states) have weak interactions between the XO radical and DMS such that the spin-orbital coupling effect may not be fully quenched.

The SOCs have been calculated for X, XO, XO/DMS complexes and XO/OAT transition states (X=Cl, Br, and I) and compared with other calculations and experiment in Table 2. The calculations used full Breit-Pauli spin-orbit coupling,[26] an all-electron 6-311G(d) basis set, and an active space that varied with the compound ((5e,3o), (13e,8o), and (15e,10o) for X, XO and XO-DMS/XO-OAT-TS, respectively). The calculated and experimental SOCs are in reasonable agreement for X and XO (Table 2) which suggests that the XO-DMS/XO-OAT-TS SOCs may have similar accuracy. We have decided to use the experimental SOCs for X and XO and the calculated SOCs for XO-DMS/XO-OAT-TS. While the SOC for BrO and IO are large (0.92 and 1.99 kcal·mol^{-1}, respectively) and should not be ignored, the SOCs for XO-DMS and XO-OAT-TS species are all less than 0.13 kcal·mol^{-1} and could probably be ignored. Morokuma and co-workers[27] have computed SOCs at a similar level of theory for reactions including IO + $C_2H_5 \rightarrow$ HOI + C_2H_4 at the G2M(RCC) level and have obtained similar corrections.

Relative energies (and related thermodynamic properties) are given in Table 3. The structures and enthalpies of species on the XO-DMS PES are given for ClO-DMS in Figures 1 and 2, for BrO-DMS in Figures 3 and 4 and for IO-DMS in Figures 5 and 6.

Rate constants were calculated by using CHEMRATE software package.[28] Vibrational frequencies and structures were calculated at the B3LYP/6-311+G(d,p) level

for X=Cl and Br and at B3LYP/6-311+G(d,p)/ECP for X=I and used as input along with energies at the G3B3, G3B3(MP2), and G2B3(MP2) levels for X=Cl, Br, and I, respectively. The normal modes corresponding to methyl and XO rotation were treated

Table 2. Spin-orbit Corrections[a] (SOC) in kcal·mol^{-1}

	Calculated		Exptl.
	this work[b]	others	
Cl	0.78	0.82[c]	0.84[d]
ClO	0.33	0.20[e],0.30[f],0.28[g]	0.30[h]
ClO-SMe_2-c C_s	0.01		
ClO-OAT-TS-c C_s	0.00		
Br	3.20	3.63[i]	3.51[d]
BrO	0.84	0.64[e],0.92[i],0.78[g]	0.92[j]
BrO-SMe_2-c C_s	0.05		
BrO-OAT-TS-c C_s	0.02		
I	6.55	7.02[k]	7.25[l]
IO	1.48	1.60[k],1.70[e],1.75[g]	1.99[m]
IO-SMe_2-c C_s	0.13		
IO-OAT-TS-c C_s	0.08		

[a] The Spin-Orbit Correction (SOC) is the difference between the lowest spin-orbit coupled state and the J-averaged state. For the ^2P and $^2\Pi$ electronic states of X and XO (X=Cl, Br, I), respectively, the SOC is $\lambda/2$ where λ is the Spin-Orbit Coupling Constant (SOCC). Equivalently, the SOC is 1/3 of the Fine Structure Splitting (FSS) where $FSS=\Delta(^2P_{1/2}-^2P_{3/2})$ for X and $FSS=\Delta(^2\Pi_{1/2}-^2\Pi_{3/2})$ for XO, respectively.

[b] The GAMESS program was used to calculated the full Breit-Pauli spin-orbit coupling[26] with a (5e,3o), (13e,8o), and (15e,10o) active space for X, XO, and XO-SMe_2, respectively and a 6-311G(d) all-electron basis set. GAMESS: Schmidt, M. W.; Baldridge, K. K.; Boatz, J. A.; Elbert, S. T.; Gordon, M. S.; Jensen, J. J.; Koseki, S.; Matsunaga, N.; Nguyen, K. A.; Su, S.; Windus, T. L.; Dupuis, M.; Montgomery J. A. *J. Comput. Chem.* **1993**, *14*, 1347. All-Electron 6-311G(d) basis set: Krishnan, R.; Binkley, J. S.; Seeger R.; Pople, J. A. *J. Chem. Phys.* **1980**, *72*, 650. McLean A. D.; Chandler, G. S. *J. Chem. Phys.* **1980**, *72*,

5639. Blaudeau, J.-P.; McGrath, M. P.; Curtiss, L. A.; Radom, L. *J. Chem. Phys.* **1997**, *107*, 5016. Curtiss, L. A.; McGrath, M. P.; Blandeau, J. P.; Davis, N. E.; Binning, R. C., Jr.; Radom, L. *J. Chem. Phys.* **1995**, *103*, 6104. Glukhovstev, M. N.; Pross, A.; McGrath, M. P.; Radom, L. *J. Chem. Phys.* **1995**, *103*, 1878.

[c] Iliaš, M.; Kellö, V.; Visscher, L.; Schimmelpfenning, B. *J. Chem. Phys.* **2001**, *115*, 9667.

[d] Moore, C. E. *Atomic Energy Levels* (National Bureau of Standards, Washington, D.C. 1971), Vols. II and II, NSRDS-NBS 35.

[e] Ma, N. L.; Cheung, Y.-S.; Ng, C. Y.; Li, W.-K. *Mol. Phys.* **1997**, *91*, 495.

[f] Berning, A.; Schwqeizer, M.; Werner, H.-J.; Knowles, P. J.; Palmieri, P. *Mol. Phys.* **2000**, *98*, 1823.

[g] Koseki, S.; Gordon, M. S.; Schmidt, M. W.; Matsunaga, N. *J. Phys. Chem.* **1995**, *99*, 12764.

[h] Coxon, J. A. *Can. J. Phys.* **1979**, *57*, 1538.

[i] Bladeau, J.-P.; Curtiss, L. A. *Int. J. Quantum Chem.* **1997**, *61*, 943.

[j] McKellar, A. R. W. *J. Mol. Spectrosc.* **1981**, *86*, 43.

[k] Roszak, S.; Krauss, M.; Alekseyev, A. B.; Liebermann, H.-P.; Buenker, R. J. *J. Phys. Chem. A* **2000**, *104*, 2999.

[l] Lias, S. G.; Bartmass, J. E.; Liebman, J. F.; Holmes, J. L.; Levin, R. D.; Mallard, W. G. *J. Phys. Chem. Ref. Data 17, Suppl. No 1* **1988.**

[m] Gilles, M. K.; Polak, M. L.; Lineberger, W. C. *J. Chem. Phys.* **1991**, *95*, 4723.

as torsions rather as vibrations and the experimental spin-orbit splitting of XO was included as input to the CHEMRATE program.

Natural bond orbital (NBO) analysis[29] was done at the B3LYP/6-311+G(d,p) level for X=Cl and Br and at the B3LYP/6-311+G(d,p)/ECP level for X=I to understand the nature of bonding in the XO-DMS complexes.

Table 3. Relative Energies (kcal·mol^{-1}) at the DFT and ab initio levels for various species involved in the XO + DMS Reactions (X=Cl, Br, I)

	B3LYP/6-311+G(d,p)				ab initio[a]			
	E_e	ΔH(0K)	ΔH(298K)	ΔG(298K)	ΔH(0K)	ΔH(0K) +SOC	ΔH(298K)	ΔG(298K)
ClO+DMS	0.0	0.0	0.0	0.0	0.0	0.0	0.0	0.0
ClO-SMe_2-t C_1	-7.2	-6.3	-6.1	2.1	-1.6	-1.4	-1.2	7.1
ClO-SMe_2-t C_s	-7.1	-6.3	-6.7	3.2	-1.5	-1.3	-1.6	8.3
ClO-SMe_2-c C_s	-6.1	-5.3	-5.2	3.3	-1.8	-1.6	-2.0	6.5
ClO-abst-complex	-5.2	-5.4	-5.0	1.6	-7.0	-6.8	-6.5	0.1
ClO-OAT-TS-t C_s	1.4	1.7	1.5	10.8	7.2	7.4	7.3	16.6
ClO-OAT-TS-c C_s	-1.5	-1.0	-1.1	8.9	1.5	1.7	1.3	11.3
ClO-abst-TS	2.4	-0.2	-0.6	8.5	2.3	2.5	2.1	11.2
MeS(O)Me+Cl	-12.8	-11.8	-12.0	-8.8	-22.2	-22.8	-23.0	-19.8
$MeSCH_2$+HOCl	0.5	-1.6	-0.9	-3.7	-2.2	-12.0	-1.6	-4.3
$MeS(O)CH_2$+HCl	-9.3	-12.9	-12.4	-11.7	-24.7	-24.5	-23.9	-23.2
Cl-abst-TS[b]	-12.1	-14.3	-15.0	-4.7	-23.3	-22.9	-23.8	-13.4
BrO+DMS	0.0	0.0	0.0	0.0	0.0	0.0	0.0	0.0
BrO-SMe_2-t C_1	-6.8	-6.3	-6.1	2.1	-2.8	-1.9	-1.7	6.5
BrO-SMe_2-t C_s	-6.8	-6.4	-6.1	1.9	-2.5	-1.6	-1.4	6.6
BrO-SMe_2-c C_s	-5.4	-5.0	-4.8	3.4	-2.8	-1.9	-1.7	6.5
BrO-abst-complex	-6.4	-6.9	-6.5	0.8	-10.0	-9.1	-8.7	-1.4
BrO-OAT-TS-t C_1	-0.7	-0.6	-0.8	8.7	3.2	4.1	3.9	13.4
BrO-OAT-TS-t C_s	-0.7	-0.7	-1.4	9.5	3.1	4.0	3.4	14.2
BrO-OAT-TS-c C_s	-2.7	-2.5	-2.8	7.1	-1.1	-0.2	-0.4	9.4
BrO-abst-TS	1.9	-1.0	-1.3	8.1	1.3	2.3	2.0	11.4
MeS(O)Me+Br	-15.9	-15.0	-15.2	-11.9	-27.7	-30.3	-30.5	-27.2
$MeSCH_2$+HOBr	-1.2	-3.7	-3.0	-5.7	-5.6	-4.7	-4.0	-6.7
IO+DMS	0.0	0.0	0.0	0.0	0.0	0.0	0.0	0.0
IO-SMe_2-t C_1	-8.9	-8.0	-7.8	0.4	-3.4	-1.5	-1.3	6.9
IO-SMe_2-t C_s	-8.7	-7.9	-7.7	-0.3	-2.6	-0.8	-0.5	6.8
IO-SMe_2-c C_s	-6.6	-6.0	-5.7	2.5	-2.2	-0.4	-0.1	8.1
IO-abst-complex	-10.9	-11.2	-10.8	-3.8	-13.3	-11.4	-10.9	-4.0
IO-OAT-TS-t C_1	-6.8	-6.3	-6.4	2.6	-1.1	0.8	0.7	9.8
IO-OAT-TS-t C_s	-6.7	-6.4	-7.0	3.8	-1.6	0.4	-0.3	10.6
IO-OAT-TS-c C_s	-6.6	-6.0	-6.2	3.3	-4.4	-2.4	-2.6	6.9
IO-abst-TS	-0.3	-2.8	-3.1	5.9	1.6	3.6	3.3	12.3
MeS(O)Me+I	-25.8	-24.4	-24.6	-21.3	-32.9	-38.1	-38.3	-35.0
$MeSCH_2$+HOI	-5.3	-7.7	-7.0	-9.8	-8.5	-6.5	-5.8	-8.6

Footnotes for Table 3.

[a] The values for ClO+DMS, BrO+DMS, IO+DMS at the ab initio level are calculated by using G3B3, G3B3(MP2) and G2B3(MP2) methods, respectively. The G3 methods include SOC for atoms heavier than Ne. The entries under ΔH(0K) have this correction subtracted. The entries under ΔH(0K)+SOC have SOC added for X and XO as well as the XO/DMS complexes and OAT transition states. The SOC of X and XO are from experiment and the SOC of XO-SMe_2-c (C_s) and XO-OAT-TS-c (C_s) are from calculations. The SOC of XO-SMe_2-t and XO-OAT-TS-t (trans orientation) was assumed to be the same as the corresponding cis structure. The thermodynamic properties are obtained from unscaled vibrational frequencies.

[b] The transition state "Cl-abst-TS" was located at the MP2/6-31G(d) level because the structure could not be located at the DFT level. Further calculations (DFT and ab initio) were made on this geometry.

2.3 Results and discussion

2.3a ClO+DMS: Two orientations of ClO with DMS were considered, cis and trans. At the B3LYP/6-311+G(d,p) level, the trans ClO-DMS complex (C_s complex) was 1.0 kcal·mol^{-1} more stable than the cis complex. The C_s trans complex had one imaginary frequency at the B3LYP/6-311+G(d,p) level and led to a C_1 minimum, 0.1 kcal·mol^{-1} lower in energy. At the G3B3 level, the cis complex was 0.2 kcal·mol^{-1} lower in energy than the trans complex (0.8 kcal·mol^{-1} lower with SOC at 298K). In addition, the binding enthalpy of the complex is much smaller at the G3B3 level (2.0 kcal·mol^{-1}) compared to DFT (6.7 kcal·mol^{-1}).

The oxygen-atom transfer (OAT) transition states were also computed in the cis and trans orientations where the former was lower in enthalpy than the latter by 6.0

kcal·mol^{-1} (G3B3, Table 3). While the structures of the two transition states (ClO-OAT-TS-c and ClO-OAT-TS-t) are similar, the cis TS is earlier than the trans as judged by the longer S-O distance (1.985 compared to 1.964 Å) and the shorter Cl-O distance (1.861 compared to 1.901 Å), which is consistent with the smaller activation enthalpy (3.3 compared to 8.9 kcal·mol^{-1}). The lower enthalpy of the cis TS (relative to the trans TS) is due to the electrostatic stabilization of transferring charge on the ClO unit with the methyl hydrogens of DMS. The cis TS is also favored in XO-OAT-TS (X=Br and I) for the same reason, but the difference decreases from 6.0 kcal·mol^{-1} for X=Cl to 3.8 and 2.3 kcal·mol^{-1} for X=Br and I, respectively.

The initial product of the OAT reaction is Cl + DMSO which is calculated to be 23.0 kcal·mol^{-1} more stable than ClO + DMS (22.4 kcal·mol^{-1}, exptl). However, the calculated bond dissociation enthalpy of Cl-H and MeS(O)CH$_2$-H are 103.0 kcal·mol^{-1} and 98.5 kcal·mol^{-1}, respectively, which indicates that the Cl radical can exothermically abstract a hydrogen from DMSO to form HCl + MeS(O)CH$_2$. The transition state geometry for the abstraction was taken from MP2/6-31G(d) because the transition state could not be located at the B3LYP/6-31G(d) or B3LYP/6-311+G(d,p) levels. The enthalpy of Cl-abst-TS at G3B3 (using the MP2/6-31G(d) geometry) was 0.8 kcal·mol^{-1} below Cl + DMSO. On the other hand, the free energy of Cl-abst-TS is 6.4 kcal·mol^{-1} higher than Cl + DMSO at 298K. Very similar results have been obtained by Vandresen *et al.*[30] where values of $\Delta H^{\ddagger}$=-2.5 kcal·mol^{-1} and $\Delta G^{\ddagger}$=4.6 kcal·mol^{-1} were obtained.

In the abstraction transition state (ClO-abst-TS), the forming O-H bond is 1.265 Å and the breaking C-H bond is 1.290 Å. A hydrogen-bonded complex is formed (ClO-abst-complex) which is bound by 4.9 kcal·mol^{-1} relative to HOCl + MeSCH$_2$. The small

difference between the ClO-OAT-TS and the abstraction TS (1.3 compared to 2.1 kcal·mol^{-1}) suggests that products from both pathways should be observed. However, the HOCl/$MeSCH_2$ products have not been reported from experiments.[6,7] In contrast to experimental results on the reaction between Cl + DMS, Stickel *et al.*[31] and Butkovskaya *et al.*[32] report that hydrogen abstraction is the dominant reaction pathway at low pressure in the reaction between Cl + DMS. We note that the rate of H-abstraction from DMS by Cl is much faster than the rate of OAT from ClO to DMS $(3.3\pm0.5)\times10^{-10}$ compared to $(3.9\pm1.2)\times10^{-15}$ cm^3·s^{-1} at 298K, (Table 1).

There are two ways to compute the rate constant; (1) as a bimolecular reaction with ClO and DMS as reactants and (2) as a unimolecular pathway with the ClO-DMS complex as reactant. In the first scenario, the A-factor will be less favorable but the activation energy will be smaller, while in the second scenario, the A-factor will be more favorable but the activation energy will be larger. In the unimolecular case, the rate constant was computed as $k=K_5\cdot k_6$ where k_6 is obtained from CHEMRATE (eq 6) and K_5 is obtained from $\Delta G=-RT\ln K_5$ using the calculated free energy change of eq 5.

$$ClO + DMS \rightarrow ClO\text{-}DMS \quad (5)$$

$$ClO\text{-}DMS \rightarrow Cl + DMSO \quad (6)$$

In the ClO + DMS reaction, the computed bimolecular rate constant was much faster than K_5 times the unimolecular rate constant (k_6). Thus, the enthalpy of binding of the ClO-DMS complex does not compensate for unfavorable entropy of binding and leads to K_5 much smaller than 1. Only the bimolecular rate constant is reported.

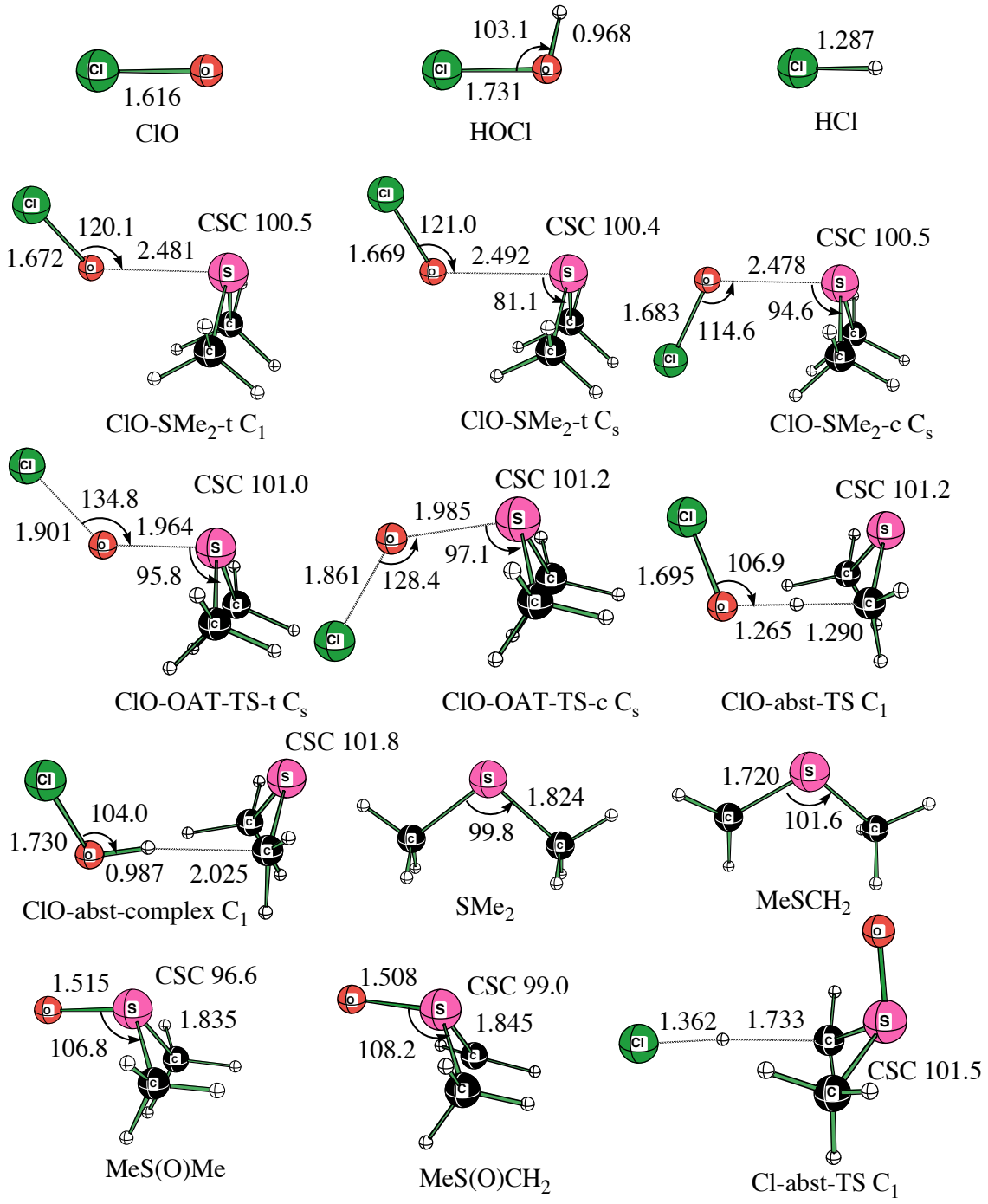

Figure 1. Optimized geometric parameters of stationary points at the

B3LYP/6-311+G(d,p) level. Bond lengths are in Å and angles are in degrees.

The optimized structure of Cl-abst-TS is at the MP2/6-31G(d) level.

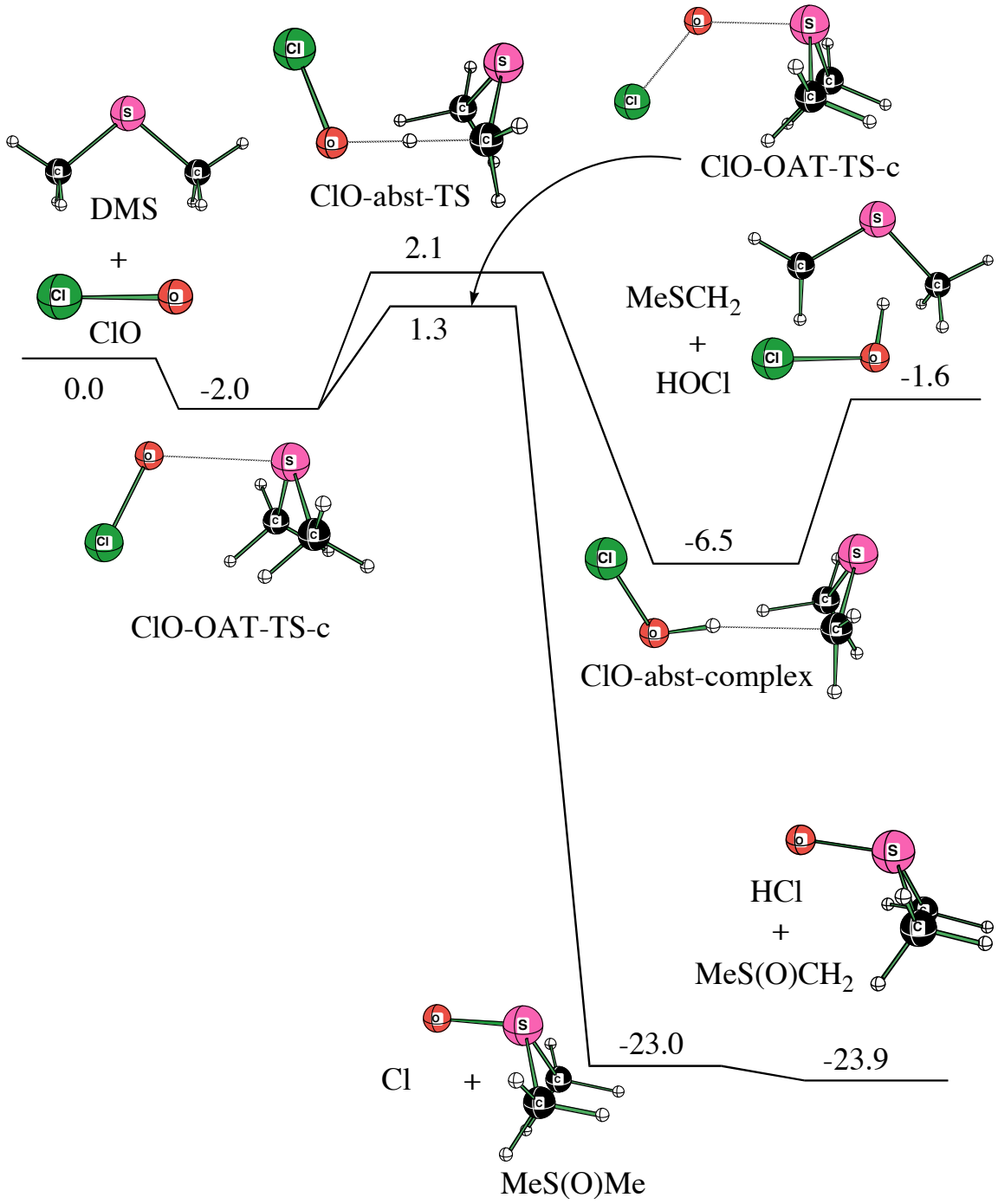

Figure 2. Schematic diagram of the potential energy surface computed at the G3B3 (298K) level for the reaction of ClO with DMS. Relative energies are given in kcal/mol at 298 K

The calculated rate constant for the OAT pathway and abstraction pathway are $3.0x10^{-15}$ and $1.1x10^{-15}$ $cm^3 \cdot s^{-1}$, respectively at 298K and 760 torr; the branching ratio is 2.7 favoring the OAT pathway. The computed rate constant for the ClO + DMS reaction is in good agreement with experiment (Table 1).

2.3b BrO + DMS: The initial complex between BrO and DMS is 1.7 $kcal \cdot mol^{-1}$ more stable than separated reactants and nearly equally stable in the cis and trans orientation. The nonbonded Br--H distance is 3.140 Å in the cis isomer (BrO-SMe_2-c) is close to the sum of the van der Waals (vdW) radii of Br (1.97 Å)[33a] and H (1.10 Å)[33b] which may indicate some interaction. In the corresponding ClO complex (ClO-SMe_2-c), the nonbonding Cl--H distance is 2.894 Å, somewhat smaller than the sum of the vdW radii between chloride (1.90 Å)[33a] and hydrogen (1.10 Å). The transition state for OAT is 3.8 $kcal \cdot mol^{-1}$ lower in the cis than in the trans orientation due to more favorable electrostatic interactions in the former. Consistent with the smaller activation enthalpy, the cis OAT TS is earlier than the trans TS as judged by the longer forming S-O bond (2.013 compared to 1.972 Å) and the shorter breaking Br-O bond (1.964 compared to 2.004 Å). The activation enthalpy for the OAT pathway is negative with respect to separated reactants (-0.4 $kcal \cdot mol^{-1}$) while the free energy of activation is 9.4 $kcal \cdot mol^{-1}$. For comparison, Bedjanian *et al.*[8] and Nakano *et al.*[10] have determined negative activation energies of -2.1 ± 0.5 $kcal \cdot mol^{-1}$ and -1.7 ± 0.5 $kcal \cdot mol^{-1}$, respectively for this reaction.

The products, Br + DMSO, are calculated to be 30.5 $kcal \cdot mol^{-1}$ exothermic which can be compared to the experimental value[17] of 27.5 $kcal \cdot mol^{-1}$. The Br radical is not expected to abstract a hydrogen from DMSO because the calculated Br-H bond enthalpy

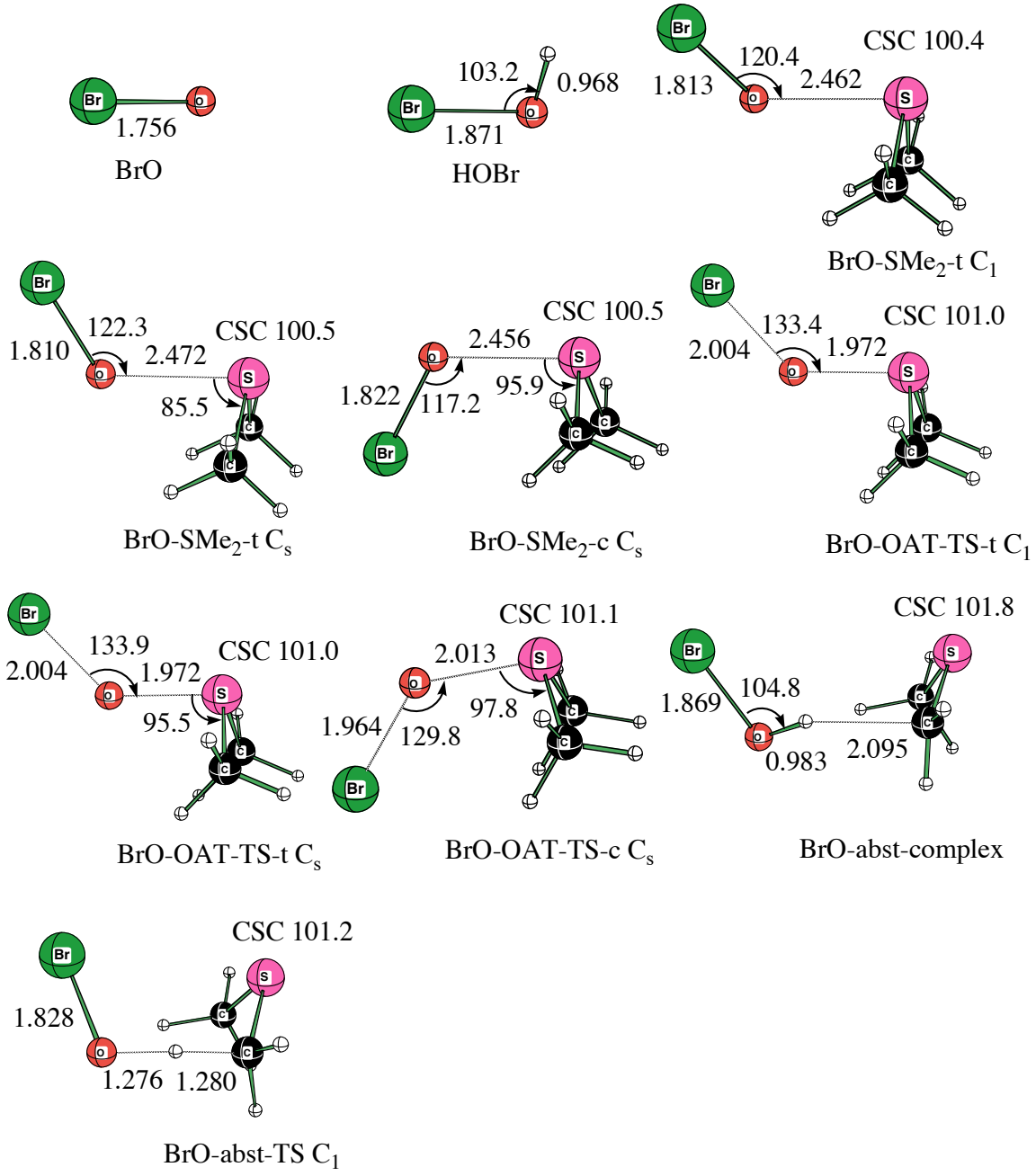

Figure 3. Optimized geometric parameters of stationary points at the B3LYP/6-311+G(d,p) level. Bond lengths are in Å and angles are in degrees.

in HBr (86.9 kcal·mol^{-1}) is smaller than the calculated C-H bond enthalpy in DMSO (98.5 kcal·mol^{-1}).

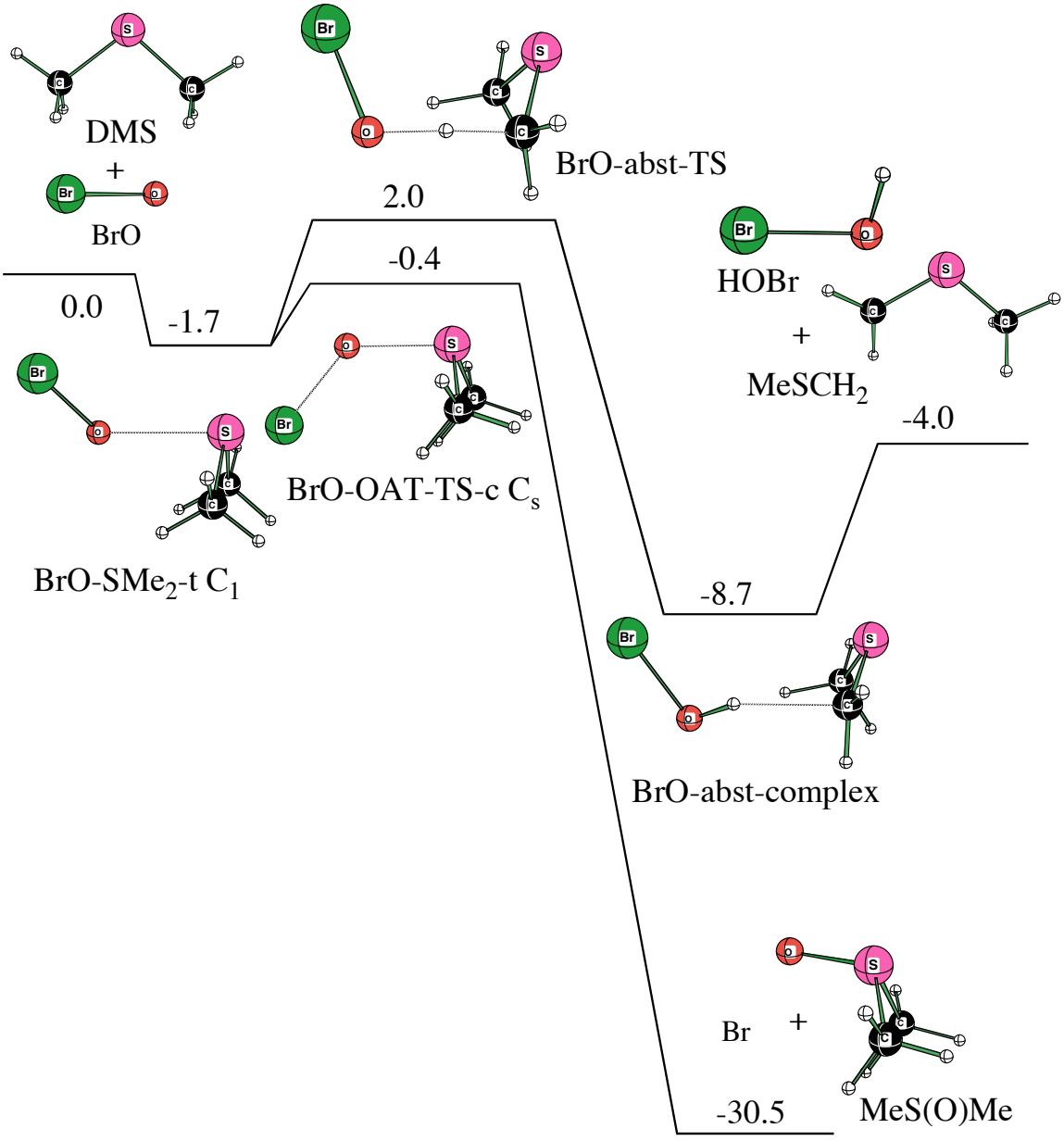

Figure 4. Schematic diagram of the potential energy surface computed at the G3B3(MP2) (298K) level for the reaction of BrO with DMS. Relative energies are given in kcal/mol at 298 K

The abstraction transition state is 2.4 kcal·mol^{-1} higher in enthalpy than the OAT transition state, consistent with the experimental results that the abstraction pathway is

not observed.[6,8-10] The calculated rate constant[34] for the OAT and hydrogen abstraction pathways are $8.7x10^{-13}$ $cm^3 \cdot s^{-1}$ and $8.9x10^{-15}$ $cm^3 \cdot s^{-1}$, respectively at 298K and 760 torr which gives a branching ratio of 98. The calculated rate constant for the OAT pathway ($8.7x10^{-13}$ $cm^3 \cdot s^{-1}$) is in good agreement with experiment (($(3\pm1)x10^{-13}$ $cm^3 \cdot s^{-1}$).

2.3c IO + DMS: The trans IO-DMS complex (IO-SMe_2-t C_1) is more stable than the cis complex (IO-SMe_2-c C_s) by 1.2 kcal·mol^{-1}. The nonbonded I--H distance in the cis IO-DMS complex (3.356 Å) is larger than the sum of the vdW radii of iodine (2.16 Å)[33a] and hydrogen (1.10 Å)[33b] which may indicate little H-bonding. While the lowest orientation of the IO-DMS complex is trans, the cis OAT transition state (IO-OAT-TS-c) is 3.3 kcal·mol^{-1} lower in energy than the trans OAT (IO-OAT-TS-t C_1). Thus, the reaction path for the OAT reaction is predicted to start with IO in the trans orientation and reach the TS in the cis orientation which would suggest that the departing iodine radical should have significant angular motion.

The enthalpy of the OAT transition state is lower than the enthalpy of the IO-DMS complex (-1.3 compared to –2.6 kcal·mol^{-1}) which is not possible on a continuous PES but does occur when enthalpies are derived from a composite method such as G2B3(MP2). It should be noted that the free energy (298K) of the OAT transition state, IO-OAT-TS-c, is 6.9 kcal·mol^{-1} higher than the free energy of IO + DMS, and the same free energy as the complex, IO-SMe_2-t C_1 (Table 3). Nakano *et al.*[10] have determined that the OAT reaction has a negative activation energy of –4.4 kcal·mol^{-1}.

The abstraction transition state is significantly higher in enthalpy than the OAT transition state (3.3 compared to –2.6 kcal·mol^{-1}). Since the bond enthalpy in the X-O

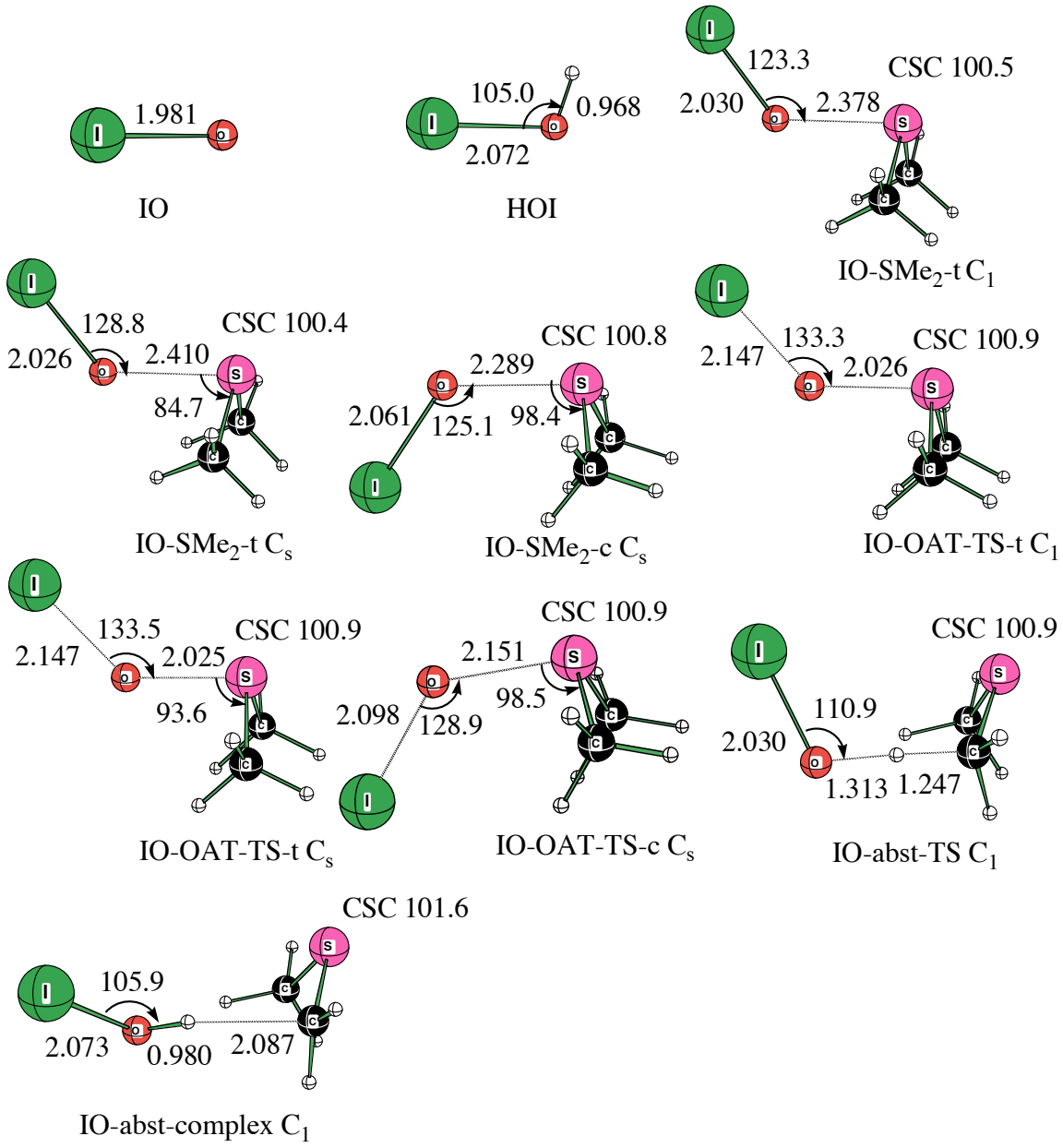

Figure 5. Optimized geometric parameters of stationary points at the B3LYP/6-311+G(d,p)/ECP level. Bond lengths are in Å and angles are in degrees.

bond should decrease in the order Cl-O > Br-O > I-O, it is expected that the OAT activation barrier should decrease in the same order. This expectation is fulfilled for the

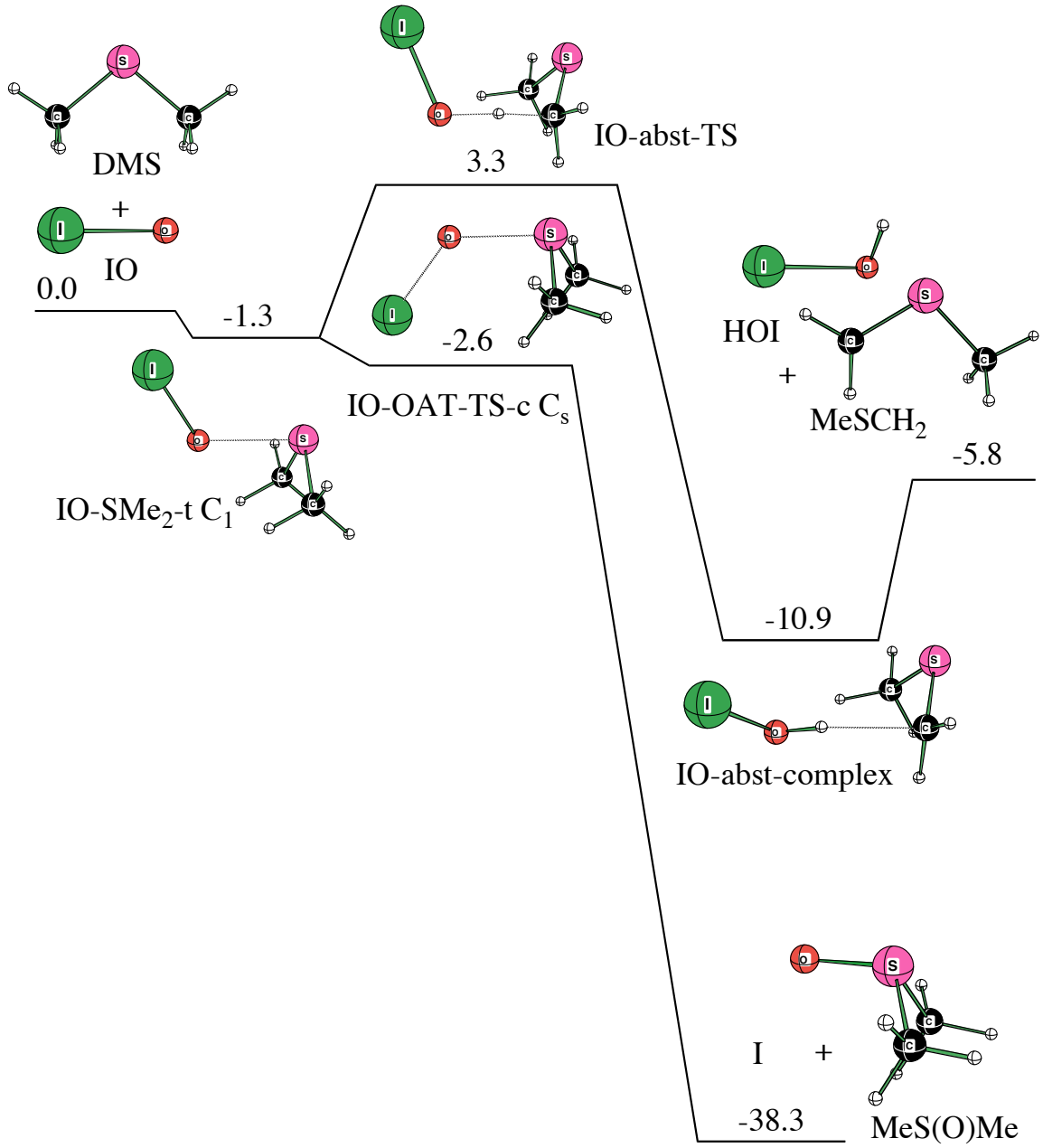

Figure 6. Schematic diagram of the potential energy surface computed at the G2B3(MP2) (298K) level for the reaction of IO with DMS. Relative energies are given in kcal/mol at 298 K.

OAT activation enthalpies (1.3 > -0.4 > -2.6 kcal·mol^{-1} for ClO, BrO, and IO, respectively). On the other hand, the abstraction of hydrogen occurs from the oxygen end of XO and is not expected to change significantly (2.1, 2.0, and 3.3 kcal·mol^{-1} for ClO, BrO, and IO, respectively).

The OAT reaction enthalpy to form I + DMSO is calculated to be –38.3 kcal·mol^{-1} which is significantly more exothermic than the experimental value[17] of –29.0 kcal·mol^{-1}. It should be noted that the SOC of the I atom (which is included in the calculations) contributes 7.25 kcal·mol^{-1} to the exothermicity. The iodine radical is not expected to abstract a hydrogen from DMSO because the calculated bond enthalpy of HI (63.6 kcal·mol^{-1}) is much smaller than the calculated H-C bond enthalpy in DMSO (98.5 kcal·mol^{-1}). The abstraction pathway generates the HOI/$MeSCH_2$ complex which is bound by 5.1 kcal·mol^{-1} with respect to separated products.

Table 4. Calculated Rate Constants (cm^3·s^{-1}) and Branching Ratios of XO + DMS (X=Cl, Br, I) at 298K for Oxygen-Atom Transfer (OAT) and Hydrogen Abstraction Pathways

	OAT (k_1)	Abstraction (k_2)	Branching Ratio (k_1/k_2)
ClO+DMS	3.0×10^{-15}	1.1×10^{-15}	2.7
BrO+DMS	8.7×10^{-13}	8.9×10^{-15}	98
IO+DMS	1.5×10^{-11}	1.0×10^{-15}	15000

The calculated rate constant[34] of the OAT pathway (1.5×10^{-11} cm^3·s^{-1}) is much faster than the abstraction pathway (1.0×10^{-15} cm^3·s^{-1}). While there is considerable disagreement among the experimental determinations of the rate constant (Table 1), the

present calculations support a fast reaction between IO and DMS. A summary of the calculated rate constants is given in Table 4.

2.3d Bonding in XO-DMS Adducts: An estimate of the binding enthalpy of an unsymmetrical 2c-3e complex is given by the average of the symmetrical complexes times $e^{-\Delta IE}$ (eq 7), where ΔIE is the difference (measured in eV) in ionization energies, a factor related to "orbital matching".[35]

$$D_{AB}=((D_{AA}+D_{BB})/2)\cdot e^{-\Delta IE} \quad (7)$$

An adjustment must be made for the ionization energy of XO^- to take into account that a work term for separating charge is "missing" (Table 5). If the PseudoIE of XO^- is used rather than the EA (Table 5), then an estimate of orbital matching can be made. Using the PseudoIE from Table 5, the orbital match for HO-DMS (ΔIE=0.76=8.69-7.93, eV) is much better than the orbital match for ClO-DMS (ΔIE=2.30=8.69-6.39, eV) which leads to a much greater predicted binding enthalpy for HO-DMS (eq 7, 14.8 $kcal\cdot mol^{-1}$)[36] compared to ClO-DMS (eq 7, 2.5 $kcal\cdot mol^{-1}$). The corresponding estimates of the BrO-DMS and IO-DMS binding enthalpies from eq 7 are also small, 2.8 and 3.1 $kcal\cdot mol^{-1}$, respectively. Thus, the ClO, BrO, and IO radicals are qualitatively different from OH in that the orbital match with DMS is poorer which leads to much smaller binding enthalpies. The calculated DFT binding enthalpies for XO-DMS (6.7, 6.1, and 7.8 $kcal\cdot mol^{-1}$ for ClO-DMS, BrO-DMS, and IO-DMS, respectively) are substantially larger

than the G3B3, G3B3(MP2), and G2B3(MP2) values (Table 3) due to known deficiencies in the DFT method for describing theses systems.[37]

The bonding between ClO and DMS in the ClO-DMS complex, as determined by an NBO population analysis at the B3LYP/6-311+G(d,p) level,[38] consists of one σ bond occupied by a single β-spin electron. There are no corresponding α-spin electrons in S-O bonding or antibonding orbitals, rather two unpaired α-spin electrons reside in nonbonding (singly-occupied lone-pair) orbitals (Figure 7). The β-bond is polarized toward sulfur (61.9%, Table 6). Since DMS donates 0.34 electrons to ClO, a most

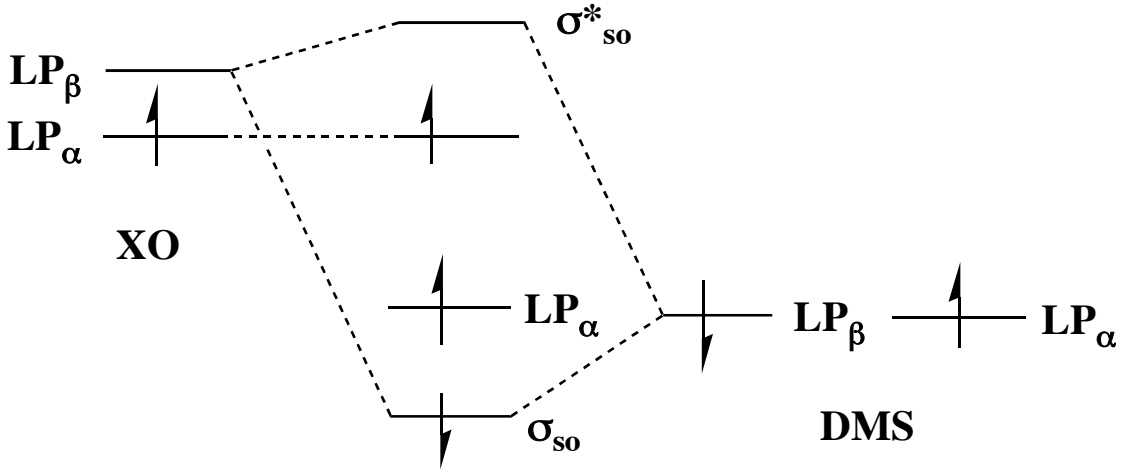

Figure 7. Interaction diagram of the singly occupied molecular orbital (SOMO) of XO (X=Cl, Br, I) interacting with the highest occupied molecular orbital (HOMO) of DMS.

consistent interpretation of the bonding in the ClO-DMS complex is the formation of a β-electron dative bond (Figure 7), i.e. a β-bond (ClO←SMe_2). The interpretation of the XO-DMS bonding for X=Br and I is very similar to ClO-DMS.

Table 5. Experimental Binding Enthalpies (kcal·mol^{-1}) of X$\therefore$X$^-$, Calculated Binding Enthalpies (kcal·mol^{-1}) of XO$\therefore$OX$^-$, and PseudoIE (eV) of X$^-$ and XO$^-$

A	Binding Enthalpy[a] of A$\therefore$A$^-$	exptl. EA (eV) of A	Work term[b] (eV)	PseudoIE (eV) of A$^-$
F	30.2	3.40	6.09	9.49
Cl	31.8	3.62	5.18	8.80
Br	27.9	3.36	4.52	7.88
I	24.3	3.06	4.12	7.18
OH	33.6[c]	1.84	6.09	7.93
OCl	20.6	2.27	4.12	6.39
OBr	21.4	2.35	4.12	6.47
OI	26.5	2.37	4.12	6.49

a) The binding enthalpies of X$\therefore$X$^-$ (X=F, Cl, Br, I) are exptl. values (see: Braïda, B.; Hiberty, P. C. *J. Phys. Chem. A* **2000**, *104*, 4618 and Chermette, H.; Ciofini, I.; Mariotti, F.; Daul, C. *J. Chem. Phys.* **2001**, *115*, 11068). The binding enthalpies (298K) of XO$\therefore$OX$^-$ (X=H, Cl, Br, I) are calculated at the B3LYP/6-311+G(2df,p) level of theory. The IO$\therefore$OI$^-$ calculation used a basis set of similar size on Iodine with an ECP replacing the core electrons. The assumed symmetry of the XO$\therefore$OX$^-$ complex was C_2 for X=H and Cl and C_{2h} for X=Br and I. The optimized O$\therefore$O distances in the XO$\therefore$OX$^-$ complexes were 2.419, 2.294, 3.517, and 3.428 Å for X=H, Cl, Br, and I, respectively. The calculated binding enthalpy (298K) of $(DMS)_2^+$ at the B3LYP/6-31+G(d) level of theory is 29.8 kcal·mol^{-1}. Spin-orbital corrections are not included in the calculation of XO$\therefore$OX$^-$ binding enthalpies.

b) Work necessary to separate unit charges (work=$qQ/4\pi\varepsilon_o R$) where R is assigned a reasonable value (Wine, P. H.; McKee, M. L. to be published). This term is added to the EA of A to give the PseudoIE of the anion (A$^-$). A comparison of the PseudoIE of A$^-$ and the IE of DMS (exptl. 8.69 eV) will give an indication of orbital matching. A better orbital match between A$^-$ and DMS will lead to a stronger 2c-3e interaction.

c) The 2c-3e structure of HO$\therefore$OH$^-$ is known to collapse to lower-energy structures. See: Braïda, B.; Thogersen, L.; Hiberty, P. C. *J. Am. Chem. Soc.* **2002**, *124*, 11781.

Table 6. NPA Charges, Total Atomic Spin Densities, and β-bond Polarization of the σ_{so} bond in the XO-DMS complex (X=Cl, Br, I)[a]

	NPA Charge		Spin Densities		β-bond Polarization	
	XO	DMS	O	S	O	S
ClO-SMe_2-c C_s	-0.34	0.34	0.54	0.37	38.1%	61.9%
BrO-SMe_2-t C_1	-0.36	0.36	0.54	0.38	39.7%	60.3%
IO-SMe_2-t C_1	-0.40	0.40	0.54	0.41	41.9%	58.1%

[a] At the B3LYP/6-311+G(d,p) for X=Cl, and Br and at the B3LYP/6-311+G(d,p)/ECP level for X=I.

2.4 Conclusions

The reaction rates between XO and DMS were computed for the oxygen-atom transfer (OAT) and hydrogen abstraction pathways. The relative reactivity of XO toward DMS is IO > BrO > ClO at 298K and 760 torr with rate constants of $3.0x10^{-15}$ $cm^3 \cdot s^{-1}$, $8.7x10^{-13}$ $cm^3 \cdot s^{-1}$ and $1.5x10^{-11}$ $cm^3 \cdot s^{-1}$ for ClO, BrO and IO, respectively at 298K and 760 torr. The abstraction pathway is less favored with calculated branching ratios of 2.7, 98, and 15000 for ClO, BrO and IO, respectively. The calculated rate constants for ClO and BrO with DMS are in good agreement with experiment, while the calculated rate constant for the IO plus DMS reaction overlaps at the "fast" end of experimental results. The binding enthalpies for ClO-DMS, BrO-DMS and IO-DMS complexes (2.0, 1.7, and 1.3 $kcal \cdot mol^{-1}$, respectively) are much weaker than the HO-DMS complex (13±3 $kcal \cdot mol^{-1}$) due to a poorer orbital match between XO and DMS (compared to OH and DMS).

2.5 References

1. Charlson, R. J.; Lovelock, J. E.; Andreae, M. O.; Warren, S. G. *Nature* **1987**, *326*, 655.
2. Barone, S. B.; Turnipseed, A. A.; Ravishankara, A. R. *J. Chem. Soc. Faraday Trans.* **1995**, *100*, 39.
3. Tyndall, G.; Ravishankara, A. R. *Int. J. Chem. Kinet.* **1991**, *23*, 483.
4. Yin, F.; Grosjean, D.; Seinfeld, J. H. *J. Atmos. Chem.* **1990**, *11*, 309.
5. Barnes, I.; Becker, K. H.; Martin, D.; Carlier, P.; Mouvier, G.; Jourdan, J. L.; Laverdet, G.; Le Bras, G. "Impact of Halogen Oxides on Dimethyl Sulfide Oxidation in the Marine Atmosphere", In *Biogenic Sulfur in the Enviroment*, E. S. Saltzman, E. S, Cooper, W. J., Eds, ACS Symposium Series, **1989**, *393*, 464.
6. Barnes, I.; Bastian, V.; Becker, K. H.; Overath, R. D. *Int. J. Chem. Kinet.* **1991**, *23*, 579.
7. Díaz-de-Mera, Y.; Aranda, A.; Rodríguez, D.; López, R.; Cabañas, B.; Martínez, E. *J. Phys. Chem. A* **2002**, *106*, 8627.
8. Bedjanian, Y.; Poulet, G.; Le Bras, G. *Int. J. Chem. Kinet.* **1996**, *28*, 383.
9. Ingham, T.; Bauer, D.; Sander, R.; Crutzen, P.J.; Crowley, J. N. *J. Phys. Chem. A.* **1999**, *103*, 7199.
10. Nakano, Y.; Goto, M.; Hashimoto, S.; Kawasaki, M.; Wallington, T. J. *J. Phys. Chem. A* **2001**, *105*, 11045.
11. Barnes, I.; Becker, H. K.; Carlier, P.; Mouvier, G. *Int. J. Chem. Kinet.* **1987**, *19*, 489.

12. Martin, D.; Jourdain, J. L.; Laverdet, G.; Le Bras, G. *Int. J. Chem. Kinet.* **1987**, *19*, 503.

13. Daykin, P. E.; Wine, P. H. *J. Geophys. Res.* **1990**, *95*, 18547.

14. Maguin, F.; Mellouki, A.; Laverdet, G.; Poulet, G.; Le Bras, G. *Int. J. Chem. Kinet.* **1991**, *23*, 237.

15. Knight, G. P; Crowley, J. N. *Phys. Chem. Chem. Phys.* **2001**, *3*, 393.

16. Nakano, Y.; Enami, S.; Nakamichi, S.; Aloisio, S.; Hashimoto, S.; Kawasaki, M. *J. Phys. Chem. A* **2003**, *107*, 6381.

17. The webbook (http://webbook.nist.gov/chemistry) was used as the source of all thermochemistry except for the heat of formation of BrO and IO. (a) BrO: Bedjanian, Y.; Le Bras, G.; Poulet, G. *Chem. Phys. Lett.* **1997**, *266*, 233. (b) IO: Bedjanian, Y.; Le Bras, G.; Poulet, G. *J. Phys. Chem.* **1996**, *100*, 15130.

18. Gaussian 98 (Revison A11), Frisch, M. J.; Trucks, G. W.; Schlegel, H. B.; Scuseria, G. E.; Robb, M. A.; Cheeseman, J. R.; Zakrzewski, V. G.; Montgomery, J. A., Jr.; Stratmann, R. E.; Burant, J. C.; Dapprich, S.; Millam, J. M.; Daniels, A. D.; Kudin, K. N.; Strain, M. C.; Farkas, O.; Tomasi, J.; Barone, V.; Cossi, M.; Cammi, R.; Mennucci, B.; Pomelli, C.; Adamo, C.; Clifford, S.; Ochterski, J.; Peterson, G. A.; Ayala, P. Y.; Cui, Q.; Morukuma, K.; Salvador, P.; Dannenberg, J. J.; Mallick, D. K.; Rabuck, A. D.; Raghavachari, K.; Foresman, J. B.; Cioslowski, J.; Ortiz, J. V.; Baboul, A. G.; Stefanov, B. B.; Liu, G.; Liashenko, A.; Piskorz, P.; Komaromi, I.; Gomperts, R.; Martin, R. L.; Fox, D. J.; Keith, T.; Al-Laham, M. A.; Peng, C. Y.; Nanayakkara, A.; Challacombe, M.; Gill, P. M.

W.; Johnson, B.; Chen, W.; Wong, M. W.; Andres, J. L.; Gonzalez, C.; Head-Gordon, M.; Replogle, E. S.; Pople, J. A. Gaussian, Inc., Pittsburgh PA, 2001.

19. MOLDEN, Schaftenaar, G.; Noordik, J. H. *J. Comput.-Aided Mol. Design* **2000**, *14*, 123.

20. Curtiss, L. A.; Raghavachari, K.; Redfern, P. C; Rassolov, V.; Pople, J. A. *J. Chem. Phys.* **1998**, *109*, 7764.

21. Curtiss, L. A.; Raghavachari, K.; Pople, J. A. *J. Chem Phys.* **1993**, *98*, 1293.

22. Glukhovtsev, M. N.; Pross, A.; McGrath, M. P.; Radom, L. *J. Chem. Phys.* **1995**, *103*, 1878. Erratum: **1996**, *104*, 3407.

23. Curtiss, L. A.; Redfern, P. C.; Raghavachari, K.; Rassolov, V.; Pople, J. A. *J. Chem. Phys.* **1999**, *110*, 4703.

24. Curtiss, L. A.; Redfern, P. C.; Rassolov, V.; Kedziora, G.; Pople, J. A. *J. Chem. Phys.* **2001**, *114*, 9287.

25. (a) Schwerdtfeger, P.; Dolg, M.; Schwarz, W. H.; Bowmaker, G. A.; Boyd, P. D. W. *J. Chem. Phys.* **1989**, *91*, 1762. (b) Bergner, A.; Dolg, M.; Küchle, W.; Stoll, H.; Preuss, H. *Mol. Phys.* **1993**, *80*, 1431.

26. Furlani, T. R.; King, H. F. *J. Chem. Phys.* **1985**, *82*, 5577. King, H. F.; Furlani, T. R. *J. Comput. Chem.* **1988**, *9*, 771. Fedorov, D. G.; Gordon M. S. *J. Chem. Phys.* **2000**, *112*, 5611.

27. Stevens, J. E.; Cui, Q.; Morokuma, K. *J. Chem. Phys.* **1998**, *108*, 1554.

28. Mokrushin, V.; Tsang, W. *CHEMRATE. A Calculational Data Base for Unimolecular Reactions*; National Institute of Standards and Technology: Gaithersburg, MD, 2000.

29. (a) NBO Version 3.1, Glendening, E. D.; Reed, A. E.; Caroenter, J. E.; Weinhold, F. (b) Ree d, A. E.; Curtiss L. A.; Weinhold, F. *Chem. Rev.* **1988**, *88*, 899.

30. Vandresen, S.; Resende, S. M. *J. Phys. Chem. A* **2004**, *108*, 2248.

31. Stickel, R. E.: Nicovich, J. M.; Wang, S.; Zhao, Z.; Wine, P. H. *J. Phys. Chem.* **1992**, 96, 9875.

32. Butkovskaya, N. I.; Poulet, G.; Le Bras, G. *J. Phys. Chem.* **1995**, 99, 4536.

33. (a) Batsanov, S. S. *J. Chem. Soc. Dalton Trans.* **1998**, 1541. (b) Mandal, P. K.; Arunan, E. *J. Chem. Phys.* **2001,** *114*, 3880.

34. Due to a limitation of the CHEMRATE program, we could not use a negative activation barrier. Therefore, we assumed an activation barrier as zero and multiplied the rate by $e^{-\Delta H/RT}$ where ΔH is the activation enthalpy (i.e ΔH_a=-0.4 or ΔH_a=-2.6 kcal·mol^{-1} for the OAT reaction of BrO and IO with DMS, respectively).

35. Clark, T. *J. Am. Chem. Soc.* **1988**, *110*, 1672.

36. The experimental binding enthalpy is 13.0 kcal·mol^{-1}: (a) Hynes, A. J.; Stoker, R. B.; Pounds, A. J.; McKay, T.; Bradshaw, J. D.; Nicovich, J. M.; Wine, P. H. *J. Phys. Chem.* **1995**, *99*, 16967. The calculated binding entrhalpy is 9-10 kcal·mol^{-1}: (b) Tureček, F. *Collect. Czech. Chem. Commun.* **2000**, *65*, 455. (c) Wang, L.; Zhang, J. *THEOCHEM* **2001**, *543*, 167. (d) McKee, M. L. *J. Phys. Chem. A* **2003**, *107*, 6819.

37. For a summary of deficiencies of the DFT methods for describing 2c-3e systems see: (a) Gräfenstein, J.; Kraka, E.; Cremer, D. *Phys. Chem. Chem. Phys.* **2004**, *6*, 1096. (b) Fourré, I.; Bergès, J. *J. Phys. Chem. A* **2004**, *108*, 898.

38. A NBO analysis at the MP2/6-311G(d,p) level (with the MP2 density matrix, i.e. DENSITY=CURRENT) gives a very similar description of the bonding for the ClO-DMS complex.

CHAPTER 3

THEORETICAL STUDY OF THE MECHANISM OF NO_2 PRODUCTION FROM NO + ClO

3.1 Introduction

The concentrations and chemistry of the ClO_x and NO_x radicals are important for understanding the global atmospheric chemistry.[1] The ClO_x and NO_x radicals are involved in tropospheric ozone production and stratospheric ozone loss.[2,3] Generally, chlorine (Cl) is oxidized by ozone in the stratosphere and forms ClO which can be removed by other reactions. Nitrogen oxides (NO_x) act as sinks for ClO, which are transformed into temporary reservoir species, such as $ClONO_2$ and HCl. These reservoir species do not react with ozone and are slowly removed from the stratosphere.

Although there have been many studies on atmospheric chlorine chemistry, there are still discrepancies concerning the atmospheric chlorine budget.[4,5] Specifically, there is a missing reservoir of inorganic chlorine in the stratosphere which may not be accounted for by $ClONO_2$ and HCl alone. For example, it is possible that nitryl chloride ($ClNO_2$) could also be an important chlorine reservoir.[6] Photolysis of $ClNO_2$ is predicted to be rapid in sunlight and may be the dominant loss mechanism, yielding primarily atomic chlorine.

The recombination of ClO and NO radicals is known to produce NO_2 and Cl radicals[8-13] (eq 1-4) through possible involvement of ONOCl and/or $ClNO_2$ as intermediates.

$$ClO + NO \rightarrow ONOCl \quad (1)$$

$$ONOCl \rightarrow Cl + NO_2 \quad (2)$$

$$ONOCl \rightarrow ClNO_2 \quad (3)$$

$$ClNO_2 \rightarrow Cl + NO_2 \quad (4)$$

Experimental studies on the NO and ClO reaction between 200 and 400K,[9,10,13] have shown the reaction to have a negative activation barrier. While the pressure dependence of the reaction has not been reported, the concentration of the bath gas in the Leu *et al.* study[10] was much higher than the concentration of the reactants which may suggest that their results may be near the high-pressure limit. Several studies[8,11,12] report rate constants at only one temperature (298K), and these results are in agreement with the temperature-dependence experimental results.[9,10,13]

The ONOX (X=OH, F, Cl) potential energy surfaces are expected to share some similarity.[14-18] When X=OH, the concerted formation of HNO_3 from HOONO is still very much in doubt.[14,17,18] Zhao *et al.*[14] showed that there is no direct isomerization between HOONO and $HONO_2$. They explained the mechanism of O-O cleavage from *cis*-HOONO to the formation of NO_2 + OH and calculated a 18-19 kcal/mol activation barrier for this process. On the other hand when X=F, Ellison *et al.*[15] showed that ONOF forms FNO_2 on a continuously connected PES through a very loose transition state with an activation barrier of 22±3 kcal/mol. Zhu and Lin[16] recently calculated an

isomerization path between *cis*-ONOCl and $ClNO_2$ with an activation barrier of 21.2 kcal/mol (through NO_2 + Cl).

In the following study, we will use electronic-structure methods to calculate the potential energy surface for the formation of NO_2 + Cl from NO + ClO. We will calculate the rate constant for disappearance of reactants (k_{dis}) as well as the rate constant for formation of products (k_{obs}) over the temperature range 200-1000K. At the temperatures and pressures used in the experimental studies, it is not known whether the dependence of the rate constant on temperature is in the fall-off or pressure-independent regime. Since the concentration of bath gas is much larger than the concentration of reactants, the reaction may be close to pressure independent. All the calculated rate constants reported below are at the high-pressure limit.

3.2 Computational Method

Since B3LYP density functional theory (DFT) has been shown to give reasonable structures and vibrational frequencies for halogen compounds,[19-22] we decided to use that method to calculate the PES. However, to check the DFT results, we also decided to use a more accurate method to determine the minima, transition states, and thermodynamic properties.

Since the CCSD(T) method (with a reasonable basis set) yields very good results for difficult chemical systems such as O_3 and FOOF,[23,24] we used it (with finite-difference derivatives) to optimize all of the stationary points on the PES.

All electronic structure calculations have used the Gaussian03[25] and Molcas6[26] program systems. Optimization and frequency calculations for the NO + ClO potential

energy surface were carried out at the B3LYP/6-311+G(d) and CCSD(T) levels. All imaginary frequencies for transition states were animated by using the graphical program MolDen[27] to make sure that the motion was appropriate for converting reactants to products.

In transition states involving bond formation or bond breaking, a lower-energy spin broken symmetry solution was obtained at the UDFT or UHF levels. For DFT calculations, we used the spin-broken symmetry results. However, for the CCSD(T) calculations, it was not clear whether the spin-restricted (RCCSD(T)) or spin-unrestricted (UCCSD(T)) method would produce more reliable results. In the work by Ellison *et al.*[15] on the ONOF $\rightarrow$ FNO_2 transition state a variety of post-SCF methods were used. At the RCCSD(T)/DZP and RCCSD(T)/pVTZ levels, the activation energies were 3 and 4 kcal/mol lower than at the UCCSD(T)/DZP and UCCSD(T)/pVTZ levels, respectively and in better agreement with their best computational results. Thus, while the UHF reference state is lower in energy than the RHF for these transition states, it appears that the RHF reference may be a better choice as the reference function for the post-SCF perturbative expansion.

Our RCCSD(T) and UCCSD(T) results for the NO + ClO reactions exhibit the same behavior, but more extreme. With respect to separated NO + ClO radicals computed at the UCCSD(T) level, the activation barriers for cis and trans addition were 5.36 and 7.49 kcal/mol, respectively. This result is in contrast to the B3LYP/6-311+G(d) results, where no transition state could be located, as well as CASPT2 results on fixed ON-OCl geometries, where the energy decreased monotonically as the N-O distance decreased. The RCCSD(T) method located transition states for cis and trans addition

which were 4.31 and 3.49 kcal/mol *below* NO + ClO. Thus, the RCCSD(T) potential energy surface has a maximum for the formation of the N-O bond, but the stability of the entire surface at these large N-O distances is overestimated since it is below the energy of the reactants (NO + ClO).

Table 1. Relative Energies[a] (kcal/mol) at the B3LYP/6-311+G(d), G3B3, CCSD(T)/cc-pVTZ//CCSD(T)/cc-pVDZ Levels for Various Species Involved in the NO + ClO Reaction

	ΔH(0K)			ΔH(298K)			ΔG(298K)		
	B3LYP	G3B3	CCSD(T)/ cc-pVTZ	B3LYP	G3B3	CCSD(T)/ cc-pVTZ[b]	B3LYP	G3B3	CCSD(T)/ cc-PVTZ
NO+ClO	0.00	0.00	0.00	0.00	0.00	0.00	0.00	0.00	0.00
t-ONOCl	-27.08	-31.10	-27.37	-27.94	-31.94	-28.21(-28.3)	-18.03	-22.02	-18.28
c-ONOCl	-31.07	-32.78	-30.34	-32.06	-33.75	-31.34(-31.3)	-21.99	-23.68	-21.15
ONOCl-ts	-16.71	-21.99	-18.31	-17.85	-23.12	-19.46(-19.3)	-7.61	-12.88	-9.12
ON-OCl-ts-c			-3.86			-4.31			3.94
ON-OCl-ts-t			-3.17			-3.49			3.76
ON-OCl-ts-c[c]			5.94			5.36			14.00
ON-OCl-ts-t[c]			8.10			7.49			16.43
NO_2Cl-ts	-18.84	-21.66	-17.20	-20.16	-22.96	-18.45(-18.0)	-9.66	-12.46	-7.64
Abst-Cl-ts-t	-3.88	10.71	4.54	-4.88	9.71	3.62	5.23	19.82	13.56
Abst-Cl-ts-c			-10.75			-11.59			-2.93
Cl-add-NO_2-ts	-16.29	-12.17	-10.17	-16.92	-12.77	-11.01	-11.46	-2.53	-1.85
Cl-add-NO_2-ts[c]			-13.62			-15.77			-6.60
NO_2 + Cl	-15.49	-10.12	-10.14	-15.79	-10.40	-10.42(-10.1)	-13.79	-8.41	-8.86
$ClNO_2$	-46.01	-44.85	-41.04	-47.34	-46.13	-42.30(-42.2)	-36.34	-35.13	-31.32

[a] The Spin-Orbit Correction (SOC) of NO (Ref. 31), ClO (Ref. 32), and Cl (Ref. 33) are included in G3B3 and CCSD(T)/cc-pVTZ level.

[b] The values in parentheses are taken from Ref. 16.

[c] Geometries are optimized at the UCCSD(T)/cc-pVDZ level.

The CCSD(T) optimizations and frequency calculations were carried out with the correlation-consistent cc-pVDZ basis of Dunning[28] with single-point calculations using

the cc-pVTZ basis set[29] (i.e. CCSD(T)/cc-pVTZ//CCSD(T)/cc-pVDZ). The G3B3 method[30] was used with manual assembly of the components where we used B3LYP/6-311+G(d) optimized geometries and unscaled vibrational frequencies with all other calculations and corrections at standard levels. For transition states which were lower in energy using the UDFT spin broken-symmetry approach, the corresponding G3B3 calculations (including the post-SCF steps) were based on the spin-broken symmetry UHF wave function. The first-order spin-orbit corrections are included for NO,[31] ClO,[32] and Cl[33] (0.11, 0.30, and 0.78 kcal/mol, respectively) in all of the relative energy comparisons in Table 1.[34]

The reaction coordinate for cis and trans approach of NO and ClO was constructed by optimizing the structure with spin broken-symmetry UDFT while fixing the N…O distance between the two radicals. In this way a set of structures, where the N…O distance was fixed to 4.00, 3.75, 3.50, 3.25, and 3.00 Å, was obtained. Harmonic vibrational frequencies were computed for each structure along the cis and trans reaction coordinate. At each structure, one imaginary frequency was obtained corresponding to the N…O stretch. The only exception was at a 4.00 Å separation along the trans reaction coordinate which was not used in the subsequent rate calculations.

The large difference between the UCCSD(T) and RCCSD(T) energies for the transition states of the NO+ClO addition reactions indicates that electron correlation methods based on a single reference are not appropriate for this part of the potential energy surface. For that reason, single-point calculations were made with a 12-electron 12-orbital complete active space[35] (CAS(12,12)) and the ANO-L basis set[36] with dynamic electron correlation introduced at the MP2 level (CASPT2).[37] At each structure, four

singlet electronic states were computed, two ^{1}A' states and two ^{1}A" states. Both radicals, NO and ClO, have $^2\Pi$ ground states. As the two radicals approach, the electronic and spatial degeneracy will be lifted to give rise to a total of sixteen microstates, four singlet states and four triplet states. The "reactive" state will correspond to ^{1}A' where the unpaired electron on each radical approaches in the reaction plane. The other electronic states will be occupied according to the Boltzmann distribution. We computed the electronic partition function to determine the fraction of reactive encounters which are in the "reactive" electronic state. At a short N…O separation where the "reactive" electronic state is already stabilized, the fraction is 0.98 at 200K and 0.54 at 1000K (3.00 Å, cis addition). At 4.00 Å the fraction is 0.36 at 200K and 0.27 at 1000K (cis addition). Since we are only considering the four close-lying singlet states, complete degeneracy would result in a 0.25 factor for each state.

Rate constants for the NO + ClO → NO_2 + Cl reaction were calculated with Polyrate-9.3[38] and VariFlex-1.0.[39] Rate constants were computed at each N-O separation (4.00, 3.75, 3.50, 3.25, and 3.00 Å) as a function of temperature (Table S4). For the cis approach, the smallest rate constant was found at 4.0 Å at each temperature. Technical difficulties prevented us from calculating rate constants at longer N-O separations. For the trans approach, the smallest rate constant was obtained at a N-O separation of 3.50 Å.

Since the formation of NO + ClO occurs without a barrier on the potential energy surface, we used VariFlex, a program designed for this task, to calculate the rate constants for cis and trans addition. VariFlex is a variational RRKM code that solves the master equation involving multistep vibrational energy transfer for the excited intermediate ONOCl. The enthalpy barrier for trans → cis isomerization of ONOCl is

8.75 kcal/mol (11.88 kcal/mol reverse barrier). We calculated rate constants with ChemRate[40] with harmonic frequencies at B3LYP/6-311+G(d) and energies at CCSD(T)/cc-pVTZ//CCSD(T)/cc-pVDZ. For calculations using Polyrate, we used B3LYP/6-311+G(d) for the IRC and harmonic frequencies and G3B3//B3LYP/6-311+G(d) for energies.

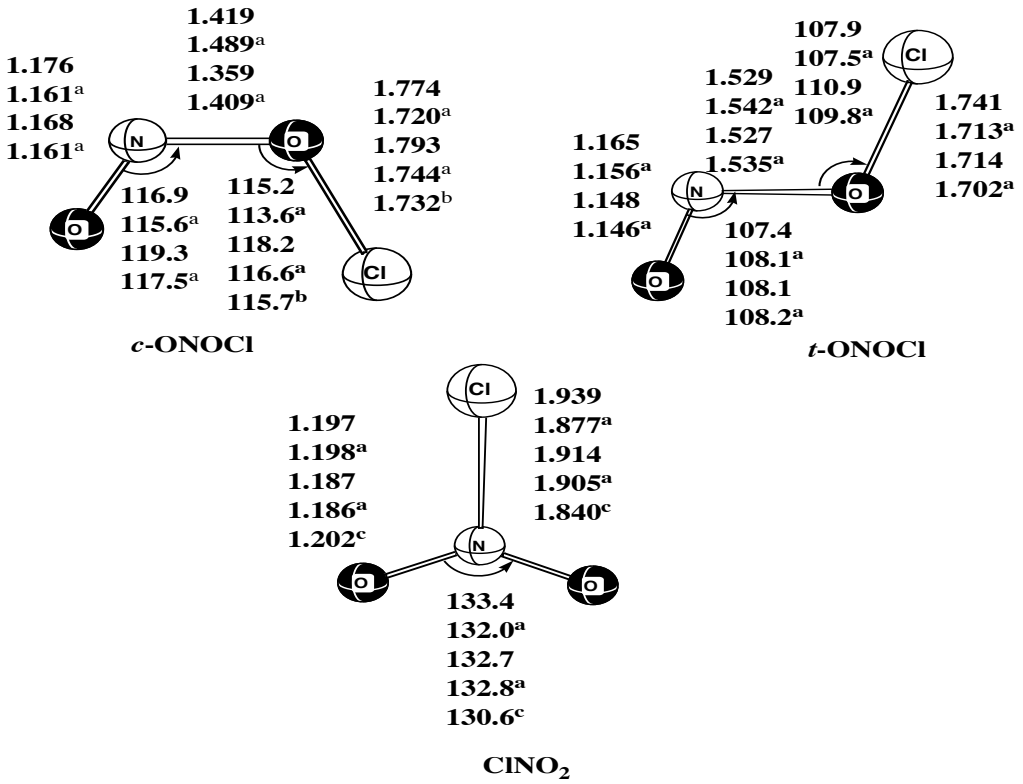

Figure 1. Optimized geometry of *cis*-, *trans*-ONOCl and $ClNO_2$ isomers. Bond lengths are in Å and angles are in degrees. Data in the first row and third row are calculated at the CCSD(T)/cc-pVDZ and B3LYP/6-311+G(d) level, respectively. (a) Calculated values at the CCSD(T)/TZ2P and B3LYP/TZ2P level, respectively are taken from Ref. 19. (b) and (c) are experimental values, are taken from Ref. 42 and Ref. 52, respectively.

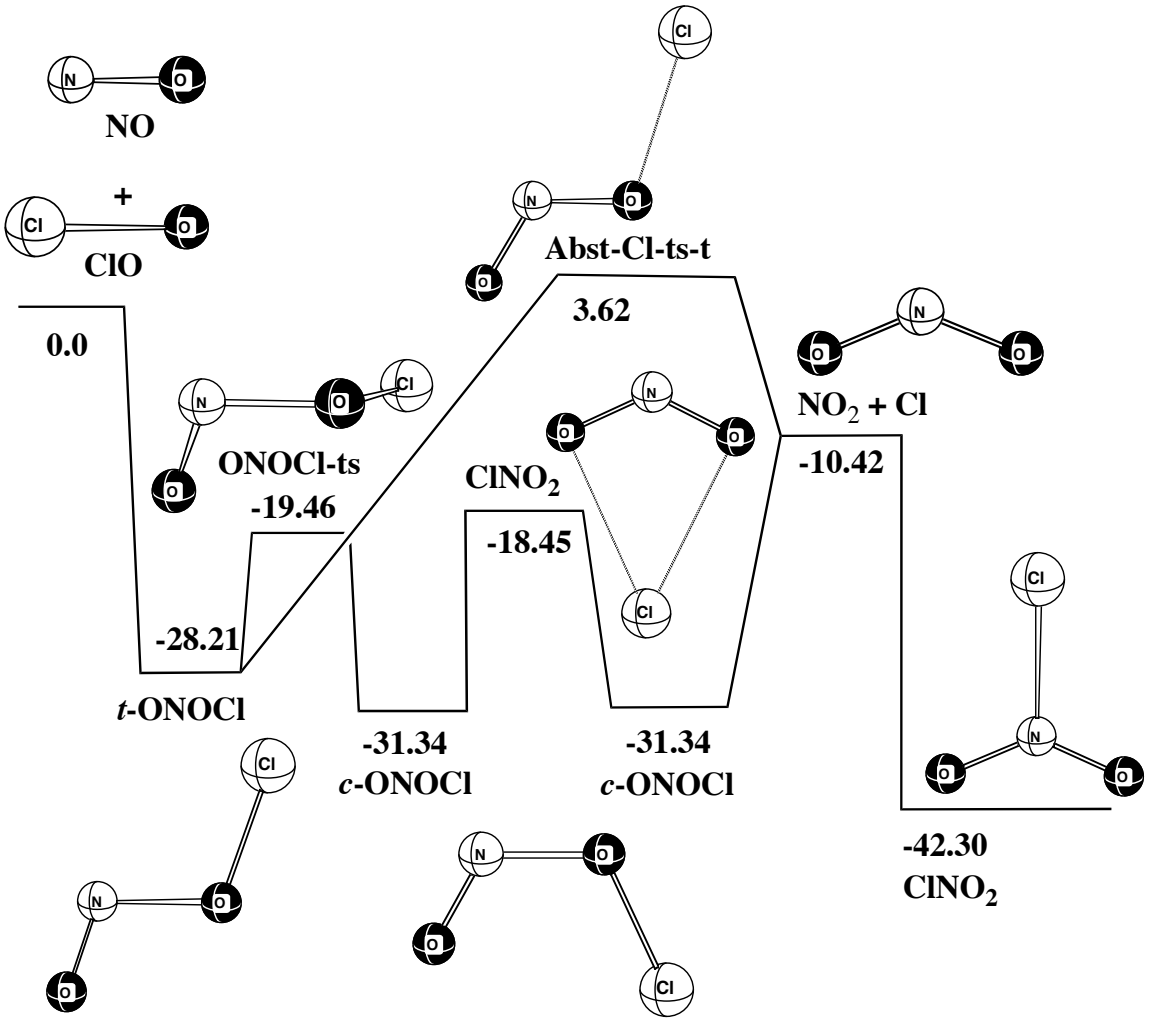

Figure 3. Schematic diagram of the potential energy surface for the NO + ClO system computed at the CCSD(T)/cc-pVTZ//CCSD(T)/cc-pVDZ level. Relative energies are given in kcal/mol at 298K.

3.3 Results and Discussion

It is widely accepted that the reaction NO + ClO → NO_2 + Cl involves the ONOCl intermediate which has two distinct conformers *cis*- and *trans*-ONOCl as well as the $ClNO_2$ isomer for which there exists reliable experimental data. However, there is little reliable experimental data available for the other ONOCl compounds. Since there is

no evidence for OClNO,[41] we did not include this isomer in our study. The equilibrium structure for *cis*-ONOCl (Figure 1) is consistent with the earlier studies and experimental results.[19,42]

Figure 1 shows that the Cl-N bond distance of $ClNO_2$ has the largest sensitivity with respect to the method with CCSD(T)/cc-pVDZ giving the longest Cl-N bond distance and CCSD(T)/TZ2P the shortest. Experimentally,[43] the enthalpy of reaction of eq 3 is -42.87 kcal/mol which is almost same as the CCSD(T)/cc-pVTZ//CCSD(T)/cc-pVDZ result of -42.30 kcal/mol. The experimental[43] enthalpy difference between *cis*-ONOCl and reactants (NO + ClO) is 32.17 kcal/mol which is excellent agreement with CCSD(T)/cc-pVTZ//CCSD(T)/cc-pVDZ (31.34 kcal/mol Figure 2) .

A comparison of calculated and measured frequencies of the *cis*- and *trans*-ONOCl and $ClNO_2$ is presented in Table 2. The calculated frequencies are in agreement with each other for *cis*-ONOCl with slightly less agreement for the torsion (ω_6(a")). For $ClNO_2$, the calculated frequencies agreed with each other and are close to the experimental results.

The NO + ClO system studied here is similar to the reaction of XO (X=H, F, Cl) and alkylperoxy radicals (ROO) with NO.[14,44] A negative activation energy is observed for the NO + ClO reaction, which strongly implies the involvement of an ONOCl intermediate. The observed negative activation enthalpy is consistent with the negative activation barriers calculated for the trans and cis transition states (ON-OCl-ts-t and ON-OCl-ts-c, respectively) at the RCCSD(T)/cc-pVTZ//RCCSD(T)/cc-pVDZ level (Table 1, -3.49 and –4.31 kcal/mol, respectively).

Table 2. Harmonic frequencies of *trans*-ONOCl, *cis*-ONOCl and $ClNO_2$ in cm^{-1}

Method						
t-ONOCl	$\omega_1(a')$	$\omega_2(a')$	$\omega_3(a')$	$\omega_4(a')$	$\omega_5(a')$	$\omega_6(a'')$
B3LYP/TZ2P[a]	1834	879	660	404	259	178
B3LYP/6-311+G(d)	1854	874	645	403	255	182
CCSD(T)/TZ2P[a]	1754	855	607	407	212	170
CCSD(T)/cc-pVDZ	1800	852	646	403	263	173
c-ONOCl	$\omega_1(a')$	$\omega_2(a')$	$\omega_3(a')$	$\omega_4(a')$	$\omega_5(a')$	$\omega_6(a'')$
B3LYP/TZ2P[a]	1741	868	647	365	229	398
B3LYP/6-311+G(d)	1732	868	673	363	212	426
CCSD(T)/TZ2P[a]	1715	850	638	416	249	341
CCSD(T)/cc-pVDZ	1731	859	618	430	245	378
Expt[b]	1715	858	644	406	260-280	344
$ClNO_2$	$\omega_1(a_1)$	$\omega_2(a_1)$	$\omega_3(a_1)$	$\omega_4(b_1)$	$\omega_5(b_2)$	$\omega_6(b_2)$
B3LYP/TZ2P[a]	1339	810	370	673	1748	409
B3LYP/6-311+G(d)	1350	809	364	668	1774	411
CCSD(T)/TZ2P[a]	1290	805	371	658	1688	409
CCSD(T)/cc-pVDZ	1342	798	345	640	1801	390
Expt[c]	1286	793	370	652	1685	408

[a] Ref. 19.

[b] Janowski, B.; Knauth, H. D.; Martin, H. *Ber. Bunsunges. Phys. Chem.* **1977**, *81*, 1262.

[c] Shimanouchi, T. *J. Phys. Chem. Ref. Data* **1977**, *6*, 993.

Computational studies to find a low activation barrier for the ROONO and HOONO unimolecular isomerization have failed.[14,18,44] In the study by Zhao *et al.*,[14] the transition state for *cis*-HOONO to NO_2 + OH was located 3 kcal/mol above NO_2 + OH radicals at the UCCSD(T)/6-31+G(d)//UCCSD/6-31+G(d) level. In our system, the transition state for *cis*-ONOCl to NO_2 + Cl is found at the RCCSD(T)/cc-pVDZ level. The stationary point has one imaginary frequency and is 1.17 kcal/mol lower than NO_2 + Cl at the RCCSD(T)/cc-pVTZ//RCCSD(T)/cc-pVDZ level. The *trans*-ONOCl → $ClNO_2$

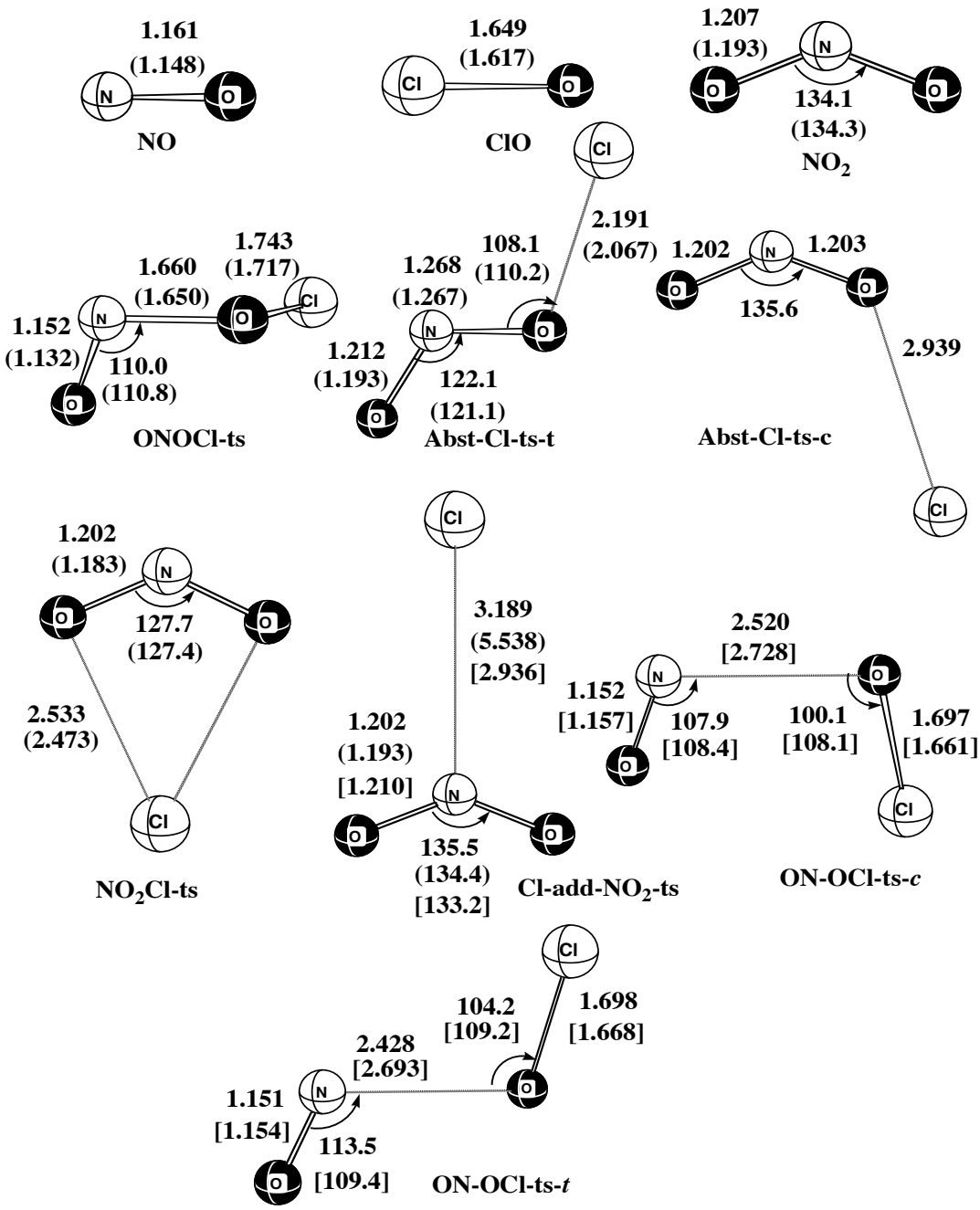

Figure 2. Optimized geometric parameters of stationary points at the CCSD(T)/cc-pVDZ level with B3LYP/6-311+G(d) values in parentheses. Bond lengths are in Å and angles are in degrees. The geometric parameters for ON-OCl-ts-c and ON-OCl-ts-t are at the RCCSD(T)/cc-pVDZ level with values at the UCCSD(T)/cc-pVDZ level given in brackets.

reaction has a much higher activation barrier than the cis isomer. The N…Cl distance in the transition state (Figure 3, abst-Cl-ts-t) is much shorter (2.191 Å) than the N…Cl distance in abst-Cl-ts-c (2.939 Å). In addition, the two N-O distances are much more asymmetric in abst-Cl-ts-t compared to abst-Cl-ts-c.

Basically, the abst-Cl-ts-c and abst-Cl-ts-t transition states are indistinguishable from fragmentation into NO_2 + Cl radicals. In their study of the c-HOONO → $HONO_2$ reaction, Dixon *et al.*[18] located a transition state with an activation energy of 21.4 kcal/mol using MP2/cc-pVTZ where the transition state was 1.6 kcal/mol higher than NO_2 + OH. Zhao *et al.*[14] located a similar transition state at the CBS-QB3 (Complete Basis Set) level 21.0 higher than c-HOONO and 2.7 kcal/mol higher than a NO_2/OH complex, but they were unable to say whether the transition state corresponded to fragmentation or isomerization. The N…O distance in the two studies were quite long (2.784 and 3.070 Å at MP2/cc-pVTZ and CBS-QB3, respectively). In contrast to the c-HOONO → $HONO_2$ reaction,

the t-ONOF → FNO_2 and t-ONOCl → $ClNO_2$ reactions have much tighter transition states. Ellison *el al.*[15] calculated a short breaking O…F distance in the t-ONOF → FNO_2 transition state (1.726 and 1.693 Å at RCCSD(T)/pVTZ and UCCSD(T)/pVTZ, respectively) while we calculate a 2.191 Å N…Cl distance at RCCSD(T)/cc-pVDZ.

The energy difference between abst-Cl-ts-t and abst-Cl-ts-c is 15.21 kcal/mol at the RCCSD(T)/cc-pVTZ//RCCSD(T)/cc-pVDZ level. The reason for the large activation energy difference can be explained with a similar explanation as given in the study of O-O cleavage in ONOONO[45] and the mechanism of peroxynitrous acid and methyl

peroxynitrite (ROONO).[14] The singly-occupied a_1 and doubly occupied b_2 orbitals of NO_2 fragment can mix through the lowering of symmetry from C_{2v} to C_S caused by the

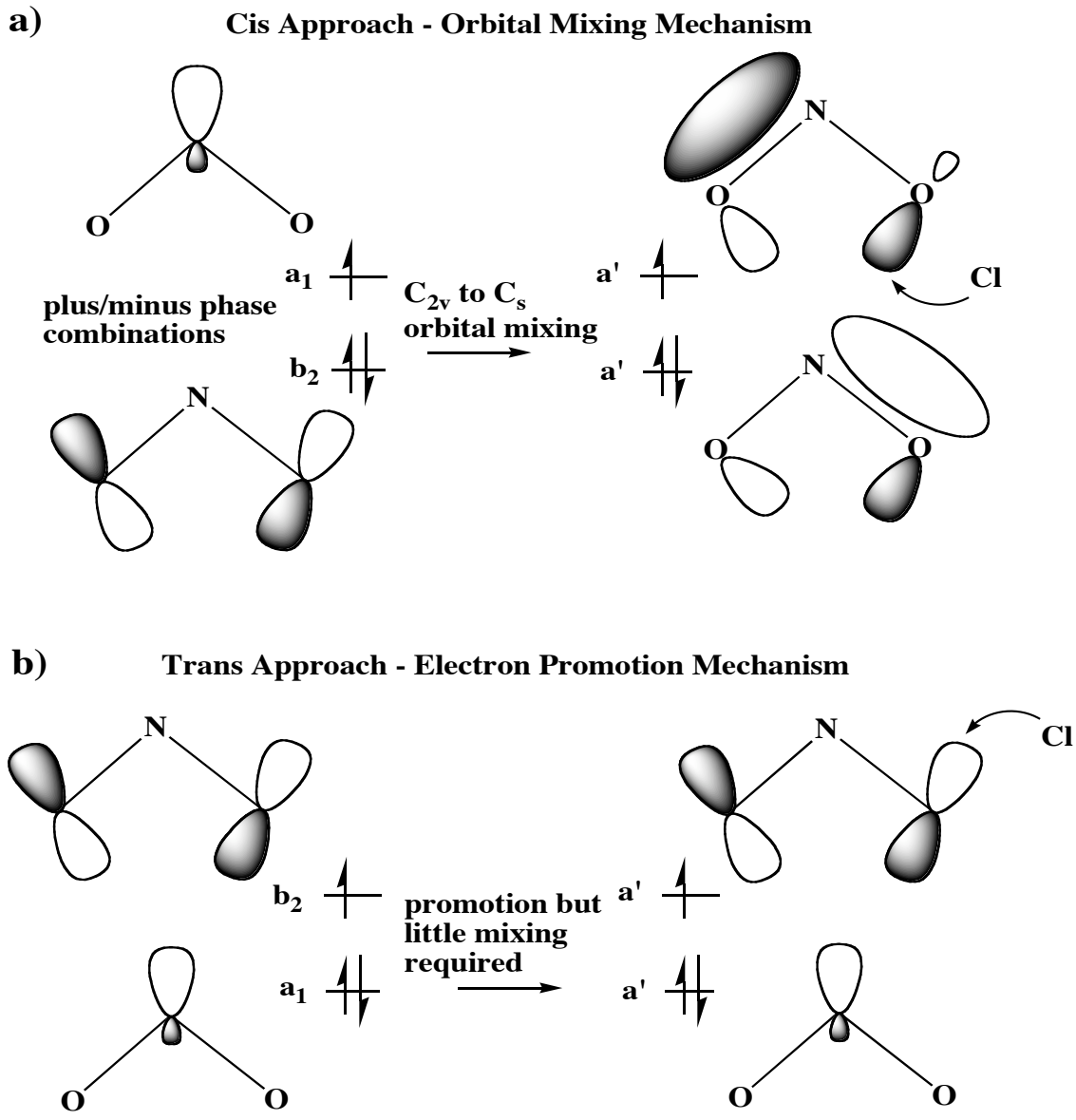

Figure 4. Illustration of cis and trans chlorine addition to NO_2 to form (a) *cis*-ONOCl and (b) *trans*-ONOCl. Cis addition can be rationalized by an orbital mixing mechanism. Trans addition has a higher activation barrier and involves an electron promotion mechanism.

approaching Cl radical (Figure 4a). The mixing causes unpaired spin density to reside on the oxygen atoms. The oxygen atom that will form a bond with chlorine has the larger lobe pointing toward the interior angle of the NO_2 fragment. A better overlap between this lobe and the chlorine atom results when the chlorine atom approaches from the cis side compared to the trans side.

The mechanism for N…Cl bond formation in $NO_2 + Cl \rightarrow$ *trans*-ONOCl (Figure 4b) can be viewed as initial electronic promotion followed by bond formation. The electronic reorganization involves the promotion of a β-spin electron from a b_2 orbital to an a_1 orbital which leaves an unpaired electron on oxygen in an orbital with significant extent away from the interior angle and suitable for bond formation with a chlorine atom approaching from that direction. Thus, bond formation from the "cis side" of NO_2 requires orbital mixing while bond formation from the "trans side" of NO_2 requires electronic promotion. The need for electronic promotion is source of the greater energy of abst-Cl-ts-t compared to abst-Cl-ts-c. An alternative explanation in term of correlating the reaction path with the $^2A_1$ or $^2B_2$ electronic state of NO_2 is also possible.[14,45]

3.4 Rate calculations

Radical-radical recombinations have long presented experimental and theoretical difficulties.[46,47,48] The very fast rates require specialized experimental techniques while reactions with no activation barriers are difficult to model theoretically. The phase-space-integral based VTST (PSI-VTST) method, as implemented in VariFlex, was used to evaluate the reactive flux as the N-O distances increased from 1.6 to 4.0 Å with a step size 0.1 Å for *cis*-ONOCl and *trans*-ONOCl intermediates. In order to evaluate the

reactive flux accurately, the transition from free rotation to hindered rotation must be treated correctly.

We also used variational transition state theory, as implemented in Polyrate, to calculate the rate constant for disappearance (k_{dis}) of reactants (NO + ClO). The reactive flux is calculated at a set of structures optimized at the UB3LYP/6-311+G(d) level with fixed central N-O distances of 3.0, 3.25, 3.50, 3.75, and 4.00 Å. The minimum reactive flux was found at 3.50 Å for *trans*-ONOCl. For *cis*-ONOCl the smallest flux was at 4.00 Å which we used as the minimum value because we could not compute the rate constant at larger N…O separations.

We also considered the electronic partition function which was explained in detail in study of the O(^{3}P) + OH reaction by Graff and Wagner.[49] The factor was calculated from eq 5 where p(T) is the

$$p(\mathrm{T})k_0(\mathrm{T}) = \frac{1}{\sum_j e^{\frac{-\varepsilon_j}{\mathrm{kT}}}} k_0(\mathrm{T}) \qquad (5)$$

probability that the collision involves the "reactive" electronic state and k_0(T) and ε_j are the rate constant and the electronic energy (relative to lowest energy) summed over j states. Four singlet states were calculated (j=4, two ^{1}A' and two ^{1}A") at the CASPT2(12,12)/ANO-L level using B3LYP/6-311+G(d) structures at fixed N…O separations.

The rate constant for disappearance of reactants (k_{dis}) is the sum of k_1 and k_3 from the mechanism in Scheme 1. The rate constant for formation of products k_{obs} is

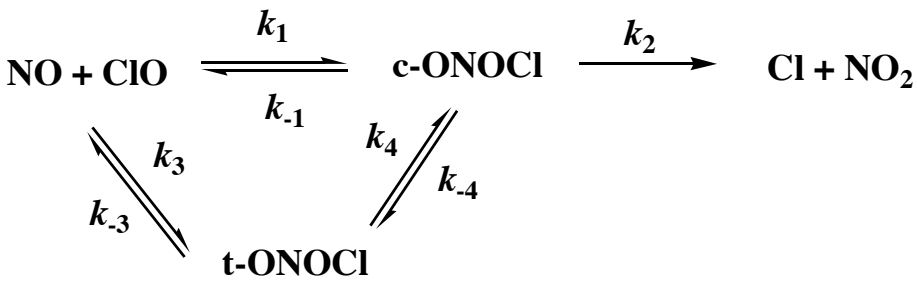

Scheme 1

derived with a steady state approximation for *cis*- and *trans*-ONOCl ($k_{obs} = \frac{k_1 k_2 (k_{-3} + k_4) + k_2 k_3 k_4}{(k_{-3} + k_4)(k_{-1} + k_2) + k_{-3} k_{-4}}$). The barrier for direct formation of NO_2 + Cl (31.83 kcal/mol) from *trans*-ONOCl is much higher than the barrier for isomerization to *cis*-ONOCl (8.75 kcal/mol). Thus, our mechanism includes direct formation of NO_2 + Cl from *cis*-ONOCl, but isomerization then fragmentation of *cis*-ONOCl for *trans*-ONOCl.

Figure 5 compares the calculated VariFlex and Polyrate rate constants (high-pressure limit) with experiments and the calculations of Zhu and Lin.[16] Our rate constants are in good agreement with experiment over the temperature range of 200-400K. Over the temperature range 200-1000K, we fit our VariFlex rate constant data (k_{obs}) to the form $7.38 \times 10^{-13} T^{0.413} \exp(286/T)$ $cm^3 \cdot molecule^{-1} \cdot s^{-1}$. In comparison, the VariFlex rate constant for k_{dis} ($k_1 + k_3$) can be fit to the form $k_{dis} = 3.30 \times 10^{-13} T^{0.558} \exp(305/T)$ $cm^3 \cdot molecule^{-1} \cdot s^{-1}$. Before computing the Polyrate rate constants k_{dis}, the CASPT2 energies (relative to the NO + ClO asymptote) were raised by 1.0 kcal/mol in order achieve better agreement with experiment.

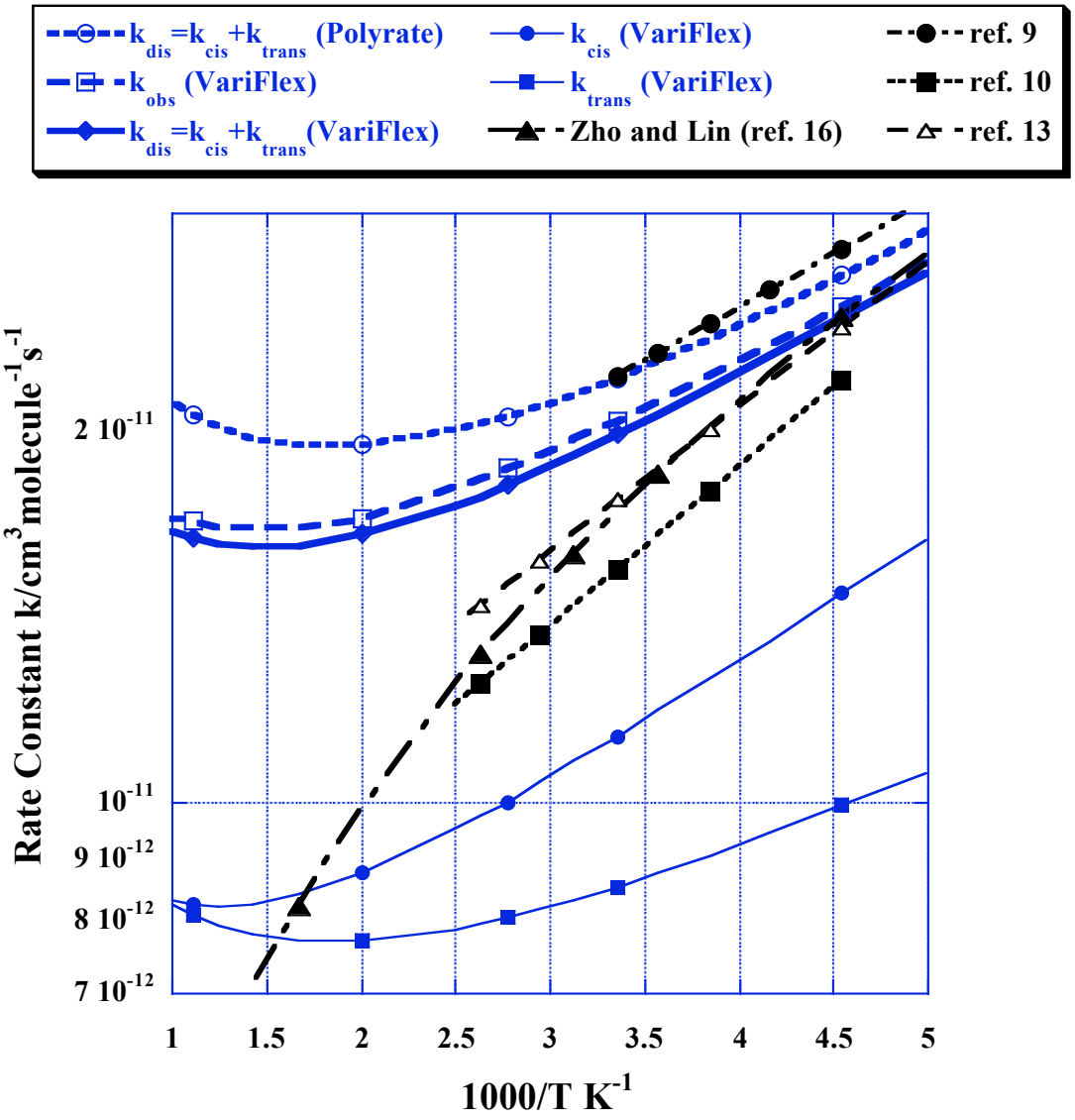

Figure 5. Calculated and experimental rate constants for the ClO + NO reaction. All references are experimental rate data except Ref. 16 which is computational. The computational rate data are for the bimolecular rate constant at the high-pressure limit. The thin lines for the cis and trans rate constants are added together to give k_{dis}.

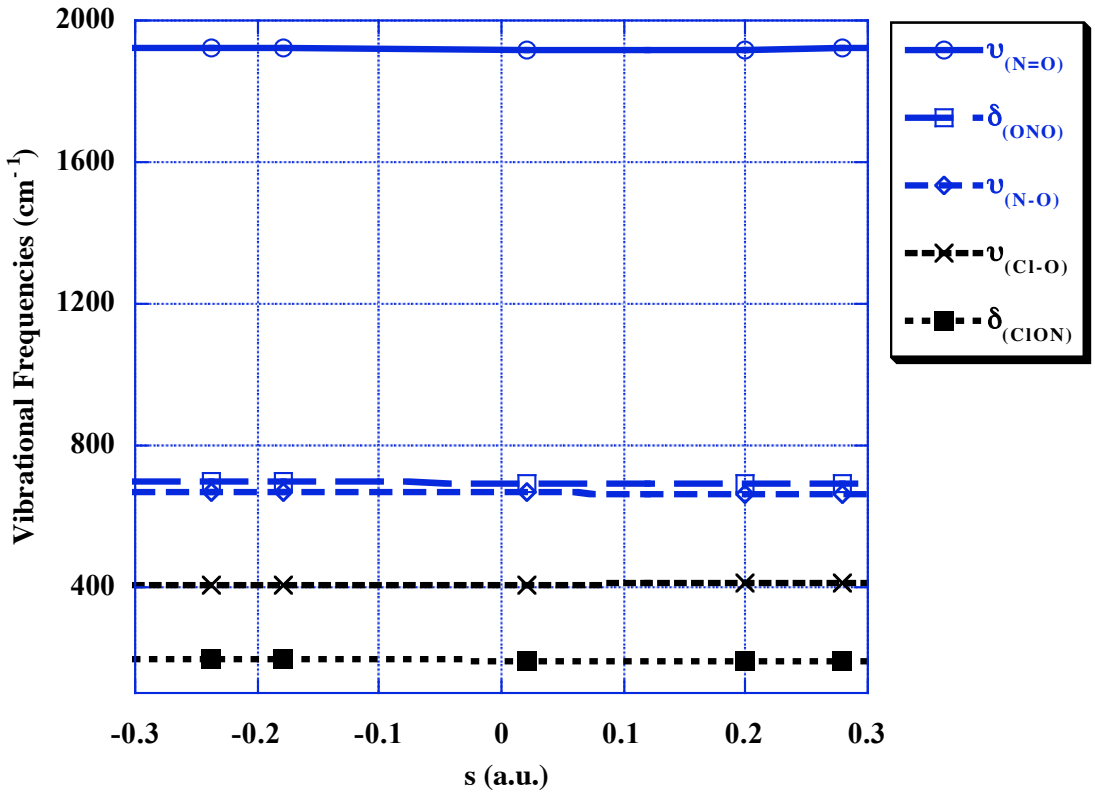

Figure 6. Plot of vibrational frequencies (cm^{-1}) along the IRC for trans → cis isomerization with the reaction projected out. The level of theory is B3LYP/6-311+G(d).

The downward (convex) curve of the Zhu and Lin plot reveals non-Arrhenius behavior at high temperature and is due to the negative exponent of temperature in their expression $k_{obs}=1.43x10^{-9}T^{-0.83}exp(92/T)$ $cm^3 \cdot molecule^{-1} \cdot s^{-1}$. Our plot indicates an upward (concave) curve due to the positive exponent of temperature in our rate constant expression $k_{obs}=7.38x10^{-13}T^{0.413}exp(286/T)$ $cm^3 \cdot molecule^{-1} \cdot s^{-1}$. The experimental data does not extend to a high enough temperature range to indicate either a concave or

convex high-temperature deviation of the rate constant from Arrhenius behavior. We note that both VariFlex and Polyrate indicate a concave curve for k_{dis}.

Generally, nonlinearity in an Arrhenius plot at low temperature is explained by quantum-mechanical tunneling effect and/or the appearance of an additional reaction channel. However in our system, there is no tunneling and no competition between two channels. The curvature in the Arrhenius plot at high temperatures can be explained by the excitation of vibrational modes.[50,51] As the population of the excited vibrational modes increase with increasing temperature, the reaction probability increases. Therefore, enhancement of the reactivity causes an increase in reaction rate at high temperatures.

The individual values of k_1 (k_{cis}) and k_3 (k_{trans}) by VariFlex are given in Figure 5 and can be used to compute a cis:trans branching ratio for the initial formation of isomers. At low temperature, the ratio of *cis*-ONOCl is much greater than *trans*-ONOCl (1 : 0.65, 200K), but the ratio is reduced at high temperature (1 : 0.83, 500K).

ChemRate and Polyrate were used to calculate the isomerization (*trans*-ONOCl ↔ *cis*-ONOCl) rate constant. ChemRate contains a master equation solver so that rate constants for unimolecular reactions in the energy transfer region and chemical activation processes under steady and non-steady conditions can be determined on the basis of RRKM theory. The input from the electronic structure programs was very similar except that CCSD(T)/cc-pVTZ//CCSD(T)/cc-pVDZ energies were used in ChemRate while G3B3//B3LYP/6-311+G(d) energies were used in Polyrate.

The vibrational frequencies as a function of *s* for the *trans*-ONOCl → *cis*-ONOCl isomerization reaction are shown in Figure 6 where positive values of *s* correspond to the

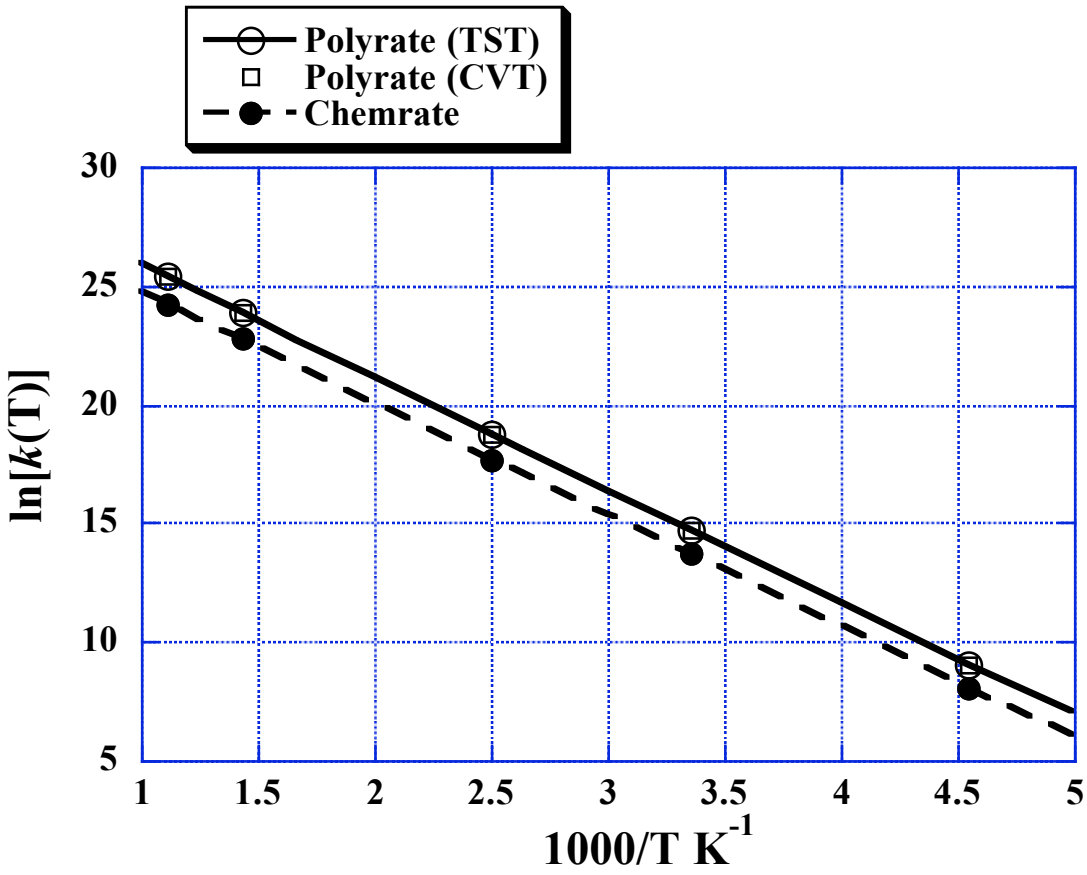

Figure 7. Comparison of ln(k) versus 1/T for transition state theory (TST) and variational transition state theory (CVT). The ChemRate results are RRKM.

product side and negative values to the reactant side. The torsion mode is not represented in Figure 6 because it is the imaginary frequency in this range of the reaction coordinate. There is little variation in reaction coordinate, which indicates that these modes do not have a strong contribution to the reaction dynamics.

The Arrhenius plots in Figure 7 show that the TST and CVT curves nearly overlap which indicates that the variational effect on the calculation of rate constant is

very small and can be ignored. The rate constant for trans → cis isomerization (k_4=1.92x10^{13}exp(-4730/T) s^{-1}; Polyrate-TST) is found to obey the Arrhenius equation at 1 atm in the temperature range of 200-2000K.

3.5 Conclusion

The NO + ClO → NO_2 + Cl reaction has been a challenge to experiment and theory. This reaction and ones similar to it such as NO + OH, NO + O_2H, and NO + OF, have been used as a test-bed for computational methods. We have used a series of theoretical methods to elucidate the reaction mechanism. Variational transition state theory was used to compute initial rate constants for the addition reaction to form cis- and trans-ONOCl. The branching ratio favors the cis isomer at lower temperature (1:0.65 at 200K). The N…Cl bond fragmentation is predicted to have a significantly different barrier in *cis*-ONOCl (19.75 kcal/mol) compared to *trans*-ONOCl (31.83 kcal/mol). This difference leads to the interesting prediction that the trans isomer must first isomerize to the cis isomer before a chlorine atom leaves. The rate constant for disappearance of reactants (k_{dis}) and appearance of products (k_{obs}) are almost identical and show a pronounced concave curvature indicating non-Arrhenius behavior at higher temperature. Over the temperature range 200-400K the activation energy is -0.35 kcal/mol (k_{dis}).

3.6 Reference

(1) Wofsy, S. C.; McElroy, M. B. *Can. J. Chem.* **1974**, *52*, 1582.

(2) Farman, J. C.; Gardiner, B. G.; Shanklin, J. D. *Nature* **1985**, *315*, 207.

(3) Stolarski, R. S.; Cicerone, R. J. *Can. J. Chem.* **1974**, *52*, 1610.

(4) Brune, W. H.; Toohey, D. W.; Anderson, J. G.; Chan, K. R. *Geophys. Res. Lett.* **1990**, *17*, 505.

(5) Waters, J. W.; Froidevaux, L.; Read, W. G.; Manney, G. L.; Elson, L. S.; Flower, D. A.; Jarnot, R. F.; Harwood, R. S. *Nature* **1993**, *362*, 597.

(6) Fickert, S.; Helleis, F.; Adams, J. W.; Moortgat, G. K.; Crowley, J. N. *J. Phys. Chem.* A **1998**, *102*, 10689.

(7) Carter, R. T.; Hallou, A.; Huber, J. R. *Chem. Phys. Lett.* **1999**, *310*, 166.

(8) Clyne, M. A. A.; Watson, R. T. *J. Chem. Soc. Faraday Trans.* **1974**, *70*, 2250.

(9) Zahniser, M. S.; Kaufman, F. *J. Chem. Phys.* **1977**, *66*, 3673.

(10) Leu, M. T.; DeMore, W. B. *J. Phys. Chem.* **1978**, *82*, 2049.

(11) Clyne, M. A. A.; MacRobert, A. J. *Int. J. Chem. Kinet.* **1980**, *12*, 79.

(12) Ray, G. W.; Watson, R. T. *J. Phys. Chem.* **1981**, *85*, 2955.

(13) Lee, Y.-P.; Stimpfle, R. M.; Perry, R. A.; Mucha, J. A.; Evenson, K. M; Jennings, D. A.; Howard, C. J. *Int. J. Chem. Kinet.* **1982**, *14*, 711.

(14) Zhao, Y.; Houk, K. N.; Olson, L. P. *J. Phys. Chem. A* **2004**, *108*, 5864.

(15) Ellison, G. B.; Herbert, J. M.; McCoy, A. B.; Stanton, J. F.; Szalay, P. G. *J. Phys. Chem. A* **2004,** *108*, 7639.

(16) Zhu, R. S.; Lin, M. C. *Chem. Phys. Chem.* **2004**, *5*, 1.

(17) Bach, R. D.; Dmitrenko, O.; Estévez, C. M. *J. Am. Chem. Soc.* **2003**, *125*, 16204.

(18) Dixon, D. A.; Feller, D.; Zhan, C.-G.; Francisco, J. S. *J. Phys. Chem. A* **2002**, *106*, 3191.

(19) Lee, T. J.; Bauschlicher, C. W.; Jayatilaka, D. *Theor. Chem. Acc.* **1997**, *97*, 185.

(20) Guha, S.; Francisco, J. S. *J. Phys. Chem. A* **1997**, *101*, 5347.

(21) Francisco, J. S.; Clark, J. *J. Phys. Chem. A* **1998**, *102*, 2209.

(22) Parthiban, S.; Lee, T. J. *J. Chem. Phys.* **2000**, *113*, 145.

(23) Lee, T. J.; Scuseria, G. E. *J. Chem. Phys.* **1990**, *93*, 489.

(24) Scuseria, G. E. *J. Chem. Phys.* **1991**, *94*, 442.

(25) *Gaussian03, (Revision B.4)*, Frisch, M. J.; Trucks, G. W.; Schlegel, H. B.; Scuseria, G. E.; Robb, M. A.; Cheeseman, J. R.; Montgomery, J. A. Jr.; Vreven, T.; Kudin, K. N.; Burant, J. C.; Millam, J. M.; Iyengar, S. S.; Tomasi, J.; Barone, V.; Mennucci, B.; Cossi, M.; Scalmani, G.; Rega, N.; Petersson, G. A.; Nakatsuji, H.; Hada, M.; Ehara, M.; Toyota, K.; Fukuda, R.; Hasegawa, J.; Ishida, M.; Nakajima, T.; Honda, Y.; Kitao, O.; Nakai, H.; Klene, M.; Li, X.; Knox, J. E.; Hratchian, H. P.; Cross, J. B.; Adamo, C.; Jaramillo, J.; Gomperts, R.; Stratmann, R. E.; Yazyev, O.; Austin, A. J.; Cammi, R.; Pomelli, C.; Ochterski, J. W.; Ayala, P. Y.; Morokuma, K.; Voth, G. A.; Salvador, P.; Dannenberg, J. J.; Zakrzewski, V. G.; Dapprich, S.; Daniels, A. D.; Strain, M. C.; Farkas, O.; Malick, D. K.; Rabuck, A. D.; Raghavachari, K.; Foresman, J. B.; Ortiz, J. V.; Cui, Q.; Baboul, A. G.; Clifford, S.; Cioslowski, J.; Stefanov, B. B.; Liu, G.; Liashenko, A.; Piskorz, P.; Komaromi, I.; Martin, R. L.; Fox, D. J.; Keith, T.; Al-Laham, M. A.; Peng, C. Y.; Nanayakkara, A.; Challacombe, M.; Gill, P. M. W.; Johnson, B.;

Chen, W.; Wong, M. W.; Gonzalez, C.; Pople, J. A. Gaussian, Inc., Pittsburgh PA, 2003.

(26) Karlström, G.; Lindh, R.; Malmqvist, P.-Å.; Roos, B. O.; Ryde, U.; Veryazov, V.; Widmark, P.-O.; Cossi, M.; Schimmelpfennig, B.; Neogrady, P.; Seijo, L. *Computational Material Science* **2003**, *28*, 222.

(27) Schaftenaar, G.; Noordik, J. H. *J. Comput.-Aided Mol. Design* **2000**, *14*, 123.

(28) Woon, D. E.; Dunning, T. H. *J. Chem. Phys.* **1993**, *98*, 1358.

(29) Kendall, R. A.; Dunning, T. H.; Harrison, R. J. *J. Chem. Phys.* **1994,** *100*, 7410.

(30) Curtiss, L. A.; Raghavachari, K.; Redfern, P. C; Rassolov, V.; Pople, J. A. *J. Chem. Phys.* **1998**, *109*, 7764.

(31) Moore, C. E. *Atomic Energy Levels*, National Bureau of Standards, Washington, D.C. 1971, Vols. II and II, NSRDS-NBS 35.

(32) Coxon, J. A. *Can. J. Phys.* **1979**, *57*, 1538.

(33) Sayin, H.; McKee, M. L. *J. Phys. Chem. A* **2004**, *108*, 7613.

(34) The standard G3B3 method includes spin-orbit corrections for atoms but not for diatomic. We have included spin-orbit effects for NO and ClO in the G3B3 energies.

(35) Roos, B. O. "The complete active space self-consistent field method and its applications in electronic structure calculations" In: Lawley, K. P., Ed. *Advances in Chemical Physics; Ab Initio Methods in Quantum Chemistry-II*; John Wiley & Sons: Chichester, UK, 1987.

(36) (a) Roos, B. O.; Andersson, K.; Fülscher, M. P.; Malmqvist, P.-Å.; Serrano-Andrés, L.; Pierloot, K.; Merchán, M. "Multiconfigurational perturbation theory:

Applications in electronic spectroscopy" In: Prigogine, I; Rice, S. A., Ed. *Advances in Chemical Physics: New Methods in Computational Quantum Mechanics*; John Wiley & Sons: New York, 1995. (b) Andersson, K.; Malmqvist, P.-Å.; Roos, B. O.; Sadlej, A. J.; Wolinski, K. *J. Phys. Chem.* **1990**, *94*, 5483. (c) Andersson, K.; Malmqvist, P.-Å.; Roos, B. O. *J. Phys. Chem.* **1992**, *96*, 1218.

(37) (a) Widmark, P. O.; Malmqvist, P.-Å.; Roos, B. O. *Theor. Chim. Acta* **1990**, *77*, 291. (b) Widmark, P. O.; Malmqvist, P.-Å.; Roos, B. O. *Theor. Chim. Acta* **1991**, *79*, 419.

(38) Corchado, J. C.; Chuang, Y.-Y.; Fast, P. L.; Villa, J.; Hu, W.-P.; Liu, Y.-P.; Lynch, G. C.; Nguyen, K. A.; Jackels, C. F.; Melissas, V. S.; Lynch, I. R.; Coitino, E. L.; Fernandez-Ramos, A.; Pu, J.; Albu, T. V.; Steckler, R.; Garrett, B. C.; Isaacson, A. D.; Truhlar, D. G. Polyrate, Version 9.3, University of Minnesota, MN, 2004.

(39) Klippenstein, S. J.; Wagner A. F.; Dunbar, R. C.; Wardlaw, D. M.; Robertson, S. H. VariFlex, Version 1.00, Argonne National Laboratory, Argonne, IL, 1999.

(40) Mokrushin, V.; Bedanov, V.; Tsang, W.; Zachariah, M. R.; Knyazev, V. D. ChemRate, Version 1.19, National Institute of Standards and Technology, Gaithersburg, MD, 2002.

(41) Tevault, D. E.; Smardzewski, R. R. J. Chem. Phys. **1977**, *67*, 3777.

(42) Kawashima, Y.; Takeo, H.; Matsumura, C. *Chem. Phys. Lett.* **1979**, *63*, 119.

(43) The NIST Standard Reference Database (http://webbook.nist.gov/chemistry) was used as the source of all thermochemistry.

(44) Zhang, D.; Zhang, R.; Park, J.; North, S. W. *J. Am. Chem. Soc.* **2002**, *124*, 9600.

(45) Olson, L. P.; Kuwata, K. T.; Bartberger, M. D.; Houk, K. N. *J. Am. Chem. Soc.* **2002**, *124*, 9469.

(46) Slagle, I. R.; Gutman D.; Davies, J. W.; Pilling, M. J. *J. Phys. Chem.* **1988**, *92*, 2455.

(47) Song, S.; Hanson, R. K.; Bowman, C. T.; Golden, D. M. *J. Phys. Chem. A* **2002**, *106*, 9233.

(48) Miller, J. A.; Klippenstein, S. J. *J. Phys. Chem.* A **2000**, *104*, 2061.

(49) Graff, M. M.; Wagner, A. F. *J. Chem. Phys.* **1990**, *92*, 2423.

(50) Kandel, S. A.; Zare, R. N. *J. Chem. Phys.* **1998**, *109*, 9719.

(51) Michelsen, H. A. *Acc. Chem. Res.* **2001**, *34*, 331.

(52) Millen, D. J.; Sinnot, K. M. *J. Chem. Soc.* **1958**, 350.

CHAPTER 4

THE DISSOCIATION MECHANISM OF A STABLE INTERMEDIATE: PERFLUOROHYROXYLAMINE

4.1 Introduction

Perfluorohydroxylamine, F_2NOF, is an interesting example of an electron-rich molecule that may have a number of competitive rearrangement pathways. There are several theoretical studies reported for this molecule;[1,2] semi-empirical,[3] Hartree-Fock methods,[4] and Coupled Cluster theory[1,2] which find that the *cis* conformation is more stable than *trans*. While the structure, stability, and thermochemistry of this compound have not been investigated experimentally, Antoniotti et al.[1] suggested that F_2NOF is an intermediate in the reaction between $O(^1D)$ and NF_3 which produced F_2N and FO radicals and Bedzhanyan et al.[6] suggested that F_2NOF can be an intermediate in the F_2N + FO reaction.

On the other hand, the F_3NO isomer has been structurally characterized and possesses a N-O bond with a high degree of double bond character (r_{N_O}=1.159 Å).[5] Antoniotti and Grandinetti studied[1] the dissociation pathway of F_3NO at the CCSD(T)/aug-cc-pVTZ//CCSD/cc-pVDZ level and found a transition state for the rearrangement of *trans*-F_2NOF to F_3NO with a 22.1 kcal/mol enthalpy barrier. As

discussed below, their transition state corresponds to a higher-lying structure with strong zwitterionic character. The true transition state has much higher radical character. Bedzhanyan et al.[6] studied the reaction between F_2N and FO radicals and found the dominant channel to be eq 1. A reasonable mechanism would have the

$$F_2N + FO \rightarrow FNO + 2F \quad (1)$$

radicals associate to form F_2NOF which could then dissociate to FNO + 2F through a stepwise cleavage of F atoms.

To our knowledge, the experimental vibrational spectrum for F_2NOF has not been reported. Misochko et al.[7] measured the infrared absorption spectra and EPR spectra of the F_2NO radical at 20K in an argon matrix, as well as infrared absorption spectra for FNO, F_2NO and F_3NO, but did not identify F_2NOF. Although postulated as an intermediate in several reaction mechanisms, F_2NOF has not been identified experimentally.

A reasonable mechanism of F_2NOF dissociation would include eq. 2-6.

$$F_2NOF \rightarrow F_2N + OF \quad (2)$$

$$F_2NOF \rightarrow FNO + F_2 \quad (3)$$

$$F_2NOF \rightarrow F_2NO + F\bullet \quad (4)$$

$$F_2NO \rightarrow FNO + F\bullet \quad (5)$$

$$F\bullet + F\bullet \rightarrow F_2 \quad (6)$$

Equation 4, the O-F dissociation step, has some similarities with O-X dissociations in ONO-X (X=F,Cl,Br,OH,OCl). When X=F, Ellison et al.[8] showed that there is direct isomerization between *cis*-ONOF and FNO_2 with an activation energy of 22±3 kcal/mol. When X=Cl, the *cis*-ONOCl → $ClNO_2$ transition state corresponds to fragmentation with a 20.9 kcal/mol barrier.[9] Kovačič et al.[10] recently calculated an isomerization path between *cis*-ONOBr and $BrNO_2$ with an activation barrier of 20.2 kcal/mol. On the other hand, when X=OH, the concerted formation of HNO_3 from HOONO is still not well established.[11] Zhao et al.[11a] showed that there is no direct isomerization between HOONO and $HONO_2$. On the other hand, a recent analysis using master equation simulation[11b] found that the best fit with experimental data occurs when the transition state for *trans*-HOONO → $HONO_2$ is 5.2 kcal/mol lower in energy than HO + NO_2. The O-O cleavage occurs from *cis*-HOONO with an activation barrier 18-19 kcal/mol to form NO_2 + OH. A similar mechanism of O-O cleavage occurs in the *cis*-ClOONO → $ClONO_2$ reaction with an activation energy of 28.4 kcal/mol and 6.7 kcal/mol from studies by Kovačič et al.[12] and Zhu et al,[13] respectively.

Fox et al.[14] reported the synthesis of F_3NO from FNO plus F in a fluorine-nitric oxide flame. The authors suggested that fluorination of an excited state of F_2NO (formed in the 2000K flame) might be involved in the mechanism.

In this paper, we will use theoretical methods to calculate the potential energy surface for the dissociation of F_2NOF molecule and calculate the rate constant for formation of products over the temperature range 200-1000K. All the calculated rate constants reported below are at the high-pressure limit.

4.2 Computational Method

Density functional theory (DFT), widely used as a computational chemistry tool providing reasonable accuracy at modest computational cost, is used in this study because it has been shown to give reasonable structures and vibrational frequencies for halogen compounds.[15-18] We optimized geometries at the B3LYP/6-311+G(d) level, but we checked our results by reoptimizing with BB1K[19] and MPWB1K[20] which are hybrid meta DFT methods specifically designed to yield good results for kinetics. Beside the 6-311+G(d)[21] basis set, we also used the MG3S[22] basis set which is equivalent to 6-311+G(2df,2p) for systems without elements heavier than F. We also checked some of the stationary points with multi-configurational SCF to determine the effect of adding additional configurations to the wave function. Lastly, we reoptimized most structures at the CCSD/6-31+G(d) level as a further check on consistency of prediction. Since the CCSD(T) method with a reasonable basis set yields very good results for different chemical systems such as O_3[23] and FOOF,[24] we based our kinetics calculations on energies at CCSD(T)/cc-pVQZ//B3LYP/6-311+G(d) unless indicated otherwise.

All electronic structure calculations have used the Gaussian03[25] and Gamess[26] program systems. All imaginary frequencies for transition states were animated by using the graphical program MolDen[27] to make sure that the motion of the transition vector was appropriate for converting reactants to products.

The transition states involving bond formation or bond breaking were computed with an unrestricted method (UDFT or UHF) to determine the lower-energy spin broken-symmetry solution at the UDFT or UCCSD levels. Single-point calculations were made with a 16-electron 11-orbital complete active space[28] (CASSCF(16e,11o)) and the

6-311+G(d) basis set with dynamic electron correlation introduced at the MP2 level (MCQDPT2).[29] Optimization of radical fragments and most F_2NOF stationary points were also carried out at the CASSCF(16e,11o) level (Table 2 and Table S5). However, the transition states that were characterized by a loosely associated F atom (Abst$-F_2-$ts$-$c, Add-F-N-ts, and F_2-FON-ts) could not be located at the CASSCF level probably due to the lack of dynamic electron correlation in the CASSCF method. T1 diagnostics were computed at the CCSD level (Table 2) for several of the transition states. Values larger than 0.02 are often used as an indicator of significant multireference character. It is noteworthy that F_2NO-F-ts had a value of 0.02.

The intrinsic reaction coordinate[30] (IRC) is constructed starting from the saddle point geometry and going downhill to both the asymptotic reactant and product channels in mass-weighted Cartesian coordinates. Along each IRC, the reaction coordinate, "*s*" is defined as the signed distance from the saddle point, with $s>0$ referring to the product side. Once accurate approximations to the stationary points on the potential energy surface (PES) are available, reaction rate constants can be calculated using variational transition-state-theory (VTST).[31-33]

Three programs were used to compute rate constants. For reactions without a transition structure, Variflex-1.0[34] was used (k_1, k_5, k_6, and k_{11}, see below). For the conversion of *cis*-F_2NOF to *trans*-F_2NOF, Chemrate-1.21[35] was used (k_3, see below). For other reactions with a transition state structure, Polyrate-9.3[36] was used either with conventional transition state theory (k_4, k_7, k_8, see below) or with variational transition state theory (k_2, see below).

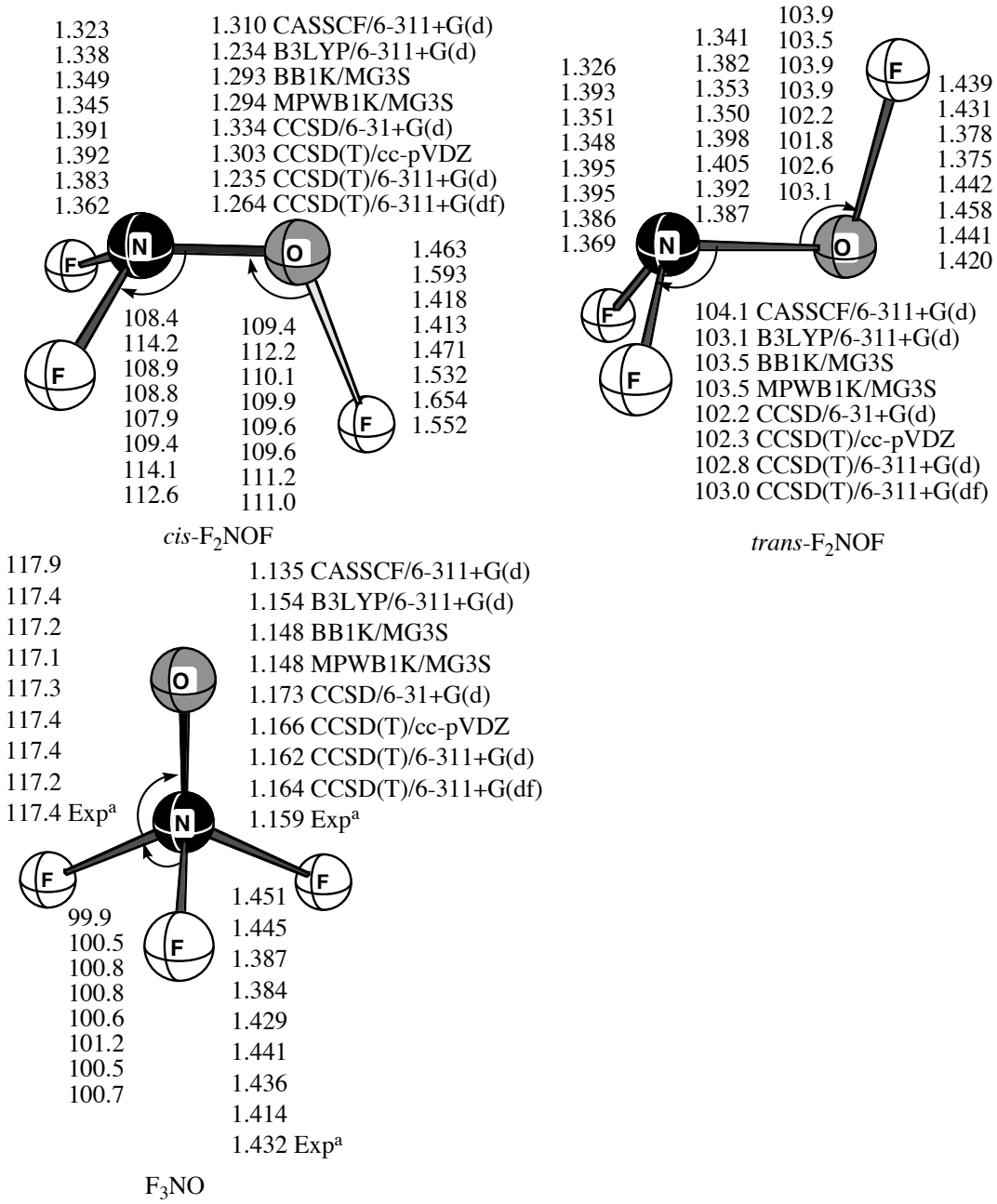

Figure 1. Optimized geometry of *cis*-, *trans*-F_2NOF and F_3NO isomers. Bond lengths are in Å and angles are in degrees. For each isomer, methods are shown with the data. The last row in F_3NO isomers are experimental values. (a) Frost, D. C.; Herring, F. G; Mitchell, K. A. R; Stenhouse, I. R. *J. Am. Chem. Soc.* **1971**, *93*, 1596.

Table 1. Harmonic frequencies of *cis*-F_2NOF, *trans*-F_2NOF and F_3NO in cm^{-1}

Method									
cis-F_2NOF	$\omega_1(a')$	$\omega_2(a'')$	$\omega_3(a')$	$\omega_4(a')$	$\omega_5(a'')$	$\omega_6(a')$	$\omega_7(a')$	$\omega_8(a')$	$\omega_9(a'')$
B3LYP/6-311+g(d)	1242	914	838	742	584	531	474	207	195
BB1K/MG3S	1150	1040	994	852	798	595	559	296	215
CCSD/6-31+G(d)	1065	975	895	823	733	549	518	277	196
CCSD(T)/cc-pVDZ	1046	910	850	750	556	547	474	232	194
CCSD(T)/6-311+G(d)	1230	951	827	696	578	518	346	189	113
CCSD(T)/6-311+G(df)	1181	1023	887	748	589	533	385	204	101
trans-F_2NOF	$\omega_1(a')$	$\omega_2(a')$	$\omega_3(a'')$	$\omega_4(a')$	$\omega_5(a')$	$\omega_6(a')$	$\omega_7(a'')$	$\omega_8(a')$	$\omega_9(a'')$
B3LYP/6-311+G(d)	1031	937	866	733	597	474	463	394	53
BB1K/MG3S	1144	1084	1029	941	668	518	512	431	63
CCSD/6-31+G(d)	1058	967	957	876	612	477	471	395	-28
CCSD(T)cc-pVDZ	1007	883	878	764	586	465	460	384	-19
CCSD(T)/6-311+G(d)	1028	910	897	797	596	473	467	391	40
CCSD(T)/6-311+G(df)	1073	968	951	849	627	489	477	401	43
F_3NO	$\omega_1(a_1)$	$\omega_2(e)$	$\omega_3(e)$	$\omega_4(a_1)$	$\omega_5(a_1)$	$\omega_6(e)$	$\omega_7(e)$	$\omega_8(e)$	$\omega_9(e)$
B3LYP/6-311+G(d)	1787	881	881	758	533	520	520	393	393
BB1K/MG3S	1785	974	974	857	609	602	602	438	438
CCSD/6-31+G(d)	1735	936	936	788	561	560	560	406	406
CCSD(T)/cc-pVDZ	1790	899	899	729	534	514	514	397	397
CCSD(T)/6-311+G(d)	1764	896	895	742	541	522	522	402	402
CCSD(T)/6-311+G(df)	1741	932	932	785	573	556	556	415	415
Exp[a]	1852	874		741		529		403	

(a) Smardzewski R. R.; Fox, W. B. *J. Chem. Phys.* **1974**, *60*, 2193.

4.3 Results and Discussions

The calculated equilibrium structures of F_3NO are in good agreement with each other and with experiment (Figure 1). The O-F bond distance of *cis*-F_2NOF has the largest sensitivity with respect to method, with CCSD(T)/6-311+G(d) giving the longest

Table 2. Relative Enthalpies[a] (kcal/mol) for Various Species Involved in the Dissociation of F_2NOF Molecule

					//B3LYP/6-311+G(d)[b]			
	BB1K/ MG3S	MPWB1K/ MG3S	CCSD/ 6-31+G(d)	MCQDPT2/ 6-311+G(d)[b,c]	B3LYP/ 6-311+G(d)	MCQDPT2/ 6-311+G(d)	CCSD(T)/ cc-pVTZ[d]	CCSD(T)/ cc-pVQZ[d]
cis-F_2NOF	0.00	0.00	0.00	0.00	0.00	0.00	0.00	0.00
trans-F_2NOF	5.89	5.84	4.51	10.76	9.06	9.36	3.80	4.31
F_3NO	-35.38	-35.36	-28.55	-39.80	-33.98	-33.44	-34.07	-34.63
Abst-F_2-ts-*c*[e]	10.98				8.94	12.05	13.80(0.07)	[15.25][g]
Add-F-N-ts	27.06	27.69	34.01		21.27	36.06	29.77(0.04)	27.37
F_2NO-F-ts[e]	17.15	17.44	18.57	17.31	13.90	15.66	14.11(0.02)	14.10(0.02)
F_2NOF-ts	14.06	14.05	12.37	11.01	16.13	15.35	10.91	11.31
F-F_2NO-ts[e]				7.73[f]	9.54	1.67	14.25(0.08)	[14.51][h]
F_2-FON-ts[e]					18.92	12.27	23.00(0.04)	[24.45][g]
Complex[e]				8.17	7.56	8.44	16.54(0.04)	[9.89][h]
F_2NO + F	9.48	10.13	9.12	14.76	10.45	8.23	14.52	15.97
FNO + F_2	-7.79	-6.30	-17.56	-8.23	-10.73	-11.64	-16.46	-15.55
FNO + 2F				16.52	20.48	24.33	17.74	20.54
F_2N + OF	33.78	34.73	29.41	50.16	35.24	36.03	35.57	38.16
NO + 3F					79.12		71.12	81.98

[a] Thermodynamic corrections to produce enthalpies at 298K are made from frequencies computed at the given level except where indicated.

[b] Thermodynamic corrections are made at the B3LYP/6-311+G(d) level.

[c] Geometries are optimized at the CASSCF(16e,11o)/6-311+G(d) level.

[d] T1 diagnostic at the CCSD level is given in parentheses.

[e] Geometries are optimized at the UDFT and UCCSD level. Spin-squared $<S^2>$ values at UB3LYP/6-311+G(d) are 0.93, 0.13, 0.93 0.95 and 0.80 for Abst-F_2-ts-*c*, F_2NO-F-ts, F-F_2NO-ts, F_2-FON-ts, and complex, respectively.

[f] Did not fully meet optimization criterion.

[g] The energy at the CCSD(T)/cc-pVQZ level is estimated by taking the energy difference with F_2NO + F at the CCSD(T)/cc-pVTZ level and adjusting to the CCSD(T)/cc-pVQZ energy of F_2NO + F (15.97 kcal/mol).

[h] The effect of spin contamination was projected out of the B3LYP/6-311+G(d) energies using the formula $E_{singlet}=(2E_{BS}-<S^2>\cdot E_{triplet})/(2-<S^2>)$, where $<S^2>$ is the spin-squared value of the singlet broken-symmetry solution (E_{BS}) and $E_{triplet}$ is the energy of the triplet at the singlet geometry. In addition, the "corrected" energy difference between "F-F_2NO-ts" or "complex" and F_2NO + F at the B3LYP/6-311+G(d) level is subtracted from the CCSD(T)/cc-pVQZ relative energy of F_2NO + F (15.97 kcal/mol).

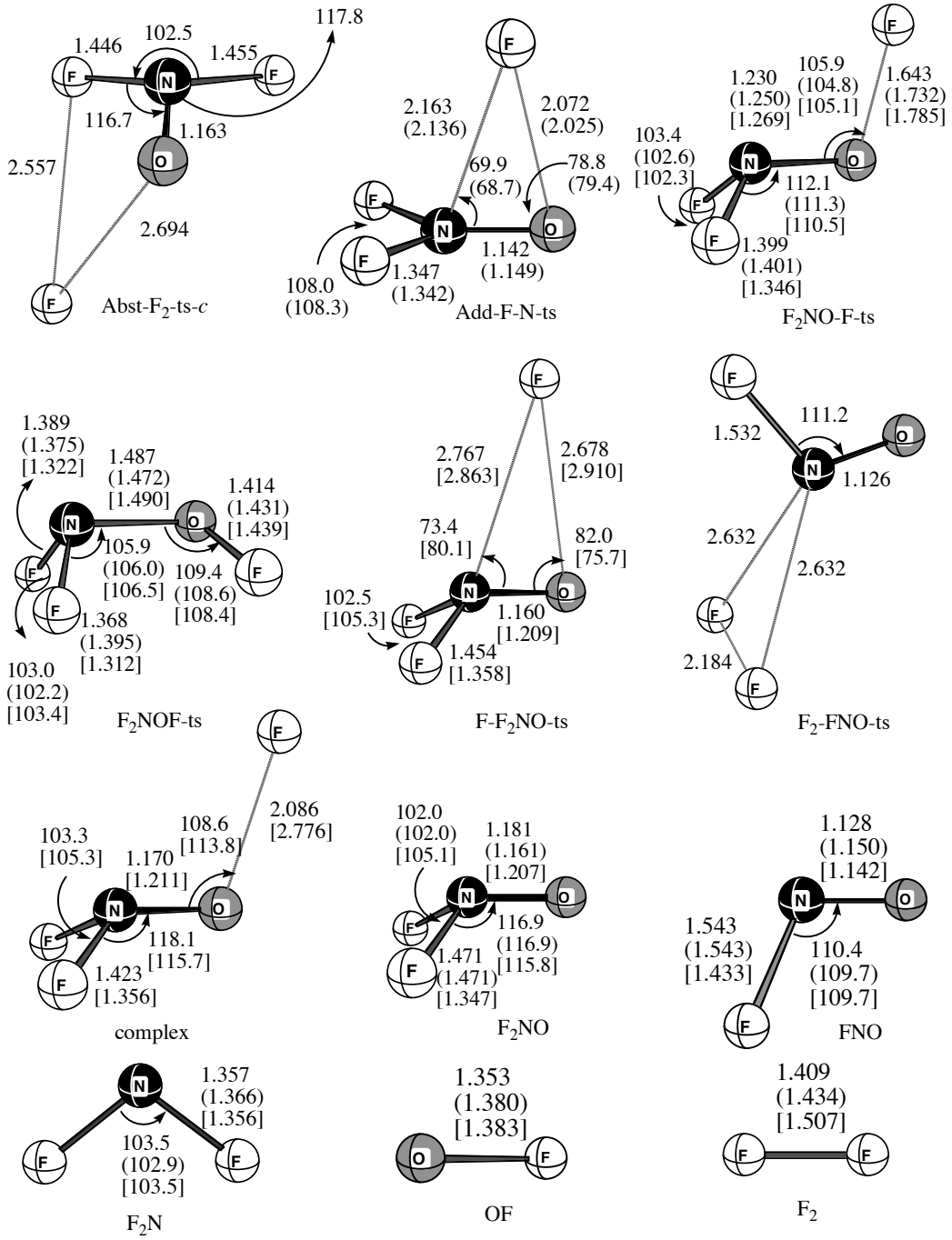

Figure 2. Optimized geometric parameters of stationary points at the B3LYP/6-311+G(d) level. Values in parentheses are at the CCSD/6-31+G(d) level and values in brackets are at the CASSCF/6-311+G(d) level. Bond lengths are in Å and angles are in degrees.

O-F bond distance and MPWB1K/MG3S the shortest. Likewise, there were large differences in the N-O bond of *cis*-F_2NOF with CCSD(T)/6-311+G(d) giving a short N-O bond distance and MPWB1K/MG3S giving a long N-O distance. The B3LYP DFT method made predictions in closest agreement with CCSD(T).

Table 1 shows the comparison of the calculated frequencies of *cis*-F_2NOF, *trans*-F_2NOF and F_3NO. The calculated frequencies are in agreement with each other for *cis*-F_2NOF with slightly less agreement for the ONF bend (ω_5). For F_3NO, the calculated frequencies are in agreement with each other and very close to experimental results. It is interesting to point out that the CCSD(T) method gave one imaginary frequency for *trans*-F_2NOF with a small basis set (cc-pVDZ),[37] but all real frequencies with bigger basis sets (6-311+G(d) and 6-311+G(df)).

A lower-energy spin broken-symmetry solution was obtained at the UDFT and UCCSD levels in transition states involving bond formation or bond breaking (Table 2). We checked two of these transition state energies by using MCQDPT2/6-311+G(d)//UB3LYP/6-311+G(d). Unfortunately we did not get reliable results at this method.

The two bonds involving fluorine in the transition state (Abst–F_2–ts–*c*) for the reaction *cis*-$F_2NOF \rightarrow FNO + F_2$ are very asymmetrical (Figure 2); one bond is almost completely broken (F-O 2.694 Å), while the other (F-N, 1.446 Å) shows no lengthening. Also, the newly forming F-F bond (2.557 Å) is very long. These factors led us to believe that the maximum along the PES might be sensitive to computational method. For these reasons, the rate constant was calculated with VTST using Polyrate. An intrinsic reaction coordinate (IRC) was calculated in mass-weighted coordinates at the B3LYP/6-311+G(d)

level. At ten points along the IRC, single-point energies were computed at the UCCSD(T)/cc-pVTZ, while a generalized normal-mode analysis was performed at the B3LYP/6-311+G(d) level projecting out the reaction coordinate. Despite expectations, the maximum at the UCCSD(T)/cc-pVTZ level occurred at a path value of s=0, the same as the maximum at the B3LYP/6-311+G(d) level.

Because the spin broken-symmetry UCCSD(T)/cc-pVQZ calculations proved to be too lengthy, we estimated the relative energy of Abst-F_2-ts-*c* at the UCCSD(T)/cc-pVQZ level by taking the Abst-F_2-ts-*c*/F_2NO+F energy difference at the UCCSD(T)/cc-pVTZ level (0.72 kcal/mol more stable than radicals) and applying it to UCCSD(T)/cc-pVQZ relative energy of $F_2NO + F$.[38] The natural population analysis (NPA) at the UB3LYP/6-311+G(d) level showed that the loosely bound fluorine has nearly a full unpaired electron and has very little charge which means the transition state is biradical rather than zwitterionic.

Unlike the reaction *cis*-$F_2NOF \rightarrow FNO + F_2$, the transition state ($F_2NOF$–ts) in the *cis*-$F_2NOF \rightarrow$ *trans*-F_2NOF isomerization did not involve bond forming or breaking, only the rotation of OF about the N-O bond which was about mid-way between cis (0^o) and trans (180^o). Therefore, we felt that the position of the transition state was probably not sensitive to method and we used normal transition state theory with Chemrate. The calculated enthalpy barrier at the CCSD(T)/cc-pVQZ//B3LYP/6-311+G(d) level was 11.31 kcal/mol which is slightly less than the barrier for the *cis*-$F_2NOF \rightarrow FNO + F_2$ reaction (15.25 kcal/mol, Table 2).

The transition state (F_2NO-F-ts) in *trans*-$F_2NOF \rightarrow F_3NO$ was found at the UB3LYP/6-311+G(d), UBB1K/MG3S, UMPWB1K/MG3S, and UCCSD/6-31+G(d)

levels. The O···F calculated distance in the transition state (Figure 2, F_2NO-F-ts) is rather short (1.643 Å, UB3LYP/6-311+G(d)). Ellison et al.[8] also found similar short O···F distances of 1.726 and 1.693 Å in the *trans*-ONOF → FNO_2 transition state at the RCCSD(T) and UCCSD(T)/cc-pVTZ levels, respectively. A similar tight transition state is obtained for O-Cl cleavage in our previous study[9] of *trans*-ONOCl → $ClNO_2$ where a O···Cl distance of 2.191 and 2.067 Å was calculated in the transition state at the RCCSD(T) and UCCSD(T)/cc-pVDZ levels, respectively.

Since little spin contamination was found at the UB3LYP/6-311+G(d) level (F_2NO-F-ts, $<S^2>=0.13$), restricted CCSD (RCCSD(T)/cc-pVQZ) was used rather than unrestricted CCSD. The enthalpy (298K) of the transition state is 1.87 kcal/mol lower than F_2NO + F which implies the product is a complex rather than free radicals. We located a complex with a spin-squared value ($<S^2>=0.80$) which was 3.45 kcal/mol lower in enthalpy (298K) than F_2NO-F-ts and 2.89 kcal/mol lower than F_2NO + F at the B3LYP/6-311+G(d) level. The O-F bond increased from 1.643 Å in the transition state (F_2NO-F-ts) to 2.086 Å in the complex. From the complex, a second transition state (F-F_2NO-ts) was reached with an enthalpy of activation of 1.98 kcal/mol and a spin-squared value of 0.93 at the B3LYP/6-311+G(d) level. At the DFT level, the description of the F_2NOF → F_3NO reaction is stepwise via a shallow intermediate which is concerted in the sense that the same fluorine that leaves oxygen adds to the nitrogen as opposed to a fragmentation/recombination mechanism where the fluorine atom added is different from the one that is cleaved.

Neither restricted nor unrestricted CCSD(T) methods do well at describing biradical character. At the UCCSD(T)/cc-pVTZ//B3LYP/6-311+G(d) level, the enthalpy

of the complex is 2.02 kcal/mol above F_2NO + F. When we projected out the effect of spin contamination from the DFT energies by an approximate method[39] (see Table 2) and referenced the enthalpy against the CCSD(T)/cc-VQZ value for F_2NO + F, the complex was 6.08 kcal/mol more stable than F_2NO + F radicals. Clearly, the relative enthalpies of the complex and F-F_2NO-ts are very uncertain. We feel that the enthalpies at the DFT level are too low, but that the enthalpies at UCCSD(T) are too high.

The electronic nature of the complex is an unsymmetrical two-center three-electron interaction (2c∴3e) between the unpaired electron on F and the lone pair on O (F_2NO∴F). The stability of this interaction is known to be exaggerated at the DFT level which is known to have excessive spin and charge delocalization.[40-43] While a stabilization of 6.0 kcal/mol is probably too large, some stabilization is reasonable. Based on our results for the F + FNO complex (see below), we would expect F to bind to F_2NO with an enthalpy of 1-2 kcal/mol.

We decided to model the reaction of F_2NOF to F_3NO in two ways. The first model assumes that F_2NOF passes over F_2NO-F-ts in competition with fragmentation to F_2NO + F such that the intermediate and second transition state (F-F_2NO-ts) are unimportant. In other words, any species that cross the first barrier will form F_3NO. The second model is the same as the first except that the first transition state (F_2NO-F-ts) is assumed to lead to an intermediate and second transition state with the same energy. Thus, in the absence of reliable energies for the intermediate and second transition state, we assume the three structures have the same energy at 0K. In the second model, the intermediate can also fragment to F_2NO + F which will reduce the F_3NO product

formation. In our calculations the branching ratio between the complex→F_3NO and complex→F_2NO+F varied from 86:14 at 298K to 70:30 at 1000K.

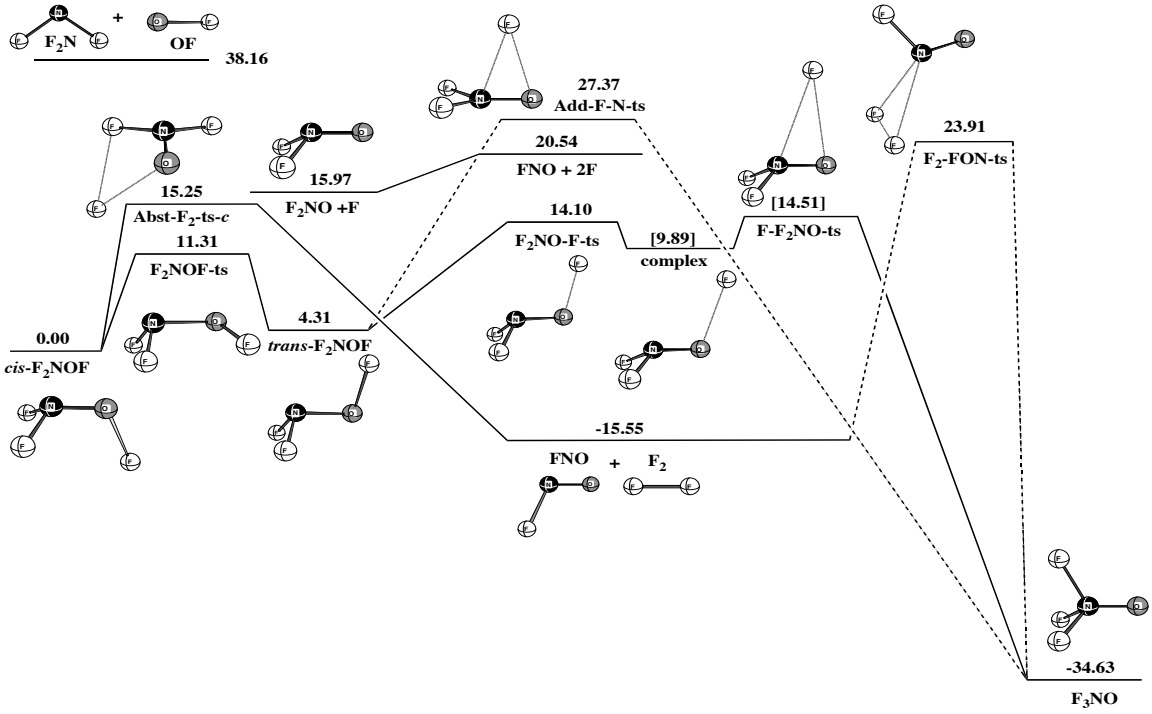

Figure 3. Schematic diagram of the potential energy surface for the dissociation of F_2NOF system computed at the CCSD(T)/cc-pVQZ//B3LYP/6-311+G(d) level. Relative enthalpies are given in kcal/mol at 298K.

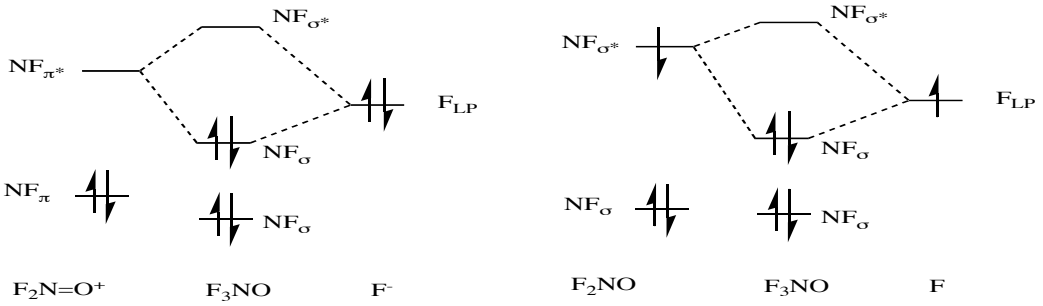

Figure 4. Interaction diagram comparing (a) the zwitterionic tansition state (Add-F-N-ts) and (b) the biradical transtion state (F-F_2NO-ts).

In comparing the first model, the rate of product formation is given by k_4, while in the second model, it is given by $k_9=k_4k_7/(k_{-4}+k_7)$. Since $k_7 >> k_{-4}$ (see Table 7), $k_4 \approx k_9$. However, the second model also includes fragmentation of the intermediate to $F_2NO + F$ which accounts for 7% of products at 298K in our calculations.

Table 3. Spin Density, Natural Population Analysis (NPA) and Geometry are calculated at the (U)B3LYP/6-311+G(d)

		Spin Density			NPA charge			Geometry		
	$<S^2>$	F	O	N	F	O	N	N-O	O-F	N-F
trans-F_2NOF	0.00	0.00	0.00	0.00	-0.11	0.01	0.56	1.38	1.43	2.21
F_2NO-F-ts	0.13	0.32	-0.12	-0.13	-0.18	-0.03	0.61	1.23	1.64	2.31
complex	0.81	0.82	-0.23	-0.41	-0.16	-0.14	0.70	1.17	2.08	2.69
F-F_2NO-ts	0.93	0.94	-0.29	-0.41	-0.05	-0.17	0.68	1.16	2.68	2.77
F_3NO	0.00	0.00	0.00	0.00	-0.22	-0.22	0.87	1.15	2.22	1.44
Add-F-N-ts	0.00	0.00	0.00	0.00	-0.61	-0.01	0.84	1.14	2.07	2.16

Antoniotti et al.[1] found a transition state for the reaction *trans*-$F_2NOF \rightarrow F_3NO$ with a barrier of 22.2 kcal/mol at the CCSD(T)/aug-cc-pVTZ//CCSD/cc-pVDZ level. In the present study, we find a zwitterionic transition state with a barrier of 23.06 kcal/mol (27.37-4.31, Table 2) which is very similar to the one found by Antoniotti et al. However, we also find a lower barrier of 9.79 kcal/mol through a biradical transition state (F_2NO-F-ts). The relevant interactions between F and F_2NO in the two transition state are given in Figure 4. In the zwitterionic transition state (Add–F–N–ts, Figure 4a), the migrating F atoms has a large negative charge (0.61 e^-). The nitrogen center is planar in the F_2NO fragment as expected for $F_2N{=}O^+$. The fluoride sits above the N=O double

bond and adds to the nitrogen side to form F_3NO. In the biradical transition state (F-F_2NO-ts, Figure 4b), the migrating F atom has little charge but large unpaired spin density (Table 3). The nitrogen center is pyramidal, as expected for a $F_2NO\bullet$ radical. The reason for the large activation energy difference can be explained by the electronic excitation (Figure 4). The β-spin electron is excited from an a" orbital to an a' orbital which leaves an unpaired electron on nitrogen in an orbital which is suitable for bond formation with a fluorine atom. The energy needed for electronic excitation is the reason for the greater energy of Add-F-N-ts compared to F_2NO-F-ts.

The reaction of *trans*-$F_2NOF \rightarrow F_3NO$ can be considered a 1,2-fluorine shift which can be compared with the 1,2-hydrogen shift of NH_2OH. In their study of *trans*-$NH_2OH \rightarrow H_3NO$, Bach et al.[44] found a transition state with a 55.9 kcal/mol barrier at the MP4/6-31G(d)//MP2/6-31G(d) level, a barrier significantly lower than the H_2NO-H bond energy of 76.5 kcal/mol (Table 4). In the 1,2-fluorine shift, the barrier and F-O bond energies are nearly the same (Figure 3).

Table 4. Enthalpies and free energies of Fluorine loss reaction at the CCSD(T)/cc-pVQZ//B3LYP/6-311+G(d) level

reaction	ΔH(298K)	ΔG(298K)	Dixon et. al. ΔH(0K)[a]	
cis-$F_2NOF \rightarrow F_2NO + F$	15.97	6.54	$H_2NOH \rightarrow$	76.5
cis-$F_2NOF \rightarrow FNO + 2F$	20.54	2.56		
cis-$F_2NOF \rightarrow NO + 3F$	81.98	56.30		
$F_2NO \rightarrow FNO + F$	4.57	-3.98	$H_2NO \rightarrow HNO+H$	61.1
$FNO \rightarrow NO + F$	61.44	53.75	$HNO \rightarrow NO+H$	47.0

(a) Dixon, D. A.; Francisco, J. S.; Alexeev, Y. *J. Phys. Chem. A* **2006**, *110*, 185.

In their study of the ClOONO → $ClONO_2$ reaction, Kovačič et al.[12] calculated an activation energy of 28 kcal/mol at the B3LYP/6-311G(d) level. The same reaction was found to have a much lower activation energy of 6.7 kcal/mol in a study in Zhu et al.[13] at the CCSD(T)/6-311+(3df)//B3LYP/6-311+G(3df) level. The 6.7 kcal/mol barrier (0K) for the ClOONO → $ClONO_2$ reaction is much more consistent with our 9.79 kcal/mol barrier (298K) for the *trans*-F_2NOF → F_3NO reaction since the propensity for migrating a OCl radical should be similar to migrating a F radical.

The calculated bond enthalpy[45] at 298K for ClO-NO_2 (28.0 kcal/mol) and BrO-NO_2 (28.9 kcal/mol) at the CCSD(T) are in good agreement with experimental results (26.8 kcal/mol and 28.2 kcal/mol, respectively). We used the same method to find the FO-NF_2 bond enthalpy of 38.16 kcal/mol at the CCSD(T)/cc-pVQZ//B3LYP/6-311+G(d) level.

Table 5. Enthalpies of the various types of F_2NO species optimized at the CCSD/cc-pVDZ level

	ΔH(0K)			ΔH(298K)		
	CCSD/ cc-pVDZ	CCSD(T)/ cc-pVTZ	CCSD(T)/ cc-pVQZ	CCSD/ cc-pVDZ	CCSD(T)/ cc-pVTZ	CCSD(T)/ cc-pVQZ
F_2NO[a]	0.00	0.00(0.00)	0.00(0.00)	0.00	0.00(0.00)	0.00(0.00)
t-F-FNO-c_s[a]	-6.95	1.24(1.35)	2.79(2.86)	-5.73	2.46(2.57)	4.01(4.08)
c-F-FNO-c_s	-6.89	1.16	2.75	-5.71	2.34	3.93
F-FNO-ts	3.38	5.67	5.66	3.44	5.75	5.74
FNO+F	-5.88	2.05(1.95)	3.57(3.44)	-4.75	3.18(3.01)	4.70(4.51)

a) The data in the parentheses are at CCSD(T)/cc-pVDZ optimized geometries.

4.4 Stability of F_2NO

The lowest energy fragmentation for *cis*-F_2NOF produces F_2NO + F radicals. The lifetime of a thermalized *cis*-F_2NOF molecule calculated from k_1 is $2.5x10^{-3}$ s at 298K. However, the N-F bond enthalpy (298K) is very small (4.57 and 3.57 kcal/mol at the CCSD(T)/cc-pVQZ//B3LYP/6-311+G(d) and CCSD(T)/cc-pVQZ//CCSD/cc-pVDZ levels, respectively, Table 4 and 5). In fact, the free energy change at 298K is spontaneous (-3.98 kcal/mol) for breaking the N-F bond in F_2NO (Table 4). It is interesting that while the N-F bond in F_2NO is very weak, the N-F in FNO is very strong. Exactly the opposite behavior is calculated for the N-H bonds in H_2NO and HNO where the first is 61.1 kcal/mol and the second one is 47.0 kcal/mol at 0K (Table 4). Fluorine is known to be a very good π donating substitutent. In FNO, fluorine can donate electron density into the π* orbital of NO while hydrogen cannot donate in HNO**.**

In contrast to F_2NOF and in spite of its lack of thermal stability, the difluoronitroxide radical (F_2NO) has been produced in solid argon matrices by addition of F atoms to NO by Misochko et al.[7] They found that F_2NO exists in equilibrium (F-FNO $\rightleftarrows$ F_2NO) with a van der Waals complex (F-FNO). Since F_2NO and the complex were formed at very low temperature (20K), we compared our results at 0K with experimental results at Table 5. The reaction mechanism of $F_2NO \rightarrow FNO + F$ are calculated at the CCSD(T)/cc-pVQZ//CCSD/cc-pVDZ in Figure 5. The complex (F-FNO) and transition state (F-FNO-ts) are located at the CCSD/cc-pVDZ level. The optimized geometries of the complex and transition state of B3LYP/6-311+G(d) level are compared with CCSD/cc-pVDZ in Figure 6. The CCSD(T)/cc-pVDZ method was used to optimized

geometries for the complex (*t*-F-FNO-c_s) and F_2NO and found to give very similar geometries with the CCSD/cc-pVDZ method. While B3LYP gives reasonable structures for halogen compounds, it is interesting that B3LYP failed for the complex. The reason for this can be understood by excessive spin delocalization in DFT that is a particular problem in asymmetric 2c-3e bonding[40-43] (Table 6).

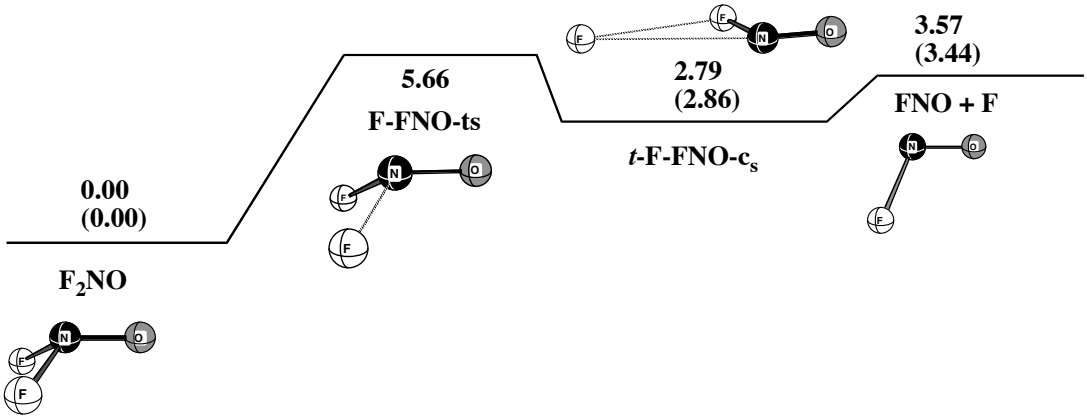

Figure 5. Schematic diagram of the potential energy surface ΔH(0K) for the dissociation of F_2NO at the CCSD(T)/cc-pVQZ//CCSD/cc-pVDZ level. Values in parentheses are at the CCSD(T)/cc-pVQZ//CCSD(T)/cc-pVDZ level.

We optimized two F-FNO complexes at the CCSD/cc-pVDZ level (*c*-F-FNO-c_s and *t*-F-FNO-c_s, Table 5) and one at the CCSD(T)/cc-pVDZ level (*t*-F-FNO-c_s). The cis complex is very slightly more stable (by 0.04 kcal/mol at 0K) but the trans complex should be formed first by the principle of least motion. Both cis and trans complexes are very different from the complex obtained at the DFT level (Figure 6). In the radical

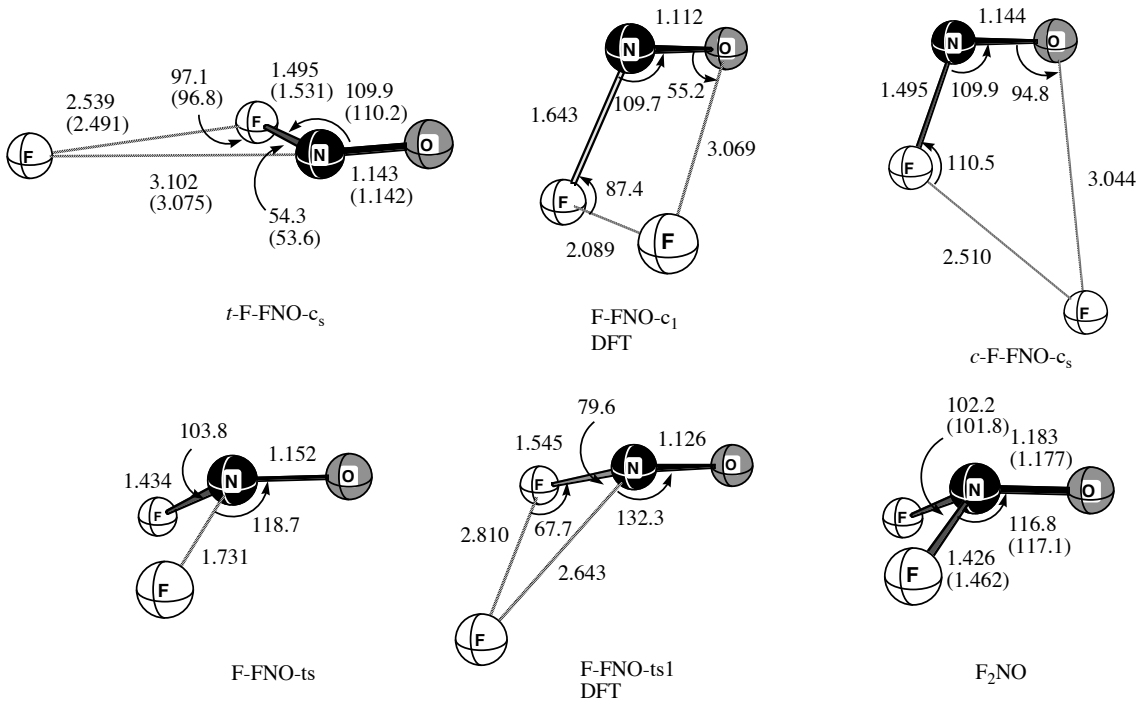

Figure 6. Optimized geometric parameters of stationary points at the CCSD/cc-pVDZ level. The parameters in parentheses are optimized at the CCSD(T)/cc-pVDZ level.

Table 6. Spin Densities and Mulliken Charges for c-F-FNO-c_s and F-FNO-c_1

	CCSD/cc-pVDZ// CCSD/cc-pVDZ *c*-F-FNO-c_s		B3LYP/6-311+G(d)// B3LYP/6-311+G(d) F-FNO-c_1	
	Spin density	Mulliken Charges	Spin density	Mulliken Charges
O	0.00	0.00	-0.02	0.24
N	0.00	0.29	-0.00	0.06
F	0.01	-0.28	0.17	-0.18
F	0.99	-0.01	0.85	-0.12

complex between FNO and F at the DFT level, the interaction is between the unpaired electron on one fluorine and the lone pair of another fluorine. The oxygen lone pair electrons in FNO have been stabilized (relative to F_2NO) which leads to a stronger interaction with the lone pairs on F of FNO.

We calculated ΔH^o=-2.75 kcal/mol enthalpy and ΔS^o=-13.76 cal/mol·K entropy for the reaction F-FNO ⇄ F_2NO at 0K (Table 5). Experimental results show that the changes in enthalpy and entropy at 20K for the equilibrium reaction (F-FNO ⇄ F_2NO) are 0.29 kcal/mol and 14.82 cal/mol·K, respectively. However, it is not possible to make a direct comparison between experiment and theory because the calculations model the gas phase while experiment takes place in an Ar matrix. A greater stabilization energy for the complex could be rationalized by greater dipole-induced dipole interactions between Ar molecules and the complex, since the complex has a higher dipole moment than F_2NO (1.548 and 0.413 D, respectively) at the CCSD/cc-pVDZ level and dipole-induced dipole interactions are directly proportional to the dipole moment. The lifetime for F_2NO is only 2.69×10^{-10} s^{-1} at 298K from k_8.

4.5 Rate Constant Calculations

Since there is no reverse barrier for *cis*-$F_2NOF \rightarrow F_2NO + F$ (k_1) and *trans*-$F_2NOF \rightarrow F_2NO + F$ (k_5), we used Variflex to calculate the rate constants (see eqs. 7-10). The reactive flux was evaluated by the phase-space-integral based VTST (PSI-VTST) method, as implemented in VariFlex[34] as the O-F distances increased from 1.5 to 4.0 Å

with a step size 0.1 Å for *cis*-$F_2NOF \rightarrow F_2NO + F$ and *trans*-$F_2NOF \rightarrow F_2NO + F$ reactions.

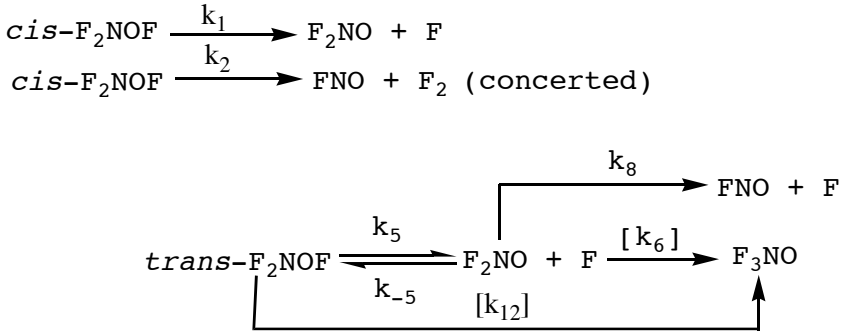

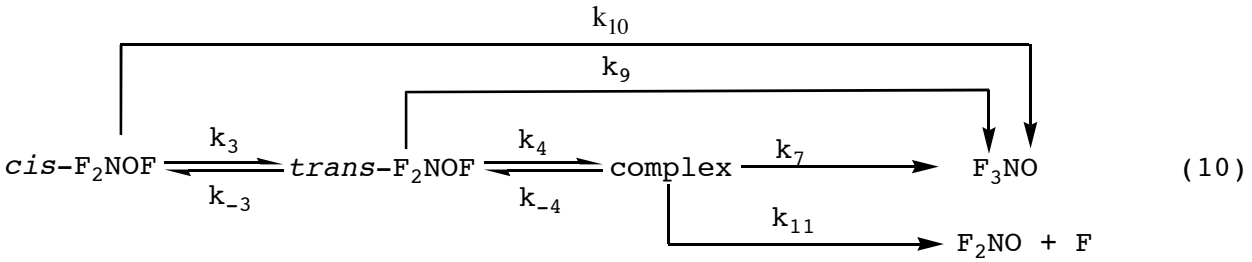

Chemrate was used to calculate the isomerization (*cis*-$F_2NOF \rightleftarrows$ *trans*-F_2NOF) rate constants (k_3, k_{-3}). Chemrate includes a master equation solver so that rate constants for unimolecular reactions can be determined on the basis of RRKM theory in the energy transfer region and chemical activation processes under steady and non-steady conditions. CCSD(T)/cc-pVQZ//B3LYP/6-311+G(d) energies are used with B3LYP/6-311+G(d) optimized geometries and thermal corrections in Chemrate.

Figure 7 compares the calculated rate constants (high-pressure limit) for production of $F_2NO + F$ (k_1) and $FNO + F_2$ (k_2). Since TST rate constants and VTST rate constants are similar for *cis*-$F_2NOF \rightarrow FNO + F_2$ (concerted) as the temperature

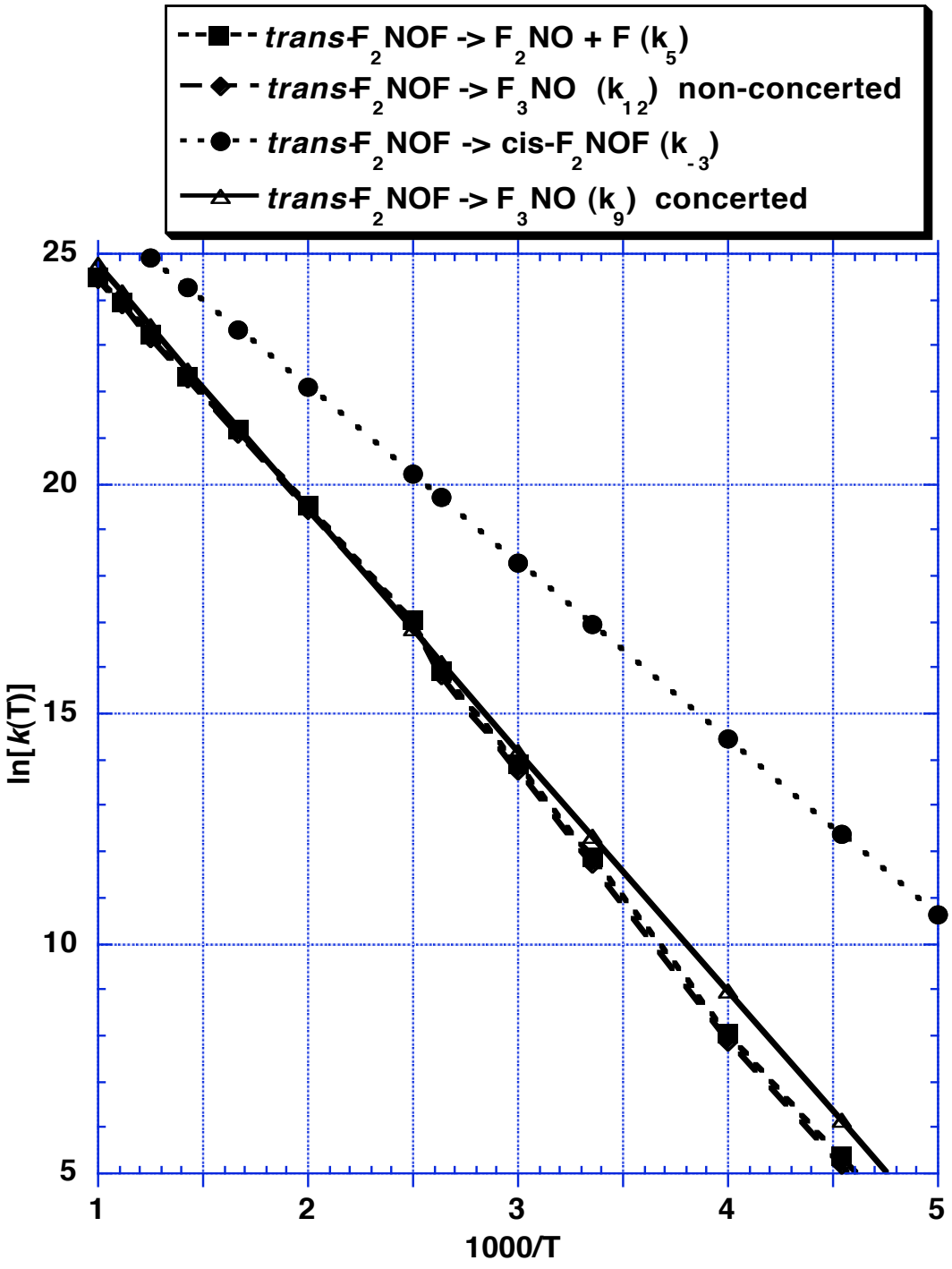

Figure 7. Calculated rate constants involving *cis*-F_2NOF. The computational rate data are for the unimolecular rate constant at the high-pressure limit.

decreases, variational effect can be ignored for this reaction. The rate constant for *cis*-$F_2NOF \rightarrow F_2NO + F$ and *cis*-$F_2NOF \rightarrow FNO + F_2$ are calculated as $k_1=6.37x10^{13}$•exp(-7855/T) and $k_2=8.14x10^{13}$•exp(-7860/T), respectively.

Table 7. Rate constant with temperature dependence at high-pressure limit for formation of F_3NO and dissociation of complex to radicals

Temp(K)	k_4	k_{-4}	k_7	k_{11}
200	4.45E+01	1.04E+12	1.09E+14	2.03E+12
220	4.68E+02	1.01E+12	1.01E+14	2.71E+12
250	7.95E+03	9.78E+11	9.22E+13	3.87E+12
298	2.28E+05	9.29E+11	8.40E+13	5.95E+12
333	1.46E+06	8.99E+11	8.02E+13	7.60E+12
380	1.01E+07	8.66E+11	7.69E+13	9.85E+12
400	2.03E+07	8.54E+11	7.58E+13	1.08E+13
500	2.83E+08	8.05E+11	7.23E+13	1.56E+13
600	1.65E+09	7.74E+11	7.05E+13	2.00E+13
700	5.83E+09	7.52E+11	6.94E+13	2.40E+13
800	1.51E+10	7.37E+11	6.87E+13	2.76E+13
900	3.15E+10	7.26E+11	6.83E+13	3.07E+13
1000	5.69E+10	7.18E+11	6.80E+13	3.35E+13

The rate constant for formation of F_3NO is derived with a steady state approximation [$k_{10}=k_3k_4k_7/(k_{-3}(k_{-4}+k_7))$] via *trans*-$F_2NOF$ in eq 10. Since the F_2NO-F-ts transition state is calculated with an accurate method (RCCSD(T)/cc-pVQZ//UB3LYP/6-311+G(d)), we used this transition state to calculate a rate constant of $1.42x10^{12}$·exp(-7420/T) for k_{10}.

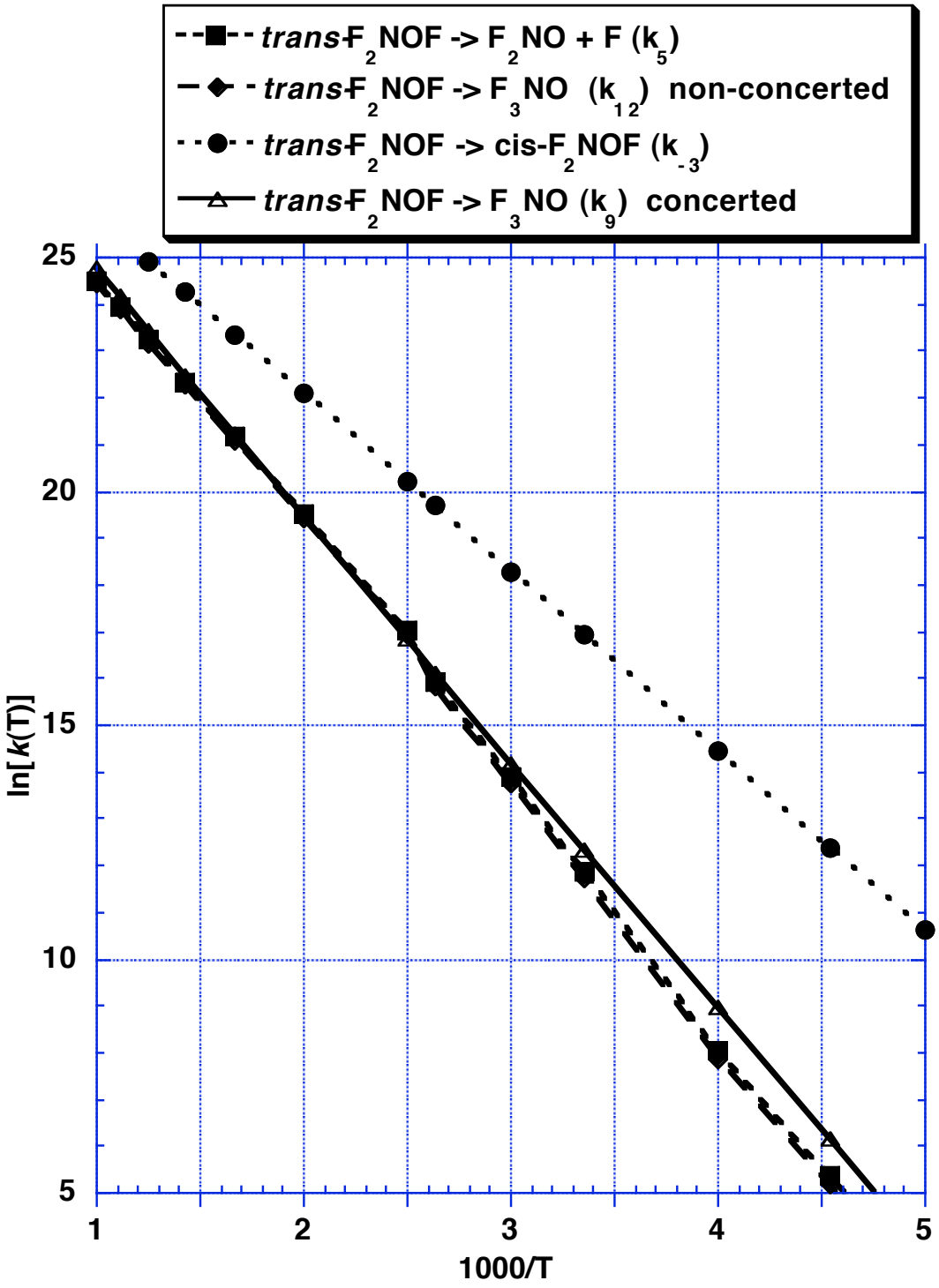

Figure 8. Calculated rate constants involving *trans*-F_2NOF.

We also checked our rate constant result corresponding to eq 10 with a steady state approximation for the complex [$k_9=k_4k_7/(k_{-4}+k_7)$]. Since the complex and F_2-NOF-ts could not be calculated accurately due to spin contamination, we assume that complex and F-F_2NOF-ts have the same energy as F_2NO-F-ts in the rate constant calculations. Rate constants k_{-4} and k_7 are calculated by Polyrate and k_8 is calculated by Variflex. Since k_{-4} is small and k_7 is large ($k_7 >> k_{-4}$), the overall rate becomes $k_9 \approx k_4$. We also include the possibility of dissociation of the complex (k_8) to radicals ($F_2NO + F$) in the rate constant for F_3NO formation. Table 7 shows that k_7 is 14 times faster than the rate constant of complex dissociation to radicals (k_{11}) at room temperature which will reduce the formation of F_3NO seven percent at room temperature.

At all temperatures the ratio of $F_2NO + F$ (k_1) formation to $FNO + F_2$ (k_2) is very similar but much faster than F_3NO formation. Since F_2NO has a very short lifetime, it can quickly dissociate to FNO + F. Depending on the rate of 2F radical-radical recombination, the dominant products from F_2NOF decomposition are expected to be FNO, F_2, and F. It is interesting to note that Fox et al.[14] suggested that the observed formation of F_3NO from the reaction of F_2 plus NO in a 2000K flame probably involved an excited-state intermediate.

While the addition of F to F_2NO does not play a role in F_3NO formation,[46] we compared this path (non-concerted path, k_{12}) with the concerted path (k_9) of *trans*-$F_2NOF \rightarrow F_3NO$ that can be formed with activation enthalpy 14.10 kcal/mol. Our calculated results show that the concerted path (k_9) is faster than the non-concerted path (k_{12}) for *trans*-$F_2NOF \rightarrow F_3NO$ at low temperatures (Figure 8). This result may have implications in reactions where the radicals generated have longer lifetimes, such as in the FONO →

FNO_2 rearrangement. In that reaction, a radical/radical complex may lead to a concerted/nonconcerted branching ratio.

4.6 Conclusion

Perfluorohydroxylamine (F_2NOF) is a challenging molecule for theory and its short lifetime suggests that it will be a challenge for experiment as well. The O-F bond enthalpy (298K) is calculated at the CCSD(T)/cc-pVQZ//B3LYP/6-311+G(d) level to be 15.97 kcal/mol. In competition with O-F bond fragmentation, *cis*-F_2NOF can eliminate F_2 or isomerize to *trans*-F_2NOF. In turn, trans-F_2NOF can cleave the O-F bond or rearrange to F_3NO via an intermediate $F+F_2NO$ complex. Rate constants have been calculated for the different pathways in order to determine the products formed. At room temperature, only 3% of products ($k_{10}/(k_1+k_2+k_{10})$ is expected to be F_3NO even though it is the global minimum.

4.7 Reference

(1) Antoniotti, P.; Grandinetti, F. *Chem. Phys. Lett.* **2002**, *366*, 676.

(2) Erben, M. F.; Diez, R. P.; Védova, C. O. D. *Chem. Phys.* **2005**, *308*, 193.

(3) Dewar, M. J. S.; Rzepa, H. S. *J. Am. Chem. Soc.* **1978**, *100*, 58.

(4) (a) Olsen, J. F.; Howell, J. M. *J. Fluorine Chem.* **1978**, *12*, 123. (b) Olsen, J. F.; O'Connor, D.; Howell, J. M. *J. Fluorine Chem.* **1978**, *12*, 179.

(5) Plato, V.; Hartford, W. D.; Hedberg, K. *J. Chem. Phys.* **1970**, *53*, 3488.

(6) Bedzhanyan, Yu. R.; Gershenzon, Yu. M.; Rozenshtein, V. B. *Kinetika i Kataliz*, **1990**, *31*, 1474.

(7) (a) Misochko, E. Ya.; Akimov, A. V.; Goldschleger, I. U. *J. Am. Chem. Soc.* **1998**, *120*, 11520. (b) Misochko, Yu. R.; Akimov, A. V.; Goldschleger, I. U.; Boldyrev, A. I.; Wight, C. A. *J. Am. Chem. Soc.* **1999**, 121, 405.

(8) Ellison, G. B.; Herbert, J. M.; McCoy, A. B; Stanton, J. F.; Szalay, P. G. *J. Phys. Chem. A* **2004**, *108*, 7639.

(9) Sayin, H.; McKee, M. L. *J. Phys. Chem.* A **2005**, *109*, 4736.

(10) Kovačič, S.; Lesar, A.; Hodošček, M. *Chem. Phys. Lett.* **2005**, *413*, 36.

(11) (a) Zhao, Y.; Houk, K. N.; Olson, L. P. *J. Phys. Chem. A* **2004**, *108*, 5864. (b) Zhang, J.; Donahue, N. M. *J. Phys. Chem. A* **2006**, ASAP. (c) Srinivasan, N. K.; Su, M.-C.; Sutherland, J. W.; Michael, J. V.; Ruscic, B. *J. Phys. Chem. A* **2006**, ASAP. (d) Hippler, H.; Krasteva, N.; Nasterlack, S.; Striebel, F. *J. Phys. Chem. A* **2006**, ASAP.

(12) Kovačič, S.; Lesar, A.; Hodošček, M. *J. Chem. Inf. Model.* **2005**, *45*, 58.

(13) Zhu, R. S.; Lin, M. C. *Chem. Phys. Chem.* **2005**, *6*, 1514.

(14) Fox, W. B.; Sukornick, B.; Mackenzie, J. S.; Sturtevant, R. L.; Maxwell, A. F.; Holmes, J. R. *J. Am. Chem. Soc.* **1970**, 92, 5240.

(15) Lee, T. J.; Bauschlicher, C. W., Jr.; Jayatilaka, D. *Theor. Chem. Acc.* **1997**, *97*, 185.

(16) Guha, S.; Francisco, J. S. *J. Phys. Chem. A* **1997**, *101*, 5347.

(17) Francisco, J. S.; Clark, J. *J. Phys. Chem. A* **1998**, *102*, 2209.

(18) Parthiban, S.; Lee, T. J. *J. Chem. Phys.* **2000**, *113*, 145.

(19) Zhao, Y.; Lynch, B. J.; Truhlar, D. G. *J. Phys. Chem. A* **2004**, *108*, 2715.

(20) Zhao, Y.; Truhlar, D. G. *J. Phys. Chem. A* **2004**, *108*, 6908.

(21) Hehre, W. J.; Radom, L.; Schleyer, P. v. R.; Pople, J. A. *Ab initio Molecular Orbital Theory*; Wiley: NewYork, 1987.

(22) Lynch, B. J.; Zhao, Y.; Truhlar, D. G. *J. Phys. Chem. A* **2003**, *107*, 1384.

(23) Lee, T. J.; Scuseria, G. E. *J. Chem. Phys.* **1990**, *93*, 489.

(24) Scuseria, G. E. *J. Chem. Phys.* **1991**, *94,* 442.

(25) *Gaussian03, (Revision B.4)*, Frisch, M. J. *et al*. Gaussian, Inc., Pittsburgh PA, 2003.

(26) Schmidt, M. W.; Baldridge, K. K.; Boatz, J. A.; Elbert, S. T.; Gordon, M. S.; Jensen, J. H.; Koseki, S.; Matsunaga, N.; Nguyen, K. A.; Su, S.; Windus, T. L.; Dupuis, M.; Montgomery, J. A. *J. Comput. Chem.* **1993**, *14*, 1347.

(27) Schaftenaar, G.; Noordik, J. H. *J. Comput.-Aided Mol. Design* **2000**, *14*, 123.

(28) Roos, B. O. "The complete active space self-consistent field method and its applications in electronic structure calculations" In: Lawley, K. P., Ed. *Advances*

in Chemical Physics; Ab Initio Methods in Quantum Chemistry-II; John Wiley & Sons: Chichester, UK, 1987.

(29) Nakano, H. *J. Chem. Phys.* **1993**, *99*, 7983.

(30) Gonzalez, C.; Schlegel, H. B. *J. Phys. Chem.* **1989**, *93*, 2154.

(31) Garrett, B. C.; Truhlar, D. G. *J. Chem. Phys.* **1984**, *81*, 309.

(32) Truhlar, D. G.; Garrett, B. C.; Klippenstein, S. J. *J. Phys. Chem.* **1996**, *100*, 12771.

(33) Chuang, Y.-Y.; Corchado, J. C.; Truhlar, D. G. *J. Phys. Chem. A* **1999**, *103*, 1140.

(34) Klippenstein, S. J.; Wagner A. F.; Dunbar, R. C.; Wardlaw, D. M.; Robertson, S. H. VariFlex, Version 1.00, Argonne National Laboratory, Argonne, IL, 1999.

(35) Mokrushin, V.; Bedanov, V.; Tsang, W.; Zachariah, M. R.; Knyazev, V. D. ChemRate, Version 1.21, National Institute of Standards and Technology, Gaithersburg, MD, **2002**.

(36) Corchado, J. C.; Chuang, Y.-Y.; Fast, P. L.; Villa, J.; Hu, W.-P.; Liu, Y.-P.; Lynch, G. C.; Nguyen, K. A.; Jackels, C. F.; Melissas, V. S.; Lynch, I. R.; Coitino, E. L.; Fernandez-Ramos, A.; Pu, J.; Albu, T. V.; Steckler, R.; Garrett, B. C.; Isaacson, A. D.; Truhlar, D. G. Polyrate, Version 9.3, University of Minnesota, MN, **2004**.

(37) Dunning-type basis sets (a) cc-pVDZ: Woon, D. E.; Dunning, T. H. *J. Chem. Phys.* **1993**, *98*, 1358. (b) cc-pVTZ: Kendall, R. A.; Dunning, T. H.; Harrison, R. J. *J. Chem. Phys.* **1992,** *96*, 6796. (c) cc-pVQZ: Dunning T, H. *J. Chem. Phys.* **1989**, *90*, 1007.

(38) When calculating the rate constant using VTST, the energy of the points along the IRC at the UCCSD(T)/cc-pVTZ level were shifted upward by 0.72 kcal/mol to be consistent with the correction for the Abst-F_2-ts-*c* transition state.

(39) (a) Noodleman, L.; Case, D. A. *Adv. Inorg. Chem.* **1992**, *38*, 423. (b) See: Bally, T.; Borden, W. T. in *Reviews Comp. Chem.* K. B. Lipkowitz, D. B. Boyd, Eds., Wiley: New York, 1999; Vol. 13, p. 1.

(40) Fourré, I.; Silvi, B.; Sevin, A.; Chevreau, H. *J. Phys. Chem. A* **2002**, 106, 2561.

(41) Braïda, B.; Thogersen, L.; Wu, W.; Hiberty, P. C. *J. Am. Chem. Soc.* **2002**, 124, 11781.

(42) Braïda, B.; Hiberty, P. C. *J. Phys. Chem. A* **2000**, 104, 4618.

(43) Braïda, B.; Hiberty, P. C.; Savin, A. *J. Phys. Chem. A* **1998**, 102, 7872.

(44) Bach, R. D.; Owensby, A. L.; Gonzalez, C.; Schlegel, H. B.; McDouall, J. J. W. *J. Am. Chem. Soc.* **1991**, *113*, 6001.

(45) Zou, P.; Derecskei–Kovacs, A.; North, S. W. *J. Phys. Chem. A* **2003**, *107*, 888.

(46) If we compare k_8/[F] and k_6 at 298K where [F] is assumed to be 0.01 atm, then the unimolecular rate ($k_8[F_2NO]$) is still 2300 times faster than the bilmolecular rate ($k_6[F_2NO][F]$).